

総合研究大学院大学 ★ 宇宙科学専攻

The Graduate University for Advanced Studies
Department of Space and Astronautical Science

**UKF Adaptation and Filter Integration for Attitude
Determination and Control of Nanosatellites with
Magnetic Sensors and Actuators**

Ph.D. Thesis

Halil Ersin Soken

July 2013

Preface and Acknowledgments

This thesis is submitted in partial fulfillment of the requirements for the Doctor of Philosophy in Space and Astronautical Science at the Graduate University for Advanced Studies (SOKENDAI). This research has been carried out under the supervision of Assoc. Prof. Shin-ichiro Sakai at the Institute of Space and Astronautical Science (ISAS), Japan Aerospace Exploration Agency (JAXA).

First of all, I would like to express my deepest gratitude to my advisor, Professor Shin-ichiro Sakai who has made this study possible with all his supports and feedbacks. I am also thankful to Prof. Chingiz Hajiyev from Istanbul Technical University and Prof. Rafael Wisniewski from Aalborg University for their valuable comments during our joint researches.

I acknowledge the Ministry of Education, Culture, Sports, Science and Technology (文部科学省) for the financial support throughout my researches in Japan.

I thank to all my colleagues with whom I have shared the same laboratory in ISAS, JAXA for three years.

Lastly, at that point, I must signify that, I am grateful to my parents and sister, who have been always with me despite the long distance between us; without their endless love this thesis would not come true.

July 2013, Sagamihara, Japan

Halil Ersin Soken

Summary

The main aim of this study is to design an accurate attitude determination and control system for the nanosatellites with magnetic sensors and actuators. This aim is achieved by discussing different estimation algorithms, integrating them and finally proposing an overall attitude determination scheme. The given methods might be regarded both as separate solutions for different practical issues or a part of a whole attitude determination and control system for a nanosatellite.

As a consequence of the progress in the miniaturization and the increase in the capability of the electronic devices, performing space missions with smaller satellites has become possible. The number of researches on such satellites is increasing day by day because of their advantages such as low investment and operational costs, enabling COTS (commercial of the shelf) technology in space and short system development periods. Despite these facts discussions on small satellite attitude control is far from being concluded. Conceptual design limitations like the size and weight are the main reasons for the complexity of the problem yet such limitations are also what make the problem more interesting. The primary target of the researchers working on this issue is to design an attitude determination and control system, which can provide the same accuracy with the system for larger competitors, but remain within the design limitations.

Magnetic sensors and actuators are popular attitude determination and control hardware for the nanosatellites since they are lighter, smaller and more economical compared to the others. On the other hand, they are regarded as coarse sensors and actuators and the accuracy that they can provide is limited because of the practical issues such as magnetic bias, residual magnetic moment and inherent complexity of the magnetic control. This study proposes new methods to overcome these limitations. In this context some of the sub-issues that are addressed are the on-orbit real time calibration of the magnetometers, adaptive tuning of the Kalman filter algorithm to increase the attitude estimation performance, robust estimation algorithm against sensor faults and estimation of the residual magnetic moments.

The main contribution of this study is to examine several basic practical problems met for the attitude determination and control of a nanosatellite with magnetic sensors and actuators, and give a whole attitude determination algorithm, which is composed of adaptive filters,

for solving these problems and increasing the attitude determination and control system performance. An approach based on the adaptation of the Unscented Kalman Filter, the estimation algorithm used as a part of the attitude determination procedure, is followed. The practical problems are solved stage by stage by using new techniques for the filter adaptation and then these filters are integrated in order to propose an overall attitude determination method. At the end a novel attitude determination scheme for nanosatellites with magnetic sensing and actuation is presented. Moreover the different estimation algorithms given in this paper have significance in terms of the estimation theory. The Robust Unscented Kalman Filter against sensor malfunctions and the Kalman filter adaptation technique used in case of unexpected instantaneous changes in the estimated parameter are newly proposed methods and can be applied for different problems.

Throughout the study, the theory is supported by simulation results. First, each problem is examined individually and then it is demonstrated how the proposed solution technique can be integrated with the main idea: attitude determination and control for nanosatellite with magnetic sensors and actuators. The results show that the accuracy for a simple nanosatellite attitude determination and control system can be increased satisfactorily. The key findings presented in this study are published (or submitted) as international papers.

Contents	Page
1. Introduction	1
1.1. Background and Motivation	1
1.2. Literature Survey	4
1.3. Contribution of the Thesis	9
1.4. Thesis Overview	12
2. Satellite Mathematical Model	15
2.1. Coordinate Systems	15
2.2. Quaternions for Attitude Representation	16
2.2.1. Vector Transformation for Quaternions	17
2.2.2. Propagation of Quaternions by Time	18
2.2.3. Euler Angles – Quaternions Relationship	20
2.3. Equations of Motion	21
2.3.1. Satellite Dynamics	21
2.3.2. Satellite Kinematics	24
3. Sensor Models	25
3.1. The Magnetometer Model	26
3.2. The Gyro Model	27
4. Sensor Bias Estimation	29
4.1. Unscented Kalman Filter for Attitude Estimation	29
4.1.1. The Unscented Kalman Filter	30
4.1.2. The UKF with Attitude Error Representation	32
4.2. Dynamics-based and Gyro-based Models	36
4.3. In-Orbit Gyro and Magnetometer Bias Estimation	37
4.3.1. Gyro and Magnetometer Bias Estimation via the UKF	37
4.3.2. Simulation Results	39
5. Adaptation Methods for the UKF	43
5.1. Adaptation Against Process Noise Uncertainties	43
5.1.1. Process Noise Covariance Scaling	44
5.1.2. Simulation Results for Process Noise Covariance Scaling	47
5.1.3. Process Noise Covariance Estimation	50
5.1.4. Simulation Results for Process Noise Covariance Estimation	54

5.2. Robust UKF Against Measurement Faults	61
5.2.1. Adaptation Using Single Scale Factor	62
5.2.2. Adaptation Using Multiple Scale Factors	63
5.2.3. Fault Detection Procedure	65
5.2.4. Simulation Results	65
6. The Residual Magnetic Moment Estimation	73
6.1. In-Orbit Estimation of the Time-Varying RMM	74
6.2. Change Detection and UKF Adaptation	78
6.2.1. Change Detection	79
6.2.2. The Adaptation of the UKF	80
6.3. Simulation Results	84
7. Demonstration of the Proposed Attitude Determination Scheme	89
7.1. Integration of the Filters	89
7.1.1. The RAUKF Algorithm	89
7.1.2. Integration of the RAUKF with the RMM Estimator	91
7.2. Overall Attitude Estimation Scheme	92
7.2.1. Demonstration of the Overall Attitude Estimation Scheme	92
7.2.2. Performance Comparison	99
8. Conclusion and Recommendations	101
Bibliography	103
A. Attitude Control of the Magnetically Actuated Nanosatellite	109
A.1. A Review for the Attitude Control by Magnetic Actuation	109
A.2. Discussion on the Recent Studies	110

Nomenclature

Acronyms and Abbreviations

ADCS	: Attitude Determination and Control System
AUKF	: Adaptive Unscented Kalman Filter
CUSUM	: Cumulative Sum
EKF	: Extended Kalman Filter
FLAS	: Fuzzy Logic Adaptive System
GMA	: Geometric Moving Average
GPS	: Global Positioning System
IGRF	: International Geomagnetic Reference Field
INS	: Inertial Navigation System
KF	: Kalman filter
LEO	: Low Earth Orbit
OKF	: Optimal Kalman Filter
RMM	: Residual Magnetic Moment
RMSE	: Root Mean Squared Error
RAUKF	: Robust Adaptive Unscented Kalman Filter
RUKF	: Robust Unscented Kalman Filter
UKF	: Unscented Kalman Filter
w.r.t	: with respect to

Notation

Vectors and Matrices

\mathbf{v}	vectors are written in bold
v_x, v_y, v_z	x, y and z components of vector \mathbf{v}
$(A)_l$	l^{th} column of matrix A
$[\mathbf{v} \times]$	cross product matrix of vector \mathbf{v}
$tr(A)$	trace of matrix A
$diag[A_{11} \ \cdots \ A_{mm}]$	$n \times n$ diagonal matrix with $A_{11} \dots A_{mm}$ diagonal components and zero non-diagonal elements

List of Symbols

\mathbf{q}	quaternion vector defining rotation of body frame w.r.t orbital frame
\mathbf{A}	Attitude matrix formed of quaternions
\mathbf{I}	identity matrix
$\boldsymbol{\omega}_{BR}$	body angular velocity w.r.t reference frame
p, q, r	angular velocity components about x , y and z axes for the body angular velocity w.r.t reference frame
φ, θ, ψ	Euler angles (roll-pitch-yaw) about x , y and z axes
\mathbf{L}	Angular momentum
\mathbf{N}	Total torque acting on the satellite
$\boldsymbol{\omega}_{BI}$	body angular velocity w.r.t inertial frame
$\omega_x, \omega_y, \omega_z$	angular velocity components about x , y and z axes for the body angular velocity w.r.t inertial frame
\mathbf{J}	moment of inertia matrix
\mathbf{N}_d	disturbance torque acting on the satellite
\mathbf{N}_c	control torque acting on the satellite
\mathbf{M}_c	Magnetic moment generated by magnetorquers
\mathbf{B}	Earth's magnetic field in the body frame
\mathbf{N}_{gg}	gravity gradient torque
\mathbf{N}_{ad}	aerodynamic torque
\mathbf{N}_{sp}	solar pressure disturbance torque
\mathbf{N}_{md}	residual magnetic torque
\mathbf{M}_r	residual magnetic moment
ω_0	angular velocity of the orbit frame w.r.t inertial frame
B_1, B_2, B_3	Earth magnetic field vector components in the orbit frame
B_x, B_y, B_z	Earth magnetic field vector components in the body frame
M_e	Magnetic dipole moment of the Earth
μ	Earth's gravitational constant
ω_e	spin rate of the Earth
i	orbit inclination
ε	magnetic dipole tilt
r_0	distance between the center of masses of the Earth and satellite.

σ_m	standard deviation of each magnetometer error
σ_v	standard deviation of each gyro random error
σ_u	standard deviation of gyro biases
η_1, η_2, η_3	zero mean Gaussian white noises
δ_{kj}	Kronecker symbol
\mathbf{b}_m	magnetometer bias vector
\mathbf{b}_g	gyro bias vector
\mathbf{x}_k	state vector
$\tilde{\mathbf{y}}_k$	measurement vector
$P(k k)$	estimated UKF covariance
P_0	initial value of the covariance
n	dimension of the state vector
$Q(k)$	process noise covariance of the UKF
$R(k)$	measurement noise covariance of the UKF
κ	scaling parameter for the UKF
$\hat{\mathbf{x}}(k k)$	estimated state vector
$\hat{\mathbf{x}}(k+1 k)$	predicted state vector
$P(k+1 k)$	predicted covariance
$\hat{\mathbf{y}}(k+1 k)$	predicted observation vector
$P_{yy}(k+1 k)$	observation covariance matrix
$P_{vv}(k+1 k)$	innovation covariance matrix
$\mathbf{y}(k+1)$	measurements vector
$P_{xy}(k+1 k)$	cross correlation matrix
$\mathbf{e}(k+1)$	innovation sequence
$K(k+1)$	Kalman gain
\mathbf{g}	vector part of quaternions
f	scale factor for the UKF with attitude error representation
a	tuning parameter for the UKF with attitude error representation
$\delta\mathbf{q}$	local error quaternion vector

$\delta \mathbf{p}$	generalized Rodrigues parameters
$\hat{\boldsymbol{\beta}}(k k)$	sensor bias vector
$P^*(k+1 k)$	predicted covariance without the additive noise
$\Lambda(k)$	adaptive factor
$\tilde{\mathbf{e}}(k+1)$	residual sequence
$P_{\tilde{\mathbf{e}}}(k+1)$	residual covariance matrix
$H(k+1 k)$	measurement matrix formed of predicted states
$H(k+1 k+1)$	measurement matrix formed of estimated states
$P_{xy}(k+1 k+1)$	cross correlation matrix for the residual
Q_q	process noise covariance for quaternions (3×3)
Q_{gb}	process noise covariance for gyro bias (3×3)
Q_{mb}	process noise covariance for magnetometer bias (3×3)
Q_{q_gb}	process noise covariance in between the quaternions and gyro bias (3×3)
$\alpha(k+1)$	adaptive parameters
MV	moving window size
C_e	innovation covariance (same as $P_{vv}(k+1 k)$)
$\Delta \mathbf{x}(k+1)$	state residual vector
γ	scale factor for the AUKF low-pass filter
Δt	sampling time
$S_s(k)$	single scale factor for the RUKF
$S_m(k)$	multiple scale factor for the RUKF
$\beta(k)$	statistical function for fault detection
$\chi_{\alpha,z}^2$	threshold for fault detection
$Z_n(k+1)$	normalized innovation sequence
$g(k+1)$	GMA parameter
λ	forgetting factor for the GMA test
ξ	threshold for the GMA test/change detection
$\Omega(k+1)$	weighting function
ϑ	tuning parameter for the weighting function
$F(k)$	system dynamics matrix

List of Figures		Page
1.1	GeneSat-1 of NASA: A nanosatellite mission example.	1
2.1	Coordinate systems.	16
4.1	Pitch angle estimation error of the UKF used for attitude, gyro and magnetometer bias estimation.	39
4.2	Estimation of the bias for the gyro aligned in the x axis by the UKF used for attitude, gyro and magnetometer bias estimation.	40
4.3	Estimation of the bias for the magnetometer aligned in the x axis by the UKF used for attitude, gyro and magnetometer bias estimation.	40
4.4	Pitch angle estimation error of the UKFs with and without magnetometer bias estimation when magnetometer bias exists in the measurements: UKF _{wb} is the filter that estimates the magnetometer biases and UKF _{wob} is the filter that disregards them.	41
4.5	Estimation of the bias for the gyro aligned in the y axis by the UKF without magnetometer bias estimation when magnetometer bias exists in the measurements.	42
5.1	The overall estimation scheme for the AUKF with process noise covariance scaling.	48
5.2	Norm of the attitude estimation errors for the conventional UKF (dashed line) and the AUKF with covariance scaling (solid line) in case of attitude, gyro bias and magnetometer bias estimation.	49
5.3	Norm of the attitude estimation errors for the UKF _a and AUKF in case where attitude and gyro biases are estimated.	55
5.4	Norm of the gyro bias estimation errors for the UKF _a and AUKF in case where attitude and gyro biases are estimated.	56

5.5	Norm of the attitude estimation errors for the UKF _a and AUKF in case where attitude, gyro biases and magnetometer biases are estimated.	57
5.6	Norm of the gyro bias estimation errors for the UKF _a and AUKF in case where attitude, gyro biases and magnetometer biases are estimated.	57
5.7	Norm of the magnetometer bias estimation errors for the UKF _a and AUKF in case where attitude, gyro biases and magnetometer biases are estimated.	58
5.8	Norm of the magnetometer bias estimation errors for the UKF _a and AUKF in case where attitude, gyro biases and magnetometer biases are estimated (zero initial error for magnetometer biases).	59
5.9	Pitch angle estimation error for attitude, gyro and magnetometer bias estimation scenario. Results for the UKF tuned by trial and error method are given with dotted line and the results for the AUKF are given with solid line.	60
5.10	Estimation of the bias for the magnetometer aligned in the x axis for attitude, gyro and magnetometer bias estimation scenario. Results for the UKF tuned by trial and error method are given with black line and the results for the AUKF are given with red line.	61
5.11	Pitch angle estimation error for the UKF and RUKF in case of continuous bias.	67
5.12	Variation of the single scale factor for the RUKF in case of continuous bias.	68
5.13	Pitch angle estimation error for the UKF and RUKF in case of measurement noise increment.	69
5.14	Variation of the single scale factor for the RUKF in case of measurement noise increment.	70
5.15	Pitch angle estimation error for the UKF and RUKF in case of zero output failure.	71
5.16	Variation of the single scale factor for the RUKF in case of zero output failure.	72

6.1	Estimation of the RMM in x axis.	76
6.2	Estimation of the RMM in x axis in case of sudden change for two different process noise levels.	77
6.3	Estimation of the angular rate about x axis by the UKF with low process noise in case of sudden change.	77
6.4	Variation of the GMA in case of change in the estimated RMM terms (change at 2000 th second).	80
6.5	The RMM estimation scheme in case of sudden change.	82
6.6	Estimation of the RMM in x axis in case of sudden change: The UKF without change detection and adaptation is referred as “w/o adaptation”; the UKF, which is reinitialized after each change detection, is named as “reint”; and the proposed estimation algorithm is shown as “adaptive”.	85
6.7	Estimation of the RMM in y axis in case of sudden change: The UKF without change detection and adaptation is referred as “w/o adaptation”; the UKF, which is reinitialized after each change detection, is named as “reint”; and the proposed estimation algorithm is shown as “adaptive”.	86
6.8	Estimation of the RMM in z axis in case of sudden change: The UKF without change detection and adaptation is referred as “w/o adaptation”; the UKF, which is reinitialized after each change detection, is named as “reint”; and the proposed estimation algorithm is shown as “adaptive”.	87
6.9	Variation of the GMA in case of change in the estimated RMM terms: The GMA for the regular UKF and UKF with the proposed change detection and adaptation procedure.	88
7.1	The proposed RAUKF.	90
7.2	Integration of the RAUKF with the RMM estimator: The overall attitude estimation scheme.	92
7.3	Estimation of the pitch angle via the RAUKF (red line) and UKF (black line) as a part of the overall estimation scheme.	95

7.4	Estimation of the RMM term in z axis via the RAUKF (red line) and UKF (black line) as a part of the overall estimation scheme.	96
7.5	Estimation of the roll angle via the AUKF (red line) and UKF (black line) as a part of the overall estimation scheme in case of measurement malfunction.	97
7.6	Estimation of the RMM term in y axis via the RAUKF (red line) and UKF (black line) as a part of the overall estimation scheme in case of measurement malfunction.	98
7.7	Estimation of the RMM term in y axis via the UKF with P adaptation (red line) and UKF without P adaptation (black line) as a part of the overall estimation scheme in case of instantaneous change in the estimated RMM parameters (figure is zoomed to the estimations in between 30000 th and 35000 th seconds).	99
A.1	Limitations of the magnetic attitude control.	110

List of Tables		Page
1.1	Typical magnetometer, MEMS gyro and magnetorquer examples for nanosatellite applications.	3
3.1	Characteristics of the attitude estimation reference sources.	25
5.1	Absolute estimation errors in case of continuous bias: Regular UKF, RUKF with single scale factor (SSF) and RUKF with multiple scale factor (MSF).	68
5.2	Absolute estimation errors in case of measurement noise increment: Regular UKF, RUKF with single scale factor (SSF) and RUKF with multiple scale factor (MSF).	70
5.3	Absolute estimation errors in case of zero output failure: Regular UKF, RUKF with single scale factor (SSF) and RUKF with multiple scale factor (MSF).	72
6.1	Absolute values of error for the RMM estimation in case of sudden change.	78
6.2	Alarm time and the adaptation values for the proposed UKF adaptation algorithm.	87
7.1	Comparison of the computational load of proposed algorithms with the EKF. (*) Here EKF is built as the Multiplicative Extended Kalman Filter which uses quaternions for the attitude representation.	100

1. Introduction

1.1. Background and Motivation

Since the world's first Earth orbiting artificial satellite, Sputnik I, was launched on 4 October 1957, mankind has always been working to reach the better in space missions. Progress in the miniaturization and the increase in the capability of the electronic devices are leading us towards a new era where performing complex space missions with small satellites will be possible.

The nanosatellite term refers to the satellites with mass less than 10kg (Fig. 1.1). The main motivation behind the nanosatellite missions is the significant cost decrease which is the direct result of reduced mass and complexity. Enabling COTS (commercial of the shelf) technology in space and short system development periods are other advantages of nanosatellites. Since the investment cost is not high the developer may take the risk of using self-developed hardware or software for the mission and the satellite can be developed from scratch in a considerably shorter time than bigger satellites. Moreover the nanosatellite missions are generally single-aimed, so the satellite is not complex and the mission failure risk is lower than usual (Rendleman 2009).

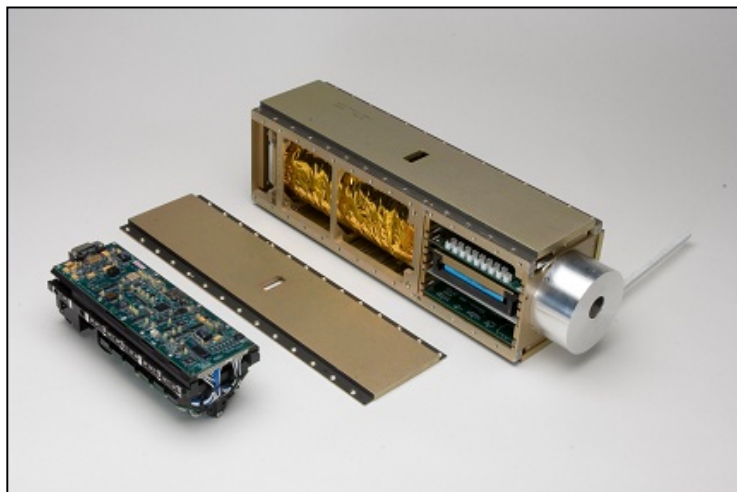





Figure 1.1: GeneSat-1 of NASA: A nanosatellite mission example (Image Credit: NASA/Ames).

Although there are numerous researches on nanosatellites and this number is increasing day by day, the investigations are still far from being concluded. In this sense maybe the most important topic for researchers to deepen their investigations is the attitude determination and control of these satellites. According to (Bouwmeester and Guo 2010) despite the advanced technology for other subsystems, the attitude determination and control system (ADCS) and the subsystems that rely on the ADCS accuracy are underdeveloped for nanosatellites. It is added that the bottleneck for nanosatellites remains the attitude control performance especially in terms of dynamic control and control accuracies. The main reason underlying this problem is the mass, size and power restrictions. Unlike the big satellites high accuracy high-tech attitude sensors and actuators such as star-trackers and reaction wheels cannot be easily used for nanosatellite missions since they are heavy, big and do consume high power. The attitude must be determined and controlled precisely by using coarse sensors and actuators which are smaller and lighter (Soken *et al.* 2010). In this context the possible candidate for attitude sensing is economic, light and small magnetometers (Table 1.1) whereas the control might be performed by magnetic torque rods (magnetorquers). The primary problem is how to get high ADCS performance by using only magnetometers and magnetorquers.

The typical attitude determination accuracy for sole magnetometer based methods is 1-2deg (Bak 1999). The dominating error sources are the magnetic field uncertainty and bias in the measurements which is caused by several reasons such as magnetic charging during the launch and electrical charge on the other subsystems. Sun sensors are usually used for aiding the magnetometer measurements but in this case the attitude determination accuracy significantly degrades during the eclipse when the sun sensors are not usable. In this sense another candidate for using together with magnetometers is the gyros since they are also light and small instruments, especially after the recent developments ended up with MEMS (Microelectromechanical systems) gyros (Table 1.1). Magnetometer is preferred as the attitude sensor for almost 30% of all nanosatellite missions by 2010 while this number is around 12% for gyros (Bouwmeester and Guo 2010).

As for the attitude control, the magnetic control is the most popular method for the nanosatellites either as passive control with magnets or active control with magnetorquers. The magnetorquers are lightweight and energy-efficient (Table 1.1). Besides they do not have any mechanical part so they are more reliable compared to the reaction wheels and control moment gyroscopes. However the control accuracy is limited for these actuators because of the inherent complexity of the problem and pointing accuracy higher than 1deg. (< 1deg) is not possible using only magnetic actuators in practice. The spacecraft should be magnetically clean also for satisfying high pointing precision with the magnetorquers.

Table 1.1: Typical magnetometer, MEMS gyro and magnetorquer examples for nanosatellite applications.

			
	Honeywell HMC 1001 Magnetometer ¹	Silicon Sensing Systems MEMS Gyro CRH01 ²	Magnetorquer ³
Mass	0.14gr	30gr	15gr
Size	1.7mm × 11.2mm × 7.3mm	35mm × 35mm × 25mm	∅6mm × 45mm
Power	50mW	< 250mW	23mW

The main motivation of this study is to provide an accurate attitude determination method for the case that nanosatellite has magnetometers and gyros as the attitude sensors, and magnetorquers as the actuators. The aimed attitude determination and control accuracies are 0.1 and 1 deg, respectively. This is challenging because the attitude determination accuracy that can be satisfied by the regular algorithms for a nanosatellite carrying magnetometers and gyros is usually around 1deg (Vinther *et al.* 2011). Moreover although the angular rates can be controlled accurately by pure magnetic control approach the accuracy for the attitude itself cannot be reduced below few degrees and usually the yaw angle estimation is worse than the others (Wisniewski 2012). Mainly there are two reasons for such poor ADCS accuracy when the magnetometer, gyros and magnetorquers are used:

- Inherent complexity of the problem: Magnetometers are not accurate sensors due to the factors such as the disturbance fields caused by the spacecraft electronics, modeling errors in the Earth's geomagnetic field and the external disturbances like ionospheric currents. For increasing attitude determination performance an accurate in-flight calibration of the magnetometers is necessary (Bak 1999). Moreover attitude control by using only magnetorquers is significantly challenging since at any instant the satellite is controllable in two-axes that are perpendicular to the magnetic field vector (Wisniewski 1996). For three axis controllability the spacecraft must experience the variation of the magnetic field along the orbit.

¹ Source: Datasheet for Honeywell HMC1001/1002 and HMC1021/1022;

<http://www.alldatasheet.com/datasheet-pdf/pdf/167569/HONEYWELL/HMC1021.html>.

² Source: Website of Silicon Sensing Systems Japan; <http://www.sssj.co.jp/en/products/gyro/crh01.html>.

³ Source: Candini *et al.* 2012.

- The size of the spacecraft: Because of the spacecraft's compactness, the interaction between the subsystems is higher than the larger spacecrafts and that affects the magnetic cleanliness of the satellite which is a necessity for accurate attitude estimation and control with magnetic sensors and actuators. Besides the attitude hardware is more vulnerable against external disturbances because of the same reason. As for the control accuracy any disturbance source will make achieving higher accuracy more challenging so a magnetically clean satellite is a preliminary necessity.

Therefore for an accurate ADCS by using magnetometers, gyros and magnetorquers these issues should be analyzed carefully and appropriate solution techniques should be given. This thesis contributes to the literature within this context. Different than the existing studies we address the problems such as in-orbit estimation of magnetometer biases and residual magnetic moment and try to increase the system accuracy by using more powerful estimation algorithms, which are proposed by the authors. First of all each problem is addressed individually and possible solution methods, which are mostly based on the adaptation of the attitude estimator algorithms, are given. Then these solution techniques are integrated in order to propose an overall attitude determination scheme for the satellite. The theory is supported by the demonstrations and performance analysis for the proposed attitude determination method. Details for the contribution are given in Section 1.3 after reviewing the current literature in Section 1.2.

1.2. Literature Survey

The attitude determination and control for nanosatellites is a widely discussed topic in the literature. In general scope, the solutions that have been proposed in order to increase the ADCS system efficiency might be considered in two categories. The first category includes the design solutions that cover the selection of the appropriate sensors, forming the layout of the subsystems in an optimal way (Han *et al.* 2012) and designing a completely new sensor or actuator (Candini *et al.* 2012). On the other hand, the algorithmic solutions which investigate the possible algorithm based techniques to solve a specific problem (Reijneveld and Choukroun 2012; Pong *et al.* 2012; Vinther *et al.* 2011) fall in the second category. The solutions in the latter category mainly aim at proposing a new method for nanosatellite implementations such that the system performance can be increased even using the existing hardware and usually they focus on a specific problem such as onboard sensor calibration, robustness of the ADCS algorithm against the external/internal disturbances etc. The studies presented in this thesis may be regarded as a part of this second category.

In this thesis the main aim is to increase the ADCS performance of a nanosatellite that carries magnetometer, gyros and magnetorquers onboard as the attitude hardware. As aforementioned this aim is accomplished by solving several interconnected practical problems.

In a broad perspective the attitude determination problems are related to magnetic disturbance compensation which is needed in order to guarantee the magnetic cleanliness of the spacecraft. Our first problem is finding an accurate estimation algorithm for the in-orbit and real time estimation of the magnetometer biases and that is an obligation as aforementioned. This is a recent topic for nanosatellite applications and since the magnetometers are popular sensors for this type of satellites there are many documented studies especially on magnetometer calibration. In (Inamori *et al.* 2009) the magnetometer biases are estimated as a part of the magnetic disturbance compensation for a nanosatellite. The Unscented Kalman Filter (UKF) is used as the estimator algorithm. Han *et al.* (2012) proposes both pre-launch on ground and post-launch in-orbit magnetometer calibration schemes for Chinese ZDPS-1A nanosatellite. In (Soken and Hajiyevev 2012) along with the magnetometer biases the scale factors are also considered and a UKF based reconfigurable attitude estimation and magnetometer calibration method is presented. Lastly Vinther *et al.* (2011) investigates the effects of magnetometer and gyro calibration on the attitude accuracy and gives a simultaneous estimation algorithm using the full-order UKF.

The biggest difficulty that arises in case of in-orbit real time sensor bias estimation is tuning the estimator. This provides a basis for the second problem which is the determination of the process noise covariance for the UKF when the sensor biases or scale factors are included in the state vector. For the case where the UKF is used for estimating only the attitude and gyro biases as a reduced-order filter the process noise covariance matrix can be approximated analytically (Crassidis and Markley 2003) likewise the general case (Farrenkopf 1978; Fosbury 2011). But this method fails if the magnetometer biases are also estimated as a part of the state vector. One possible solution technique is to use an adaptive algorithm to tune the UKF as discussed in this thesis. The adaptation of the UKF is also a necessity for building a filter which is robust against any kind of sensor malfunctions. Since the spacecraft is vulnerable against external disturbances there is a high risk for the magnetometer measurements to be affected and give faulty outputs for a period of time. Unless the filter is built robust against that kind of malfunctions, they will deteriorate the estimation performance significantly. That will be the third problem examined in this study.

In literature there are several methods to adapt the linear Kalman filter (KF). Unquestionably, the pioneering methods in this area have been proposed by Mehra (Mehra

1970; Mehra 1972). Specifically the covariance matching technique discussed in (Mehra 1972) may be considered as the fundamental of the algorithms proposed in this thesis. The main drawback of these studies, and as well their successors that examine the adaptation of the KF (Geng and Wang 2008; Kim *et al.* 2006; Odelson *et al.* 2006; Dunik *et al.* 2009), they are generally appropriate for discrete-time linear systems and cannot be used as a method for the adaptation of the UKF without any correction or modification.

In this sense, researches on the Adaptive Unscented Kalman Filter (AUKF), which can be used for nonlinear systems, should be examined. In (Han *et al.* 2009), two distinct methods are described as the AUKF algorithms. In the first method, the MIT rule is used to derive the adaptive law and a cost function is defined in order to minimize the difference between the filter computed covariance and the actual innovation covariance. The algorithm is used for the Q-adaptation (process noise covariance adaptation), which is required for tuning the filter against uncertainties. It is stated that a similar approach may be pursued for the R-adaptation (measurement noise covariance adaptation), which is necessary for building a filter robust against sensor malfunctions. As a deficiency, the presented algorithm requires calculation of the partial derivatives and that introduces a relatively large computational burden as it is also stated by the authors themselves. In the second method, two UKFs are run in parallel as master and slave filters. Its computational demand is lower than the first method but as it is known (Vinther *et al.* 2011), despite being free of the Jacobian calculations, the computational burden of the UKF is not very low because of the sigma point calculations. Therefore, using two UKF algorithms in a parallel manner still increases the required computation burden significantly. Hence the main problem for both of the methods presented in (Han *et al.* 2009) is high computational load. Nonetheless in (Liu and Lu 2009; Shi *et al.* 2009) Saga-Husa noise statistics estimator is integrated with the UKF in order to build an AUKF. Although it may give satisfactory results for the target tracking problem, this method has an instability issue; when the noise covariance loses its semi-positive definiteness, the filter diverges.

In (Cao and Tian 2009) an adaptive UKF algorithm is proposed to improve the estimation of error covariance matrices. By introducing measurement innovation into the estimation of error covariance matrices, the proposed algorithm can compute the Kalman gain adaptively and make the innovation series of the future measurement uncorrelated. However, the presented AUKF algorithm is valid, if only the model of dynamics is nonlinear, but the model of measurements is linear. In (Song and He 2009) a slave UKF is proposed to estimate the covariance of system noise online. An AUKF is developed and applied to nonlinear joint estimation of both time-varying states and modeling errors for helicopter. The filter is composed of parallel master and slave UKFs. While the master UKF estimates the states or parameters, the slave filter estimates the diagonal elements of the noise

covariance matrix for the master UKF. Such a mechanism improves the adaptive ability of the UKF and enlarges its application scope but as the second method given in (Han et al. 2009) it is complex and requires high computational load.

The UKF may be also built adaptively by using fuzzy logic based techniques. In (Jwo and Tseng 2009) Fuzzy Logic Adaptive System (FLAS) aids the interacting multiple models and by switching between filters suitable value for the process noise covariance can be determined. As a disadvantage such method also requires more than one filter running simultaneously. In (Jwo and Chung 2010) a sensor fusion method based on the combination of adaptive UKF and fuzzy logic adaptive system for the ultra-tightly coupled GPS/INS integrated navigation is presented. Through the use of fuzzy logic, the FLAS has been incorporated into the AUKF as a mechanism for timely detecting the dynamical changes and implementing the on-line tuning of the factors in the weighted covariance matrices by monitoring the innovation information so as to maintain good estimation accuracy and tracking capability. Although it is possible to get satisfactory results for some specific cases, the essences of these kinds of fuzzy methods are human experience and heuristic information; in out of experience cases they may not work.

Another practical problem, which should be solved by the UKF adaptation, is the Residual Magnetic Moment (RMM) estimation for nanosatellites and this is the fourth issue discussed in this thesis.

Generally, the RMM is the main attitude disturbance source for the low earth orbit (LEO) nanosatellites (Sakai *et al.* 2006b). Other disturbances such as the gravity gradient, sun pressure, aerodynamic drag have relatively less effect because of the small size of the satellite and can be minimized during the design process (Inamori *et al.* 2009). However, the magnetic disturbance is mainly caused by the onboard electric current loop, small permanent magnet in some devices or some special material on the satellite, and does not strongly depend on the satellite size (Sakai *et al.* 2008). Hence, the RMM must be compensated in-orbit with an active control strategy.

The effects of the RMM on the attitude determination and control accuracy for small satellites and the necessity for its compensation are well discussed in (Sakai *et al.* 2008; Inamori *et al.* 2009; Steyn and Hashida 2001; Suehiro 2010; Hosonuma *et al.* 2012). The orthodox way to cancel out the disturbance caused by the RMM is to use a feedback controller but the efficiency of the method depends on several conditions such as the sensor noise, computational performance or plant model accuracy (Sakai *et al.* 2008). Another method is to use a feedforward cancellation technique and when this technique is used the performance depends on the accuracy of the RMM estimation.

In (Sakai *et al.* 2006b; Sakai *et al.* 2008), an observer is proposed to estimate the RMM whereas in (Steyn and Hashida 2001; Hosonuma *et al.* 2012) the RMM is estimated using the Extended Kalman Filter (EKF). In (Inamori *et al.* 2009), as well as the EKF, an UKF is designed for the RMM estimation and the estimation accuracies of these two different KFs are compared. In these studies, the RMM components are considered to be constant in time. However, in practice, these parameters may change with sudden shifts because of the instantaneous variations in the onboard electrical current. Such instantaneous variations in the current may be caused by switching on/off of the onboard electronic devices or going into/out of eclipse. In such cases, the KF cannot catch the new value of the parameter quickly if it is designed with a small process noise covariance in order to increase steady state estimation accuracy. The main issue is, especially if we use the feedforward cancellation technique for the RMM compensation, then, as discussed, the estimation accuracy is essential and so the KF must be designed with small process noise covariance. In other words, the inherent tracking capacity of the KF that can be provided by choosing a high process noise covariance must be sacrificed in order to increase the overall system performance. Therefore, if we want to design a KF with good tracking capability, as well as the high steady state accuracy, then the filter should be adaptively designed such that it gives both good estimation results when there is no change in the parameter and good tracking performance when the parameter is changed.

Change detection and the KF adaptation in case of abrupt changes in the estimated parameters is a common issue in many fields from automotive to computer systems (Gustafsson 2000; Hartikainen and Ekelin 2006) and there are several documented methods investigating this topic. In general, these methods may be categorized in two: the methods that use one KF and detect the change by applying a whiteness test on the innovation vector of the filter and methods that use a bank of filters with different statistical information for changes with different characteristics (such as shifts with different magnitudes) (Gustafsson 2000). An example for the latter method is the use of two different KFs where one of them is designed with low process noise covariance for steady state accuracy and the other one is with a high process noise covariance for agility in case of change. In general the multiple model based approach with several KFs running parallel gives better results compared to the single filter based adaptive recursive estimation algorithms. However in return for the increasing accuracy, the algorithm becomes more complex and so the computational load increases as well. Besides, as a prerequisite for designing the filters the characteristics of the changes (e.g. the magnitude of different shifts) must be known (Hartikainen and Ekelin 2006).

A simple technique for change detection is to apply a whiteness test on the innovation vector of the KF in order to check whether a change in the system occurred. A well known

test is the Cumulative Sum (CUSUM) test in which the filter innovations are transformed into distance measures with different characteristics corresponding to the desired design properties and the test built upon these distance measures (Gustafsson 2000; Page 1954; Basseville and Nikiforov 1993). The next step after the change detection is to perform a correction (or adaptation) on the filter statistics in order to adapt the filter to the changing conditions and get better tracking capability. The easiest and most straightforward method is to restart the filter (Gustafsson 1996) after each change detection which basically increases the estimation covariance to get better tracking. Another way of adaptation is to increase the estimation covariance of the related state for one time step or a period of time by multiplying with a factor (Stenlund and Gustafsson 2002). Nonetheless, it is also possible to perform similar adaptation by multiplying the process noise covariance matrix with the scale factor instead of the estimation covariance of the KF (Gustafsson 2000; Gustafsson 1996). The main disadvantage of all these adaptation techniques is being heuristic; the adaptation is based on the designer's experiences. As in the first adaptation method, if the filter is restarted after each change detection then the magnitude of the change does not have any significance on the performed adaptation and after some certain changes the KF may give a bad transient behavior (Gustafsson 1996). On the other hand, when the estimation covariance or the process noise covariance matrix is multiplied with a scale factor after the change is detected, the scale factor must be selected carefully such that it represents the required response of the filter for all possible changes. However, as it is extensively discussed in (Hartikainen and Ekelin 2006) such selection is not possible and the KF response is very sensitive to the value of the scale factor. Besides, if the scale factor is applied for a period instead of just one time step (periodic correction instead of momentarily correction) then determination of the adaptation period appears as another problem. Therefore, the main drawback of the existing single KF based change detection and adaptation algorithms is the necessity to know the characteristics of the change (e.g. the magnitude of the shift) a priori in order to obtain a precise scale factor for correction and achieve successful adaptation as a result; none of them may perform well under circumstances other than they are designed for.

1.3. Contribution of the Thesis

In general this thesis proposes a simple yet accurate attitude determination method for increasing the ADCS performance of nanosatellites with magnetic sensors and actuators. In order to achieve that first we increase the accuracy of the magnetometer outputs by proposing an appropriate in-orbit calibration algorithm. The tuning problem for the filter that is used for calibration as well as the attitude estimation is overrun by the adaptive Kalman filtering approach. The same filter is made robust against faults in the

measurements. That is a necessity in the severe space environment especially for nanosatellites which are highly vulnerable against the internal and external disturbances. As the next step, the RMM is estimated to cancel out the effects of the magnetic disturbance and assure the magnetic cleanliness of the satellite for the attitude control purpose. The instantaneous changes in the RMM are regarded and the estimator UKF is adapted as it gives accurate estimations at any case. In the final section, which may be regarded as the core of this study, the given UKF adaptation techniques are integrated and an overall attitude determination scheme is introduced. The scheme is demonstrated for the attitude determination of the nanosatellite and its performance is analyzed by comparisons with the existing algorithms. Moreover, in the appendix a brief discussion about possible novel methodologies for pure magnetic attitude controller, which can work independently from the orbital periodicity of the geomagnetic field, is given.

The main contributions of this thesis can be listed as:

- In Section 4.3 a magnetometer and gyro bias estimation algorithm is presented. The UKF, a rather novel Kalman filter, which does not have so many implementation examples for the bias estimation in literature, is used as a part of the estimation system. Differently from the existing studies both magnetometer and gyro biases are estimated simultaneously as well as the attitude parameters by using a gyro-based model. The results were presented in (Soken and Sakai 2011).
- A novel adaptive scaling method for the process noise covariance of the UKF is given in Section 5.1.1. The adaptation is performed using a single adaptive factor calculated in the base of the residual sequence and the process noise covariance matrix tuned dynamically via multiplication with this factor. It is demonstrated that the given AUKF algorithm provides more accurate attitude estimation results than the regular UKF. The results were presented in (Soken and Sakai 2012a).
- In Section 5.1.2 an adaptive method for tuning the process noise covariance matrix of the UKF is proposed for the general case. This filter algorithm is also called as the AUKF. The method is based on Maybeck's maximum likelihood estimator (Maybeck 1982), which has been already investigated for several different problems. Firstly it is shown that the adaptation method can be generalized for the nonlinear systems so it holds true for a nonlinear problem where the UKF is used as the attitude estimator. Then the method is tested in various scenarios for the attitude and sensor bias estimation and the results are compared with the filter where analytically approximated process noise covariance matrix (Farrenkopf 1978) is used. The

results were presented in (Soken and Sakai 2012b) and published in (Soken and Sakai 2012c).

- A Robust Unscented Kalman Filter (RUKF) algorithm is proposed for the case of magnetometer faults in Section 5.2. With simulations it is demonstrated that the regular UKF fails about giving accurate attitude estimation results if the magnetometer output is faulty whereas the RUKF ensures estimation accuracy for any case. The applied adaptation scheme is similar to the one given in (Soken and Hajiyev 2010). However, in this study the attitude estimation problem is generalized and instead of the Euler angles the quaternions are used as the attitude representation method. Besides, the robust Kalman filters are examined for different measurement system failure cases. The results for the adaptation using single scale factor were published as a part of (Soken *et al.* 2013a).
- In Section 5.2.2 the UKF is built robust against measurement malfunctions using multiple scale factors. The key findings for the adaptation with multiple scale factors were presented in (Soken *et al.* 2012a) and published in (Soken *et al.* 2012b). Comparison of the single and multiple scale factor based adaptation schemes was given in (Soken *et al.* 2013a).
- An in-orbit RMM estimation method for small satellite applications is discussed in Chapter 6. Unlike the existing studies in the literature, the unexpected abrupt changes in the RMM are also considered. The adaptation method that tunes the covariance of the UKF regarding the magnitude of the change is a novel approach. The specific results for the UKF were presented in (Soken and Sakai 2013). The version generalized for all KF applications was published in (Soken *et al.* 2013b).
- In Chapter 7, the proposed UKF algorithms are integrated to build an overall attitude estimation scheme for the nanosatellite. The given integration method and so the overall scheme is tested via demonstrations and its performance is comprehensively analyzed by comparisons with the exiting methods. The proposed scheme is a new one that can be used for estimating all the necessary parameters for attitude determination and control of a nanosatellite with magnetic sensors and actuators.

1.4. Thesis Overview

The thesis aims at proposing an attitude determination method for increasing the ADCS performance of nanosatellites with magnetic sensors and actuators. The first two chapters constitute the preliminary basis for the next chapters by introducing the motion model for the satellite and the models for the attitude sensors. The rest of the study may be divided into two: the first part which examines several practical problems for the attitude determination and control of the nanosatellite and the second part which presents the overall attitude determination algorithm. The details are given below chapter by chapter:

- **Chapter 2: Satellite Mathematical Model**

This chapter first gives the definition of the coordinate systems used throughout the thesis. After a brief description for the quaternions for attitude parameterization, the mathematical model for the satellite's motion is presented.

- **Chapter 3: Sensor Model**

This chapter presents the models of the sensors that are used for getting attitude information. The Earth magnetic field model is presented as a part of the discussions for the magnetometer model. The magnetometer and gyro models are given for the common case that we regard the sensor biases.

- **Chapter 4: Sensor Bias Estimation**

In this chapter an UKF based magnetometer and gyro bias estimation algorithm is presented as a part of the attitude determination procedure for a nanosatellite, which has three magnetometers and three gyros as measurement sensors. Differently from the existing studies both the magnetometer and gyro biases are estimated as well as the attitude parameters. As a basis for building the bias estimation algorithm, first the UKF and its implementation method for attitude estimation are given. A comparison for the dynamics-based and gyro-based estimation models is also included. The effects of magnetometer bias estimation on the attitude determination accuracy are discussed.

- **Chapter 5: Adaptation Methods for the UKF**

This chapter presents the adaptation methods for a UKF used for nanosatellite attitude estimation. Mainly two different problems met in practice are examined. In the first part, an adaptive method for tuning the process noise covariance matrix of the UKF is given and the AUKF algorithm is tested in various scenarios for the

attitude and sensor bias estimation. Both scaling and estimation techniques for the process noise covariance adaptation are discussed. In the second part, a Robust Kalman Filtering method against the measurement faults is proposed. The adaptation is performed following both single and multiple scale factor based schemes and the results are applied for the UKF in order to build a RUKF. The RUKF is tested for the attitude estimation of the nanosatellite and the results are compared with the regular UKF for various measurement faults.

- **Chapter 6: The Residual Magnetic Moment Estimation**

In this chapter a method for in-orbit estimation of time-varying RMM is presented. First the deteriorating effects of the sudden RMM changes on the estimation accuracy are examined. Then a new method for change detection and Kalman Filter adaptation is presented. By using this simple approach, the covariance of the Kalman filter is adapted to get better tracking in case of unexpected abrupt changes in the RMM without sacrificing the estimation accuracy. The results are applied for the nanosatellite attitude estimation problem.

- **Chapter 7: Demonstration of the Proposed Attitude Determination Scheme**

In this chapter, first a possible integration scheme for the estimation algorithms, which were discussed in the previous chapters, is proposed. As a consequence, an overall attitude determination algorithm for a nanosatellite carrying magnetometers, gyros and magnetorquers as the attitude hardware is given. Then this scheme is tested by demonstrations for the ADCS of the nanosatellite. The results are evaluated regarding the main aim of the thesis and analyzed via comparisons with the existing methods.

- **Chapter 8: Conclusion and Recommendations**

In this chapter the concluding remarks and recommendations for the future work are given.

2. Satellite Mathematical Model

2.1. Coordinate Systems

The coordinate systems used in this thesis are the satellite body frame, which matches with the principal axes of inertia of the satellite, orbit reference frame and inertial reference frame which is Earth centered. The definitions of these coordinate systems are given below.

Earth Centered Inertial Frame: The origin of the frame is located at the centre of the Earth. The z axis shows the geographic North Pole while the x axis is directed toward the Vernal Equinox (γ - the point where the Sun crosses the celestial Equator in March on its way from south to north). The y axis completes the coordinate system as the cross product of z and x axes (Fig. 2.1a).

Orbit Reference Frame: The origin of the frame is at the mass centre of the spacecraft. The z axis is in nadir direction (towards the centre of the Earth) and the y axis is tangential to the orbit (aligns with velocity vector of the spacecraft in case of circular orbit). The x axis completes to the orthogonal right hand system (Fig. 2.1b).

Satellite Body Frame: The origin of the frame is located at the centre of mass of the satellite. The axes are directed towards the principal inertial axes of the spacecraft. Three parameters named as Euler angles set the condition of the body frame related to the orbital coordinate system. When the direction cosine matrix is identity matrix the satellite body frame matches with the orbital frame (Fig. 2.1c).

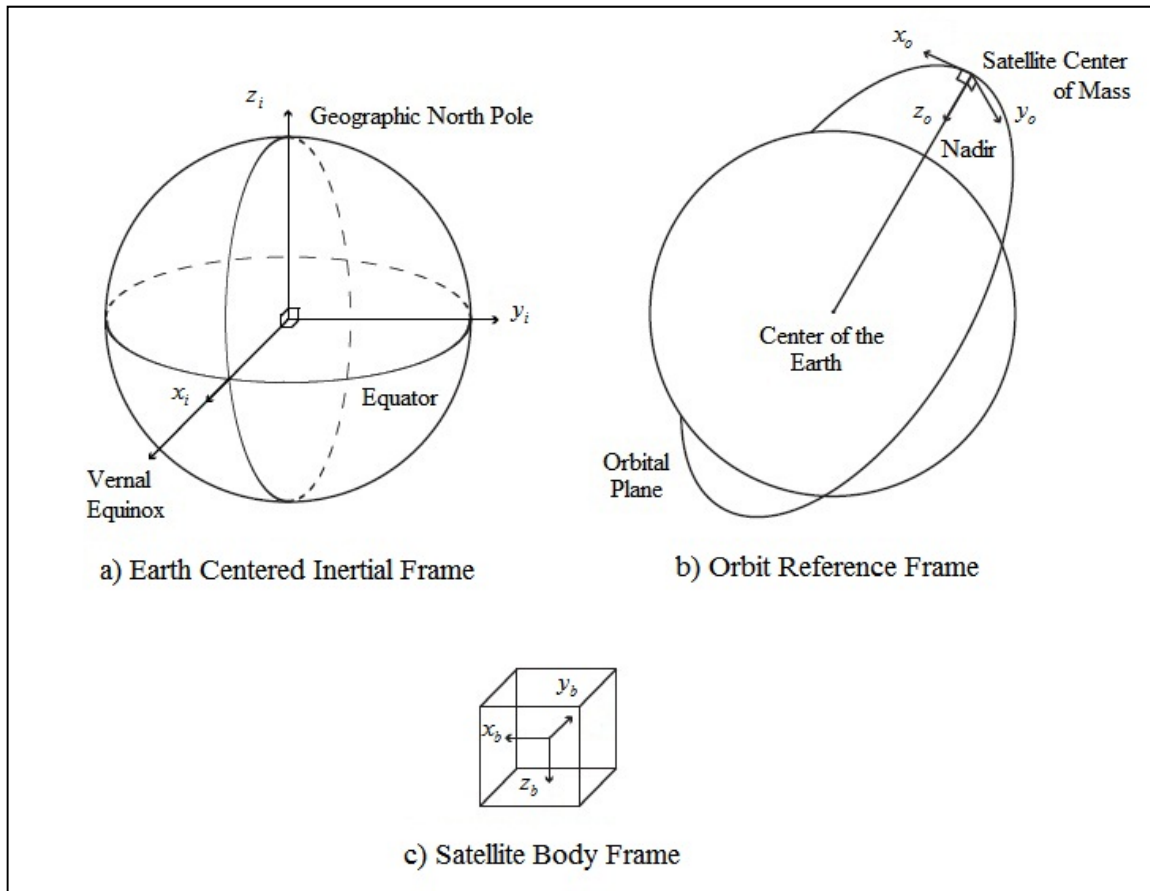


Figure 2.1: Coordinate systems.

2.2. Quaternions for Attitude Representation

The quaternion attitude representation is a technique based on the idea that a transformation from one coordinate frame to another may be performed by a single rotation about a vector e defined with respect to the reference frame. The quaternion, denoted here by the symbol q , is a four element vector, the elements of which are functions of the vector e and magnitude of the rotation, Φ :

$$q_1 = e_1 \sin \frac{\Phi}{2} \quad (2.1)$$

$$q_2 = e_2 \sin \frac{\Phi}{2} \quad (2.2)$$

$$q_3 = e_3 \sin \frac{\Phi}{2} \quad (2.3)$$

$$q_4 = \cos \frac{\Phi}{2} \quad (2.4)$$

Here e_1, e_2, e_3 are the components of the vector e . The vector which shall be transformed is rotated around e with an angle of Φ . As a result, by the use of quaternions a transfer from reference frame to body frame can be denoted by a single rotation around a vector defined in the reference frame.

A quaternion with components q_1, q_2, q_3 and q_4 may also be expressed as a four parameter complex number with a real component q_4 and three imaginary components, q_1, q_2 and q_3 as follows:

$$\mathbf{q} = q_4 + iq_1 + jq_2 + kq_3, \quad (2.5)$$

where i, j, k are hyper-imaginary numbers with the characteristics of;

$$i^2 = j^2 = k^2 = -1 \quad (2.6)$$

$$ij = -ji = k \quad (2.7)$$

$$jk = -kj = i \quad (2.8)$$

$$ki = -ik = j \quad (2.9)$$

Also, the redundancy of the quaternions must be noted as;

$$q_1^2 + q_2^2 + q_3^2 + q_4^2 = 1 \quad (2.10)$$

2.2.1. Vector Transformation by Quaternions

A vector quantity defined in the body axes, \mathbf{r}_B may be expressed in the reference axes as \mathbf{r}_R using the quaternions directly. First define a quaternion, \mathbf{r}_B^q , in which the complex components are set equal to the components of \mathbf{r}_B , and with a zero scalar component, that is, if:

$$\mathbf{r}_B = ix + jy + kz \quad (2.11)$$

$$\mathbf{r}_B^q = 0 + ix + jy + kz \quad (2.12)$$

This is expressed in the reference axes as \mathbf{r}_R^q using:

$$\mathbf{r}_R^q = \mathbf{q} \mathbf{r}_B^q \mathbf{q}^* \quad (2.13)$$

where $\mathbf{q}^* = (q_4 - iq_1 - jq_2 - kq_3)$ is the complex conjugate of \mathbf{q} .

Hence,

$$\begin{aligned}
\mathbf{r}_R^q &= (q_4 + iq_1 + jq_2 + kq_3)(0 + ix + jy + kz)(q_4 - iq_1 - jq_2 - kq_3) \\
&= 0 + \left\{ (q_4^2 + q_1^2 - q_2^2 - q_3^2)x + 2(q_1q_2 - q_4q_3)y + 2(q_1q_3 + q_4q_2)z \right\} i \\
&\quad + \left\{ 2(q_1q_2 + q_4q_3)x + (q_4^2 - q_1^2 + q_2^2 - q_3^2)y + 2(q_2q_3 - q_4q_1)z \right\} j \\
&\quad + \left\{ 2(q_1q_3 - q_4q_2)x + 2(q_2q_3 + q_4q_1)y + (q_4^2 - q_1^2 + q_2^2 - q_3^2)z \right\} k
\end{aligned} \tag{2.14}$$

Alternatively, \mathbf{r}_R^q may be expressed in matrix form as follows:

$$\mathbf{r}_R^q = A' \mathbf{r}_B^q, \tag{2.15}$$

where $A' = \begin{bmatrix} 0 & 0 \\ 0 & A \end{bmatrix}$, $\mathbf{r}_R^q = \begin{bmatrix} 0 & \mathbf{r}_B \end{bmatrix}$ and

$$A = \begin{bmatrix} q_1^2 - q_2^2 - q_3^2 + q_4^2 & 2(q_1q_2 + q_3q_4) & 2(q_1q_3 - q_2q_4) \\ 2(q_1q_2 - q_3q_4) & -q_1^2 + q_2^2 - q_3^2 + q_4^2 & 2(q_2q_3 + q_1q_4) \\ 2(q_1q_3 + q_2q_4) & 2(q_2q_3 - q_1q_4) & -q_1^2 - q_2^2 + q_3^2 + q_4^2 \end{bmatrix}. \tag{2.16}$$

which is equivalent to writing:

$$\mathbf{r}_R = A \mathbf{r}_B. \tag{2.17}$$

Here A is the same direction cosine matrix that is used for transformation from body to reference frame.

2.2.2. Propagation of Quaternions by Time

While defining the kinematic equations of motion with quaternions, time dependence of them must be used and that can be derived from the product relation (Wertz 1988).

Multiplication of quaternion is performed in a way not too different from complex number multiplications. However the order of the process is important. By using the characteristic of hyper-imaginary numbers;

$$\mathbf{q}'' = \mathbf{q}\mathbf{q}' = (q_4 + iq_1 + jq_2 + kq_3)(q_4' + iq_1' + jq_2' + kq_3'), \tag{2.18}$$

$$\begin{aligned}
\mathbf{q}'' &= (-q_1q_1' - q_2q_2' - q_3q_3' + q_4q_4')i(q_1q_4' + q_2q_3' - q_3q_2' + q_4q_1') + \\
&\quad j(-q_1q_3' + q_2q_4' + q_3q_1' + q_4q_2') + k(q_1q_2' - q_2q_1' + q_3q_4' + q_4q_3').
\end{aligned} \tag{2.19}$$

If it is written in matrix form,

$$\begin{bmatrix} q_1'' \\ q_2'' \\ q_3'' \\ q_4'' \end{bmatrix} = \begin{bmatrix} q_4' & q_3' & -q_2' & q_1' \\ -q_3' & q_4' & q_1' & q_2' \\ q_2' & -q_1' & q_4' & q_3' \\ -q_1' & -q_2' & -q_3' & q_4' \end{bmatrix} \begin{bmatrix} q_1 \\ q_2 \\ q_3 \\ q_4 \end{bmatrix}. \quad (2.20)$$

Now assume that, \mathbf{q} and \mathbf{q}'' correspond to the orientation of the body at t and $t + \Delta t$, respectively. Also \mathbf{q}' is for the representation of position at $t + \Delta t$ in a relative way to the position that has been occupied at t ,

$$q_1' \equiv e_1 \sin \frac{\Delta\Phi}{2}, \quad (2.21)$$

$$q_2' \equiv e_2 \sin \frac{\Delta\Phi}{2}, \quad (2.22)$$

$$q_3' \equiv e_3 \sin \frac{\Delta\Phi}{2}, \quad (2.23)$$

$$q_4' \equiv \cos \frac{\Delta\Phi}{2}. \quad (2.24)$$

When the necessary multiplication is done it is obvious that

$$\mathbf{q}(t + \Delta t) \approx \left\{ \cos \frac{\Delta\Phi}{2} I + \sin \frac{\Delta\Phi}{2} \begin{bmatrix} 0 & e_3 & -e_2 & e_1 \\ -e_3 & 0 & e_1 & e_2 \\ e_2 & -e_1 & 0 & e_3 \\ -e_1 & -e_2 & -e_3 & 0 \end{bmatrix} \right\} \mathbf{q}(t). \quad (2.25)$$

where e_1, e_2, e_3 are the components of rotation axis unit vector and I is the 4×4 identity matrix. After that by small angle approximation,

$$\cos \frac{\Delta\Phi}{2} \approx 1, \quad (2.26)$$

$$\sin \frac{\Delta\Phi}{2} \approx \frac{1}{2} \bar{\omega}_{BR} \Delta t. \quad (2.27)$$

It is possible to show that

$$\mathbf{q}(t + \Delta t) \approx \left\{ I + \frac{1}{2} \begin{bmatrix} 0 & r & -q & p \\ -r & 0 & p & q \\ q & -p & 0 & r \\ -p & -q & -r & 0 \end{bmatrix} \Delta t \right\} \mathbf{q}(t). \quad (2.28)$$

here p, q, r are components of $\boldsymbol{\omega}_{BR}$ and they indicate angular velocity of the rigid body with respect to the reference frame. Hence if a skew-symmetric matrix is defined as

$$\Omega(\boldsymbol{\omega}_{BR}) = \begin{bmatrix} 0 & r & -q & p \\ -r & 0 & p & q \\ q & -p & 0 & r \\ -p & -q & -r & 0 \end{bmatrix}. \quad (2.29)$$

equation becomes

$$\mathbf{q}(t + \Delta t) \approx \left\{ I + \frac{1}{2} \Omega \Delta t \right\} \mathbf{q}(t). \quad (2.30)$$

Finally it is known that

$$\frac{d\mathbf{q}(t)}{dt} \cong \frac{\mathbf{q}(t + \Delta t) - \mathbf{q}(t)}{\Delta t} = \frac{1}{2} \Omega(\boldsymbol{\omega}_{BR}) \mathbf{q}(t). \quad (2.31)$$

2.2.3. Euler Angles – Quaternions Relationship

In order to understand the physical meaning of the quaternions more easily they can be related with the Euler angles. The formula for obtaining quaternion vector by the use of the Euler angles is given as,

$$\begin{bmatrix} q_1 \\ q_2 \\ q_3 \\ q_4 \end{bmatrix} = \begin{bmatrix} \sin\left(\frac{\varphi}{2}\right) \cos\left(\frac{\theta}{2}\right) \cos\left(\frac{\psi}{2}\right) - \cos\left(\frac{\varphi}{2}\right) \sin\left(\frac{\theta}{2}\right) \sin\left(\frac{\psi}{2}\right) \\ \cos\left(\frac{\varphi}{2}\right) \sin\left(\frac{\theta}{2}\right) \cos\left(\frac{\psi}{2}\right) + \sin\left(\frac{\varphi}{2}\right) \cos\left(\frac{\theta}{2}\right) \sin\left(\frac{\psi}{2}\right) \\ \cos\left(\frac{\varphi}{2}\right) \cos\left(\frac{\theta}{2}\right) \sin\left(\frac{\psi}{2}\right) - \sin\left(\frac{\varphi}{2}\right) \sin\left(\frac{\theta}{2}\right) \cos\left(\frac{\psi}{2}\right) \\ \cos\left(\frac{\varphi}{2}\right) \cos\left(\frac{\theta}{2}\right) \cos\left(\frac{\psi}{2}\right) + \sin\left(\frac{\varphi}{2}\right) \sin\left(\frac{\theta}{2}\right) \sin\left(\frac{\psi}{2}\right) \end{bmatrix}. \quad (2.32)$$

Here φ is the roll angle about x axis, θ is the pitch angle about y axis and ψ is the yaw angle about z axis. Note that the Euler angles that we get as a result are for 3-2-1 sequence (Wertz 1988).

On the other hand, the equations for finding the Euler angles using the quaternions are

$$\varphi = \text{atan } 2 \left[2(q_4 q_1 + q_2 q_3), 1 - 2(q_1^2 + q_2^2) \right], \quad (2.33)$$

$$\theta = \arcsin \left[2(q_4 q_2 - q_3 q_1) \right], \quad (2.34)$$

$$\psi = \text{atan } 2 \left[2(q_4 q_3 + q_1 q_2), 1 - 2(q_2^2 + q_3^2) \right], \quad (2.35)$$

where $\arcsin(\cdot)$ is the arcsine function and $\text{atan } 2(\cdot)$ is the arctangent function with two arguments, which is used to generate all the rotations (not just the rotations between $-\pi/2$ and $\pi/2$) and defined as,

$$\text{atan } 2(y, x) = \begin{cases} \arctan\left(\frac{y}{x}\right) & x > 0 \\ \arctan\left(\frac{y}{x}\right) + \pi & y \geq 0, x < 0 \\ \arctan\left(\frac{y}{x}\right) - \pi & y < 0, x < 0 \\ +\frac{\pi}{2} & y > 0, x = 0 \\ -\frac{\pi}{2} & y < 0, x = 0 \\ \text{undefined} & y = 0, x = 0 \end{cases}. \quad (2.36)$$

2.3. Equations of Motion

2.3.1. Satellite Dynamics

The fundamental equation of the satellite dynamics relates the time derivative of the angular momentum vector with the overall torque affecting the satellite (Wertz 1988),

$$\frac{d\mathbf{L}}{dt} = \mathbf{N} - \boldsymbol{\omega}_{BI} \times \mathbf{L} = \mathbf{J} \frac{d\boldsymbol{\omega}_{BI}}{dt}, \quad (2.37)$$

$$\mathbf{L} = \mathbf{J} \boldsymbol{\omega}_{BI} , \quad (2.38)$$

where \mathbf{L} is the angular momentum vector, \mathbf{N} is the torque vector, $\boldsymbol{\omega}_{BI}$ is the angular velocity vector of the body frame with respect to the inertial frame and \mathbf{J} is the moment of inertia matrix. When the vectors of \mathbf{L} and $\boldsymbol{\omega}_{BI}$ are parallel, as the rotation is about the principal axis of the satellite, then the moment of inertia matrix is formed of principal moments of inertia as

$$\mathbf{J} = \begin{bmatrix} J_x & 0 & 0 \\ 0 & J_y & 0 \\ 0 & 0 & J_z \end{bmatrix} . \quad (2.39)$$

Note that, this condition is an obligation for the rotation without nutation (Wertz 1988).

By the use of (2.37) and (2.38), the dynamic equation of the satellite can be derived:

$$\frac{d\boldsymbol{\omega}_{BI}}{dt} = \mathbf{J}^{-1} \left[\mathbf{N} - \boldsymbol{\omega}_{BI} \times (\mathbf{J} \boldsymbol{\omega}_{BI}) \right] . \quad (2.40)$$

The torque vector \mathbf{N} can be defined as the sum of the disturbance torques and control torque acting on the satellites as,

$$\mathbf{N} = \mathbf{N}_d + \mathbf{N}_c . \quad (2.41)$$

Here \mathbf{N}_c is the control torque and for a satellite with pure magnetic controllers

$$\mathbf{N}_c = \mathbf{M}_c \times \mathbf{B} , \quad (2.42)$$

where \mathbf{M}_c is the magnetic dipole moment of the magnetorquers and \mathbf{B} is the Earth's magnetic field vector measured in the body frame. Furthermore, concerning the equation (2.41), \mathbf{N}_d is the vector of disturbance torque affecting the satellite which can be given as a sum of

$$\mathbf{N}_d = \mathbf{N}_{gg} + \mathbf{N}_{ad} + \mathbf{N}_{sp} + \mathbf{N}_{md} . \quad (2.43)$$

Here \mathbf{N}_{gg} is the gravity gradient torque, \mathbf{N}_{ad} is the aerodynamic disturbance torque, \mathbf{N}_{sp} is the solar pressure disturbance torque and \mathbf{N}_{md} is the residual magnetic torque which is caused by the interaction of the satellite's residual dipole and the Earth's magnetic field.

As discussed in the introduction, for a LEO nanosatellite the main attitude disturbance source is \mathbf{N}_{md} . Other disturbances such as the gravity gradient, sun pressure, aerodynamic drag have relatively less effect because of the small size of the satellite and can be minimized during the design process. Hence they are negligible. On the other hand to increase the overall ADCS performance of a satellite with magnetic sensing and actuation the RMM terms must be estimated. Similarly with the magnetic control torque, \mathbf{N}_{md} is defined as,

$$\mathbf{N}_{md} = \mathbf{M}_r \times \mathbf{B}, \quad (2.44)$$

where, $\mathbf{M}_r = [M_{r_x} \quad M_{r_y} \quad M_{r_z}]^T$ is the RMM vector. In this study, the RMM terms are modeled as constant but with unexpected abrupt changes as discussed in the introduction. Assuming the RMM as piecewise constant is valid in general since the high frequency time-varying components of the RMM are negligibly small compared to the constant components and magnitude of the changes caused by instantaneous variations in the onboard electrical current (Suehiro 2010). High frequency time-variation in the RMM should be suppressed in the design process of the satellite (Hosonuma *et al.* 2012). Hence, the general model for the RMM is

$$\dot{\mathbf{M}}_r = 0; \quad (2.45)$$

with the hypothesis that

$$\mathbf{M}_r(t) = \begin{cases} \mathbf{M}_0 & t_0 \leq t < t_1 \\ \mathbf{M}_1 & t_1 \leq t < t_2 \\ \vdots & \vdots \\ \mathbf{M}_\alpha & t_\alpha \leq t < t_{orb} \end{cases}. \quad (2.46)$$

Here t_j are the unknown time instances that a change occurs within one orbit period t_{orb} , \mathbf{M}_j are constant RMM vectors and $\Delta M_j = \|\mathbf{M}_j - \mathbf{M}_{j-1}\|$ are the magnitude of the changes in the RMM that occur at t_j for $j = 1 \dots \alpha$.

2.3.2. Satellite Kinematics

Kinematics equation of motion of the satellite is based on the time derivation of the quaternions and same as (2.31),

$$\dot{\mathbf{q}}(t) = \frac{1}{2} \Omega(\boldsymbol{\omega}_{BR}(t)) \mathbf{q}(t) . \quad (2.47)$$

Here \mathbf{q} is the quaternion vector formed of four attitude parameters, $\mathbf{q} = [q_1 \quad q_2 \quad q_3 \quad q_4]^T$, and $\Omega(\boldsymbol{\omega}_{BR})$ is the skew symmetric given with (2.29).

On the other hand, in order to define the satellite kinematics using the body angular rate vector with respect to the inertial axis frame, $\boldsymbol{\omega}_{BI}$, we need to first relate $\boldsymbol{\omega}_{BI}$ and $\boldsymbol{\omega}_{BR}$. Assuming the satellite's orbit is circular,

$$\boldsymbol{\omega}_{BR} = \boldsymbol{\omega}_{BI} - A[0 \quad -\omega_0 \quad 0]^T . \quad (2.48)$$

Here ω_0 denotes the angular velocity of the orbit with respect to the inertial frame, found as $\omega_0 = (\mu / r_0^3)^{1/2}$ - μ is the the Earth Gravitational constant and r_0 is the distance between the center of mass of the Earth and satellite. A is the attitude matrix which is related to the quaternions by (2.16).

Consequently, the kinematics equation of motion of the satellite can be given using the body angular rates with respect to the inertial frame as (Sekhavat *et al.* 2007)

$$\dot{q}_1(t) = \frac{1}{2} [\omega_x(t)q_4(t) - \omega_y(t)q_3(t) + \omega_z(t)q_2(t) + \omega_0(t)q_3(t)] , \quad (2.49)$$

$$\dot{q}_2(t) = \frac{1}{2} [\omega_x(t)q_3(t) + \omega_y(t)q_4(t) - \omega_z(t)q_1(t) + \omega_0(t)q_4(t)] , \quad (2.50)$$

$$\dot{q}_3(t) = \frac{1}{2} [-\omega_x(t)q_2(t) + \omega_y(t)q_1(t) + \omega_z(t)q_4(t) - \omega_0(t)q_1(t)] , \quad (2.51)$$

$$\dot{q}_4(t) = \frac{1}{2} [-\omega_x(t)q_1(t) - \omega_y(t)q_2(t) - \omega_z(t)q_3(t) - \omega_0(t)q_2(t)] . \quad (2.52)$$

3. Sensor Models

In this chapter, measurement sensor models for the nanosatellite attitude estimation procedure are presented.

Performing measurements with magnetometers and gyros and so having the magnetic field and an inertial sensor as the attitude estimation reference source have various advantages and drawbacks. Table 3.1 summarizes these characteristics (Wertz 1988; Bak 1999):

Table 3.1: Characteristics of the attitude estimation reference sources.

Reference	Performance	Advantages	Disadvantages
Magnetic Field (Magnetometers)	Accuracy of 0.5 deg- 5 deg	-Economical. -Low power. -Always available for LEO spacecrafts.	-Poor accuracy. -Good only for near Earth satellites. -Limited by modeling accuracy. -Orbit and attitude are strongly coupled. -Spacecraft must be magnetically clean (or in flight calibration must be done). -Sensitive to biases.
Inertial Space (Gyros)	Drift rate of 0.001deg/h - 1deg/h	-No need for external sensors. -Orbit independent. -High accuracy for limited time intervals. -Easily done onboard.	-Senses only orientation rate. -No absolute measurement. -Subject to drift.

3.1. The Magnetometer Model

Magnetometer is a favorite sensor type for the attitude estimation especially in nanosatellite applications. The model for the magnetometer measurements is given by,

$$\begin{bmatrix} B_x(\mathbf{q}, t) \\ B_y(\mathbf{q}, t) \\ B_z(\mathbf{q}, t) \end{bmatrix} = A \begin{bmatrix} B_1(t) \\ B_2(t) \\ B_3(t) \end{bmatrix} + \mathbf{b}_m + \eta_1, \quad (3.1)$$

where $B_1(t)$, $B_2(t)$ and $B_3(t)$ represent the Earth magnetic field vector components in the orbit frame as a function of time and can be modeled as (Sekhavat et al. 2007),

$$B_1(t) = \frac{M_e}{r_0^3} \left\{ \cos(\omega_0 t) [\cos(\varepsilon) \sin(i) - \sin(\varepsilon) \cos(i) \cos(\omega_e t)] - \sin(\omega_0 t) \sin(\varepsilon) \sin(\omega_e t) \right\}, \quad (3.2)$$

$$B_2(t) = -\frac{M_e}{r_0^3} [\cos(\varepsilon) \cos(i) + \sin(\varepsilon) \sin(i) \cos(\omega_e t)], \quad (3.3)$$

$$B_3(t) = \frac{2M_e}{r_0^3} \left\{ \sin(\omega_0 t) [\cos(\varepsilon) \sin(i) - \sin(\varepsilon) \cos(i) \cos(\omega_e t)] + 2 \cos(\omega_0 t) \sin(\varepsilon) \sin(\omega_e t) \right\}. \quad (3.4)$$

Here, $M_e = 7.943 \times 10^{15} \text{ Wb.m}$ is the magnetic dipole moment of the Earth; $\mu = 3.98601 \times 10^{14} \text{ m}^3 / \text{s}^2$ is the Earth Gravitational constant, i is the orbit inclination, $\omega_e = 7.29 \times 10^{-5} \text{ rad} / \text{s}$ is the spin rate of the Earth; $\varepsilon = 11.7^\circ$ is the magnetic dipole tilt; and r_0 is the distance between the centre of mass of the satellite and the Earth.

Therefore, $B_x(\mathbf{q}, t)$, $B_y(\mathbf{q}, t)$ and $B_z(\mathbf{q}, t)$ show the measured Earth magnetic field vector components in body frame as a function of time and varying quaternion vector. Furthermore, \mathbf{b}_m is the magnetometer bias vector as $\mathbf{b}_m = [b_{m_x} \quad b_{m_y} \quad b_{m_z}]^T$ and modeled as piecewise constant in time,

$$\dot{\mathbf{b}}_m = \mathbf{0}. \quad (3.5)$$

Lastly, concerning the equation (3.1), η_1 is the zero mean Gaussian white noise with the characteristic of

$$E[\eta_{1k} \eta_{1j}^T] = I_{3 \times 3} \sigma_m^2 \delta_{kj}. \quad (3.6)$$

$I_{3 \times 3}$ is the identity matrix with the dimension of 3×3 , σ_m is the standard deviation of each magnetometer error and δ_{kj} is the Kronecker symbol.

3.2. The Gyro Model

Widely used model for the gyro measurements is as follows.

$$\tilde{\boldsymbol{\omega}}_{Bl} = \boldsymbol{\omega}_{Bl} + \mathbf{b}_g + \boldsymbol{\eta}_2, \quad (3.7)$$

where, $\tilde{\boldsymbol{\omega}}_{Bl}$ is the measured angular rates of the satellite, \mathbf{b}_g is the gyro bias vector as $\mathbf{b}_g = [b_{g_x} \quad b_{g_y} \quad b_{g_z}]^T$ and $\boldsymbol{\eta}_2$ is the zero mean Gaussian white noise with the characteristic of

$$E[\boldsymbol{\eta}_{2k} \boldsymbol{\eta}_{2j}^T] = I_{3 \times 3} \sigma_v^2 \delta_{kj}. \quad (3.8)$$

Here, σ_v is the standard deviation of each gyro random error. Nevertheless, characteristic of gyro bias is given as,

$$\dot{\mathbf{b}}_g = \boldsymbol{\eta}_3, \quad (3.9)$$

where $\boldsymbol{\eta}_3$ is also the zero mean Gaussian white noise with the characteristic of

$$E[\boldsymbol{\eta}_{3k} \boldsymbol{\eta}_{3j}^T] = I_{3 \times 3} \sigma_u^2 \delta_{kj}. \quad (3.10)$$

Here, σ_u is the standard deviation of gyro biases.

4. Sensor Bias Estimation

As aforementioned magnetometers are not accurate sensors because of the factors such as the disturbance fields caused by the spacecraft electronics, modeling errors in the Earth's geomagnetic field and the external disturbances such as ionospheric currents. For increasing attitude determination performance an accurate in-orbit calibration of the magnetometers is necessary as the preliminary step. This chapter investigates the UKF based magnetometer bias estimation procedure.

4.1. Unscented Kalman Filter for Attitude Estimation

Kalman filter plays an important role in the attitude estimation procedure of the spacecrafts. Regarding the obstacles met during the development process of the attitude estimation systems, various types of KFs have been developed. One of these difficulties is the inherent nonlinear dynamics and kinematics of the satellites similarly to the many real world systems. The EKF was proposed so as to overcome this problem and since then it has been used instead of the linear KF for estimating the attitude of the satellite (Markley *et al.* 2005).

Even though still being a popular method as a spacecraft attitude estimator, the EKF has some disadvantages, especially in case of high nonlinearity, which appears to be a common problem in the attitude determination applications. Generally this is caused by the mandatory linearization phase of the EKF procedure and so the Jacobians derived with that purpose. For most of the applications, generation of the Jacobians is difficult, time consuming and prone to human errors (Julier *et al.* 1995). Nonetheless, the linearization brings about an unstable filter performance when the time step intervals for the update are not sufficiently small and as a result the filter diverges (Julier *et al.* 2000). Per contra, small time step intervals increase the computational burden because of the larger number of Jacobian calculations. These facts show that the EKF may be efficient only if the system is almost linear on the timescale of update intervals.

The UKF algorithm is a considerably new filtering method which has many advantages over the well known EKF. The essence of the UKF is the fact that; the approximation of a nonlinear distribution is easier than the approximation of a nonlinear function or transformation (Julier *et al.* 2000). The UKF introduces sigma points to catch higher order

statistic of the system and avoid the linearization step of the EKF. As a result it satisfies both better estimation accuracy and convergence characteristic (Soken and Hajiyev 2012). Moreover, the UKF is more robust against the initial attitude estimation errors than the EKF (Crassidis and Markley 2003).

4.1.1. The Unscented Kalman Filter

In order to utilize the Kalman filter for nonlinear systems without any linearization step, the unscented transformation, and so the UKF is one of the techniques. The UKF uses the unscented transform, a deterministic sampling technique, to determine a minimal set of sample points (or sigma points) from the *a priori* mean and covariance of the states. Then, these sigma points go through nonlinear transformation. The *posterior* mean and the covariance are obtained from these transformed sigma points (Julier *et al.* 1995; Crassidis and Markley 2003).

The UKF is derived for discrete-time nonlinear equations, so the system model is given by;

$$\mathbf{x}_{k+1} = f(\mathbf{x}_k, k) + \mathbf{w}_k, \quad (4.1)$$

$$\tilde{\mathbf{y}}_k = h(\mathbf{x}_k, k) + \mathbf{v}_k. \quad (4.2)$$

Here \mathbf{x}_k is the state vector and $\tilde{\mathbf{y}}_k$ is the measurement vector. Moreover \mathbf{w}_k and \mathbf{v}_k are the process and measurement error noises, which are assumed to be Gaussian white noise processes with the covariances of $Q(k)$ and $R(k)$ respectively.

The UKF procedure begins with the determination of $2n+1$ sigma points with a mean of $\hat{\mathbf{x}}(k|k)$ and a covariance of $P(k|k)$. For an n dimensional state vector, these sigma points are obtained by

$$\mathbf{x}_0(k|k) = \hat{\mathbf{x}}(k|k), \quad (4.3)$$

$$\mathbf{x}_l(k|k) = \hat{\mathbf{x}}(k|k) + \left(\sqrt{(n+\kappa)P(k|k)} \right)_l, \quad l=1 \dots n. \quad (4.4)$$

$$\mathbf{x}_{l+n}(k|k) = \hat{\mathbf{x}}(k|k) - \left(\sqrt{(n+\kappa)P(k|k)} \right)_l, \quad l=1 \dots n. \quad (4.5)$$

where, $\mathbf{x}_0(k|k)$, $\mathbf{x}_l(k|k)$ and $\mathbf{x}_{l+n}(k|k)$ are sigma points, n is the state number, and κ is the scaling parameter which is used for fine tuning. $\left(\sqrt{(n+\kappa)P(k|k)}\right)_l$ corresponds to the l^{th} column of the indicated matrix.

The next step of the UKF procedure is evaluating the transformed set of sigma points for each of the points by,

$$\mathbf{x}_l(k+1|k) = f[\mathbf{x}_l(k|k), k] \quad l = 0 \dots 2n. \quad (4.6)$$

Thereafter, these transformed values are utilized for gaining the predicted mean and covariance (Crassidis and Markley 2003; Soken and Hajiyev 2012).

$$\hat{\mathbf{x}}(k+1|k) = \frac{1}{n+\kappa} \left\{ \kappa \mathbf{x}_0(k+1|k) + \frac{1}{2} \sum_{l=1}^{2n} \mathbf{x}_l(k+1|k) \right\}, \quad (4.7)$$

$$P(k+1|k) = \frac{1}{n+\kappa} \left\{ \kappa [\mathbf{x}_0(k+1|k) - \hat{\mathbf{x}}(k+1|k)][\mathbf{x}_0(k+1|k) - \hat{\mathbf{x}}(k+1|k)]^T + \frac{1}{2} \sum_{l=1}^{2n} [\mathbf{x}_l(k+1|k) - \hat{\mathbf{x}}(k+1|k)][\mathbf{x}_l(k+1|k) - \hat{\mathbf{x}}(k+1|k)]^T \right\} + Q(k). \quad (4.8)$$

Here, $\hat{\mathbf{x}}(k+1|k)$ is the predicted mean and $P(k+1|k)$ is the predicted covariance. Note that the process noise covariance, $Q(k)$, might be added to the filtering process before and/or after the propagation. We preferred to include after the propagation as given with (4.8). Otherwise it would be added to $P(k|k)$ in (4.4) and (4.5). Furthermore, the predicted observation vector is,

$$\hat{\mathbf{y}}(k+1|k) = \frac{1}{n+\kappa} \left\{ \kappa \mathbf{y}_0(k+1|k) + \frac{1}{2} \sum_{l=1}^{2n} \mathbf{y}_l(k+1|k) \right\}, \quad (4.9)$$

where,

$$\mathbf{y}_l(k+1|k) = h[\mathbf{x}_l(k+1|k), k] \quad l = 0 \dots 2n. \quad (4.10)$$

After that, the observation covariance matrix is determined as,

$$P_{yy}(k+1|k) = \frac{1}{n+\kappa} \left\{ \kappa [\mathbf{y}_0(k+1|k) - \hat{\mathbf{y}}(k+1|k)][\mathbf{y}_0(k+1|k) - \hat{\mathbf{y}}(k+1|k)]^T + \frac{1}{2} \sum_{l=1}^{2n} [\mathbf{y}_l(k+1|k) - \hat{\mathbf{y}}(k+1|k)][\mathbf{y}_l(k+1|k) - \hat{\mathbf{y}}(k+1|k)]^T \right\}, \quad (4.11)$$

where the innovation covariance is

$$P_{vv}(k+1|k) = P_{yy}(k+1|k) + R(k+1). \quad (4.12)$$

Here $R(k+1)$ is the measurement noise covariance matrix. Conversely, the cross correlation matrix can be obtained as,

$$P_{xy}(k+1|k) = \frac{1}{n+\kappa} \left\{ \kappa [\mathbf{x}_0(k+1|k) - \hat{\mathbf{x}}(k+1|k)] [\mathbf{y}_0(k+1|k) - \hat{\mathbf{y}}(k+1|k)]^T + \frac{1}{2} \sum_{l=1}^{2n} [\mathbf{x}_l(k+1|k) - \hat{\mathbf{x}}(k+1|k)] [\mathbf{y}_l(k+1|k) - \hat{\mathbf{y}}(k+1|k)]^T \right\}. \quad (4.13)$$

The following part is the update phase of the UKF algorithm. In that phase, first by using the measurements, $\mathbf{y}(k+1)$, an innovation sequence is found as

$$\mathbf{e}(k+1) = \mathbf{y}(k+1) - \hat{\mathbf{y}}(k+1|k), \quad (4.14)$$

and then the Kalman gain is computed by,

$$K(k+1) = P_{xy}(k+1|k) P_{vv}^{-1}(k+1|k). \quad (4.15)$$

Finally, the updated states and covariance matrix are determined,

$$\hat{\mathbf{x}}(k+1|k+1) = \hat{\mathbf{x}}(k+1|k) + K(k+1)\mathbf{e}(k+1), \quad (4.16)$$

$$P(k+1|k+1) = P(k+1|k) - K(k+1)P_{vv}(k+1|k)K^T(k+1). \quad (4.17)$$

Here, $\hat{\mathbf{x}}(k+1|k+1)$ is the estimated state vector and $P(k+1|k+1)$ is the estimated covariance matrix.

4.1.2. The UKF with Attitude Error Representation

In case of quaternion utilization for the kinematic modeling of the satellite's motion, the UKF in standard format cannot be implemented straightforwardly. The reason of such drawback is the constraint of quaternion unity given by $\mathbf{q}^T \mathbf{q} = 1$. If the kinematics equations (2.49-2.52) are used in the filter directly, than there is no guarantee that the predicted quaternion mean will satisfy this constraint since the prediction is performed using the averaged sum of the quaternions (4.7).

One of the methods to solve this issue is to enforce quaternion unity constraint as a dummy measurement into the measurement output (Sekhavat *et al.* 2007). Basic of the method is to augment the measurement output with the known algebraic constraint,

$$\zeta(x, t) = 0 \quad (4.18)$$

for a nonlinear system given as

$$\dot{x} = f(x, t), \quad (4.19)$$

$$y = h(x, t). \quad (4.20)$$

Hence, the augmented measurement output becomes

$$y_A = \begin{bmatrix} h(x, t) \\ \zeta(x, t) \end{bmatrix}. \quad (4.21)$$

However when we use this method for the bias estimation, it does not work well for large bias updates.

On the other hand, another documented method to overcome the quaternion unity problem is to use an unconstrained three component vector in order to represent an attitude-error quaternion instead of using all four components of the quaternion vector. The details of this method can be found in (Crassidis and Markley 2003). In this section the method is summarized briefly and it is described how this method is used for the attitude and sensor bias estimation.

First let us define the basics. We may rewrite the quaternion vector by $\mathbf{q} = [\mathbf{g}^T \quad q_4]^T$, so $\mathbf{g} = [q_1 \quad q_2 \quad q_3]^T$. Then for $\Xi(\mathbf{q})$ matrix shown as;

$$\Xi(\mathbf{q}) = \begin{bmatrix} q_4 I_{3 \times 3} + [\mathbf{g} \times] \\ -\mathbf{g}^T \end{bmatrix}, \quad (4.22)$$

the quaternion multiplication can be denoted with

$$\mathbf{q}' \otimes \mathbf{q} = [\Xi(\mathbf{q}) \quad \vdots \quad \mathbf{q}] \mathbf{q}'. \quad (4.23)$$

Here $[\mathbf{g} \times]$ is the cross product matrix as,

$$[\mathbf{g} \times] = \begin{bmatrix} 0 & -g_3 & g_2 \\ g_3 & 0 & -g_1 \\ -g_2 & g_1 & 0 \end{bmatrix}. \quad (4.24)$$

The second step is to represent the local error-quaternion that will be used in the UKF formulations. If we denote the local-error quaternion as $\delta\mathbf{q} = [\delta\mathbf{g}^T \ \delta q_4]^T$ then it is possible to represent it by using a vector of generalized Rodrigues parameters:

$$\delta\mathbf{p} = f [\delta\mathbf{g} / (a + \delta q_4)]. \quad (4.25)$$

Here a is a parameter from 0 to 1 and f is the scale factor. When $a = 0$ and $f = 1$ then (4.25) gives the Gibbs vector and when $a = 1$ and $f = 1$ then (4.25) gives the standard vector of modified Rodrigues parameters. In (Crassidis and Markley 2003) - as well in this paper - f is chosen as $f = 2(a + 1)$. The inverse transformation from $\delta\mathbf{p}$ to $\delta\mathbf{q}$ is given by

$$\delta q_4 = \frac{-a \|\delta\mathbf{p}\|^2 + f \sqrt{f^2 + (1 - a^2) \|\delta\mathbf{p}\|^2}}{f^2 + \|\delta\mathbf{p}\|^2}, \quad (4.26)$$

$$\delta\mathbf{g} = f^{-1} (a + \delta q_4) \delta\mathbf{p}. \quad (4.27)$$

Now we can introduce the procedure for the UKF with attitude error representation. First let us define the following state vector:

$$\mathbf{x}_0(k|k) = \hat{\mathbf{x}}(k|k) = \begin{bmatrix} \delta\hat{\mathbf{p}}(k|k) \\ \hat{\boldsymbol{\beta}}(k|k) \end{bmatrix}. \quad (4.28)$$

$\delta\hat{\mathbf{p}}(k|k)$ is the three-dimensional attitude representation and comes from (4.25). Besides $\hat{\boldsymbol{\beta}}(k|k)$ is bias part of the state vector consists of the gyro and magnetometer biases. Hence the vector for the sigma points can be partitioned into two parts:

$$\mathbf{x}_l(k|k) = \begin{bmatrix} \mathbf{x}_l^{\delta p}(k|k) \\ \mathbf{x}_l^{\beta}(k|k) \end{bmatrix} \quad l = 0 \dots 2n. \quad (4.29)$$

where $\mathbf{x}_l^{\delta p}(k|k)$ is the attitude error part and $\mathbf{x}_l^{\beta}(k|k)$ is the bias part which may be also shown in two parts for gyro biases, $\mathbf{x}_l^{\beta g}(k|k)$, and magnetometer biases, $\mathbf{x}_l^{\beta m}(k|k)$, as

$\mathbf{x}_l^\beta(k|k) = \left[\mathbf{x}_l^{\beta s}(k|k)^T \quad \mathbf{x}_l^{\beta m}(k|k)^T \right]^T$. The sigma points in (4.29) can be called as error sigma points which correspond to the sigma points calculated for error quaternions. We need to calculate the full sigma points that correspond to the full state with four quaternion terms and 6 bias terms in order to propagate the model. Therefore,

$$\hat{\mathbf{q}}_0(k|k) = \hat{\mathbf{q}}(k|k), \quad (4.30)$$

$$\hat{\mathbf{q}}_l(k|k) = \delta \hat{\mathbf{q}}_l(k|k) \otimes \hat{\mathbf{q}}(k|k) \quad l = 1 \dots 2n. \quad (4.31)$$

where $\delta \hat{\mathbf{q}}_l(k|k) = \left[\delta \hat{\mathbf{g}}_l(k|k)^T \quad \delta \hat{\mathbf{q}}_{4_l}(k|k) \right]^T$ is represented by (4.26-4.27):

$$\delta \hat{\mathbf{q}}_{4_l}(k|k) = \frac{-a \|\mathbf{x}_l^{\delta p}(k|k)\|^2 + f \sqrt{f^2 + (1-a^2)} \|\mathbf{x}_l^{\delta p}(k|k)\|^2}{f^2 + \|\mathbf{x}_l^{\delta p}(k|k)\|^2} \quad l = 1 \dots 2n. \quad (4.32)$$

$$\delta \hat{\mathbf{g}}_l(k|k) = f^{-1} \left[a + \delta \hat{\mathbf{q}}_{4_l}(k|k) \right] \mathbf{x}_l^{\delta p}(k|k) \quad l = 1 \dots 2n. \quad (4.33)$$

(4.30) requires that $\mathbf{x}_0^{\delta p}(k|k)$ be zero and this is due to the reset of the attitude error to zero after each estimation step.

Next, the quaternions are propagated using the kinematic model (2.49-2.52) so we have $\hat{\mathbf{q}}_l(k+1|k)$ as the propagated quaternions for $l = 0 \dots 2n$. Note that the angular velocity terms used in (2.49-2.52) are the angular velocities estimated at the previous step as:

$$\hat{\boldsymbol{\omega}}_{Bl}(k|k) = \tilde{\boldsymbol{\omega}}_{Bl} - \mathbf{x}_l^{\beta s}(k|k) \quad l = 0 \dots 2n. \quad (4.34)$$

As a result, now we have the propagated full sigma points. The propagated error sigma points must be calculated to continue the filtering process. So as to do that, we use the representation in (4.25);

$$\mathbf{x}_0^{\delta p}(k+1|k) = \mathbf{0} \quad (4.35)$$

$$\mathbf{x}_l^{\delta p}(k+1|k) = f \frac{\delta \hat{\mathbf{g}}_l(k+1|k)}{a + \delta \hat{\mathbf{q}}_{4_l}(k+1|k)} \quad l = 1 \dots 2n \quad (4.36)$$

where

$$\begin{aligned} \left[\delta \hat{\mathbf{g}}_l(k+1|k)^T \quad \delta \hat{q}_4(k+1|k) \right]^T = \\ \delta \hat{q}_l(k+1|k) = \hat{q}_l(k+1|k) \otimes \left[\hat{q}_0(k+1|k) \right]^{-1} \quad l = 0 \dots 18. \end{aligned} \quad (4.37)$$

Note that $\delta \hat{q}_0(k+1|k)$ is the identity quaternion. Moreover we get the propagated sigma points for biases $\mathbf{x}_l^\beta(k+1|k)$, by (3.5) for the magnetometer biases and (3.9) for the gyro biases. Now using the propagated error sigma points $\mathbf{x}_l(k+1|k)$, it is possible to calculate the predicted mean and covariance (4.7, 4.8).

Next step is to calculate the predicted observation vector by using the propagated full sigma points (4.9, 4.10). Then the observation covariance, innovation covariance and cross correlation matrices can be computed using (4.11-4.13). After calculating the innovation series and the Kalman gain (4.14, 4.15), the state vector and the covariance can be updated by the use of (4.16, 4.17) with $\hat{\mathbf{x}}(k+1|k+1) = \left[\delta \hat{\mathbf{p}}(k+1|k+1)^T \quad \hat{\boldsymbol{\beta}}(k+1|k+1)^T \right]^T$ as the result for the state update.

Now we have the updated state vector for error quaternions and we need to update the full quaternion vector by

$$\hat{q}(k+1|k+1) = \delta \hat{q}(k+1|k+1) \otimes \hat{q}_0(k+1|k), \quad (4.38)$$

where $\delta \hat{q}(k+1|k+1) = \left[\delta \hat{\mathbf{g}}(k+1|k+1)^T \quad \delta \hat{q}_4(k+1|k+1) \right]^T$ is represented by (4.26, 4.27):

$$\delta \hat{q}_4(k+1|k+1) = \frac{-a \|\delta \hat{\mathbf{p}}(k+1|k+1)\|^2 + f \sqrt{f^2 + (1-a^2)} \|\delta \hat{\mathbf{p}}(k+1|k+1)\|^2}{f^2 + \|\delta \hat{\mathbf{p}}(k+1|k+1)\|^2}, \quad (4.39)$$

$$\delta \hat{\mathbf{g}}(k+1|k+1) = f^{-1} \left[a + \delta \hat{q}_4(k+1|k+1) \right] \delta \hat{\mathbf{p}}(k+1|k+1). \quad (4.40)$$

4.2. Dynamics-Based and Gyro-Based Models

The algorithm that is given in the previous section is for the case that we use a gyro-based model for the UKF (or a reduced-order filter). In other words, we only need the kinematics knowledge of the process in order to propagate the states and the dynamics given with (2.40) is not necessary. That has certain advantages such as (Fosbury 2011):

- Since the quaternion propagation can be performed using a discrete matrix and a closed-form solution to the state transition matrix has been developed for use in state-error propagation, the computational load for this method is low.
- There is no need to know the moments of inertia of the satellite accurately.
- It is not necessary to build a realistic model for the disturbance torques such as gravity-gradient, sun pressure etc.

On the other hand, in this method we do not use the gyro output as measurements but instead use them when updating the angular velocity information by the estimated gyro biases as given with (4.34). If we had known the dynamics perfectly then including the gyro outputs in the measurement vector would provide better estimation accuracy. In this case the body angular rate vector, $\boldsymbol{\omega}_{Bl}$, would be also included in the state vector and estimated throughout the filtering procedure by using the full-order UKF. For the scenario, where in-orbit calibration for the gyros and magnetometers is performed, that would increase the computational load of the UKF. Hence it is more advantageous to use a gyro-based model rather than the dynamics-based model when the gyro and magnetometer biases are estimated and specifically if the uncertainty in the dynamics caused by inaccurate moment of inertia or torque information is high.

4.3. In-Orbit Gyro and Magnetometer Bias Estimation

4.3.1. Gyro and Magnetometer Bias Estimation via the UKF

In this section we present the results of the given method for in-orbit gyro and magnetometer bias estimation. The UKF based estimation algorithm presented in the previous sections of this chapter is used.

The state vector is composed by the attitude quaternions, gyro biases and magnetometer biases as,

$$\mathbf{x} = \begin{bmatrix} \mathbf{q}^T & \mathbf{b}_g^T & \mathbf{b}_m^T \end{bmatrix}^T . \quad (4.41)$$

Besides, we use the output of three axis magnetometer as the measurements,

$$\mathbf{y} = \begin{bmatrix} H_x & H_y & H_z \end{bmatrix}^T . \quad (4.42)$$

The simulations are realized for 20000 seconds with a sampling time of $\Delta t = 10$ sec.

Nonetheless the orbit of the satellite is assumed as circular. The inclination for the satellite's orbit is $i = 31^\circ$ and the distance between the centre of the masses of the Earth and satellite is $r_0 = 7450km$.

For the magnetometer measurements, the sensor noise is characterized by zero mean Gaussian white noise with a standard deviation of $\sigma_m = 300nT$ and the constant magnetometer bias terms are accepted as $\bar{b}_m = [0.14 \ 0.019 \ 0.37]^T \times 10^4 nT$.

Moreover, the gyro random error is taken as $\sigma_v = 1 \times 10^{-3} [\text{deg}/\sqrt{h}]$, whereas the standard deviation of the gyro biases is $\sigma_u = 2 \times 10^{-3} [\text{deg}/\sqrt{h^3}]$.

As the filter parameters, κ is selected as $\kappa = -2$ where $f = 2(a+1)$ and $a = 1$. Initial attitude errors for the filter are set to 30, 25 and 25 deg for pitch, yaw and roll axes respectively. The initial estimation values for the gyro and magnetometer biases are taken as 0. Besides, the initial value of the covariance matrix is $P_0 = \text{diag}[0.5 \ 0.5 \ 0.5 \ 10^{-7} \ 10^{-7} \ 10^{-7} \ 10^{-3} \ 10^{-3} \ 10^{-3}]$ where $\text{diag}(\cdot)$ refers to diagonal matrix.

Last but not least, the value of the process noise covariance matrix for the UKF is set to,

$$Q = \begin{bmatrix} (1E-5)I_{3 \times 3} & -(1E-15)I_{3 \times 3} & 0_{3 \times 3} \\ -(1E-15)I_{3 \times 3} & (1E-12)I_{3 \times 3} & 0_{3 \times 3} \\ 0_{3 \times 3} & 0_{3 \times 3} & (1E-15)I_{3 \times 3} \end{bmatrix}. \quad (4.43)$$

The necessity for in-orbit real time magnetometer calibration is already discussed. Yet in order to show the effects of magnetometer bias estimation on the nanosatellite attitude determination accuracy, same simulation scenario is repeated with a filter which does not estimate the magnetometer biases. Apparently, in this case the state vector is,

$$\mathbf{x} = [\mathbf{q}^T \ \mathbf{b}_g^T]^T. \quad (4.44)$$

For this second UKF the scaling parameter is selected as $\kappa = 1$. The initial value of the covariance matrix is taken as $P_0 = \text{diag}[0.5 \ 0.5 \ 0.5 \ 10^{-5} \ 10^{-5} \ 10^{-5}]$ while the initial attitude and gyro bias errors are same as the first filter. The process noise covariance matrix is tuned as

$$Q = \begin{bmatrix} (1E-10)I_{3 \times 3} & -(1E-18)I_{3 \times 3} \\ -(1E-18)I_{3 \times 3} & (1E-15)I_{3 \times 3} \end{bmatrix}. \quad (4.45)$$

4.3.2. Simulation Results

At first we test the given in-orbit attitude and sensor bias estimation algorithm. In Fig.4.1 the attitude estimation error for the pitch angle is given. Obviously the attitude can be accurately estimated using the presented algorithm and the attitude estimation error settles to an error less than ± 1 deg. Results for the roll and yaw angle estimations are similar.

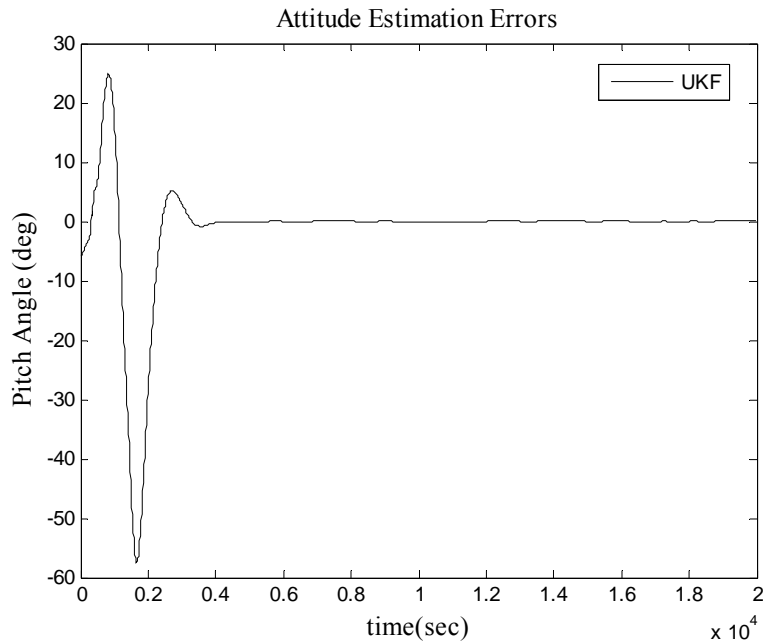


Figure 4.1: Pitch angle estimation error of the UKF used for attitude, gyro and magnetometer bias estimation.

The results for the gyro and magnetometer bias estimation prove that the filter is working properly for sensor calibration (Fig.4.2 and Fig.4.3). However the accuracy of the

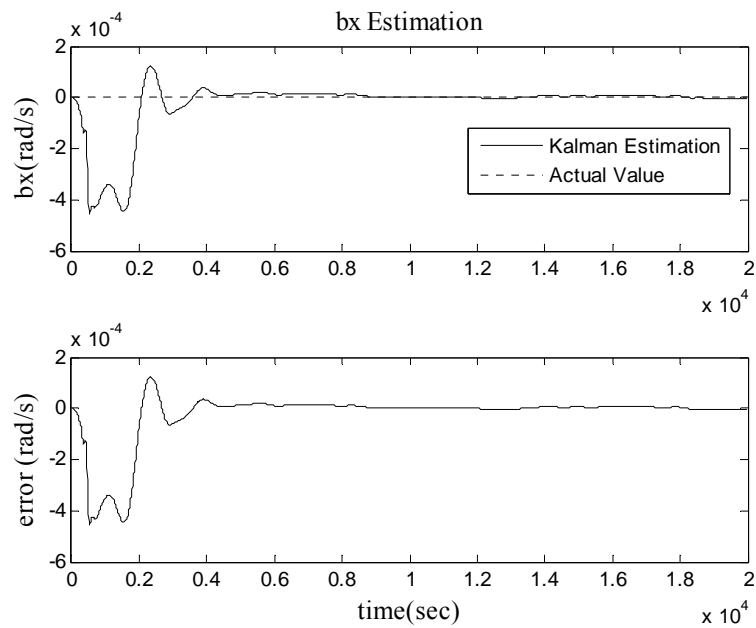


Figure 4.2: Estimation of the bias for the gyro aligned in the x axis by the UKF used for attitude, gyro and magnetometer bias estimation.

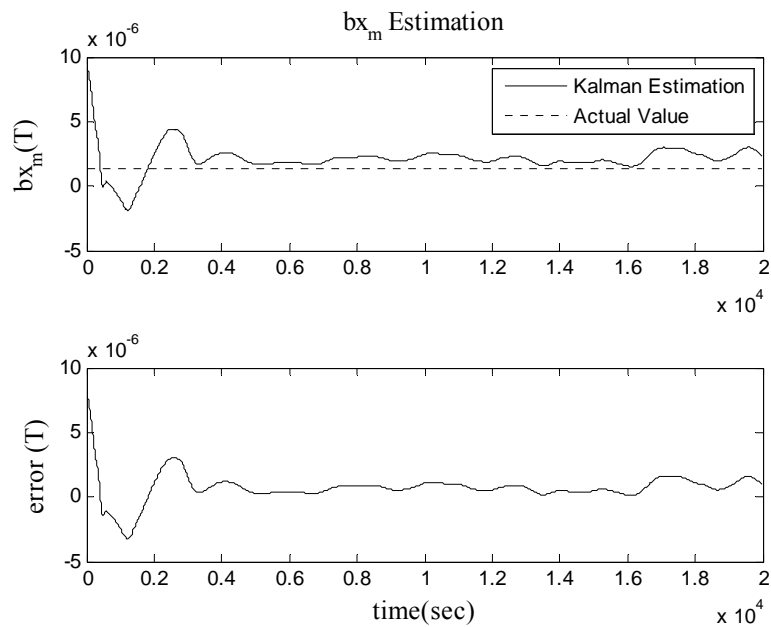


Figure 4.3: Estimation of the bias for the magnetometer aligned in the x axis by the UKF used for attitude, gyro and magnetometer bias estimation.

estimation for both of the parameters is not so high. This issue is related to the difficult tuning procedure of the UKF and will be extensively discussed in the next chapter, where an AUKF algorithm is proposed to solve the problem.

On the other hand, as expected, estimating the magnetometer biases for the case that bias exists in the measurements significantly increases the attitude estimation accuracy. In Fig. 4.4 the attitude estimation results for the UKFs with and without bias estimation are compared. As seen the UKF, which disregards the magnetometer biases and does not estimate them, provides relatively worse attitude estimation accuracy. Moreover the gyro bias estimation results via the UKF without magnetometer bias estimation are alike in the sense of accuracy (Fig. 4.5).

As a consequence, these results underline the importance of in-orbit magnetometer bias estimation for the nanosatellites. If we want to increase the attitude estimation accuracy for a nanosatellite carrying magnetometers and gyros as the attitude sensors, in-orbit calibration of the magnetometers is a requirement.

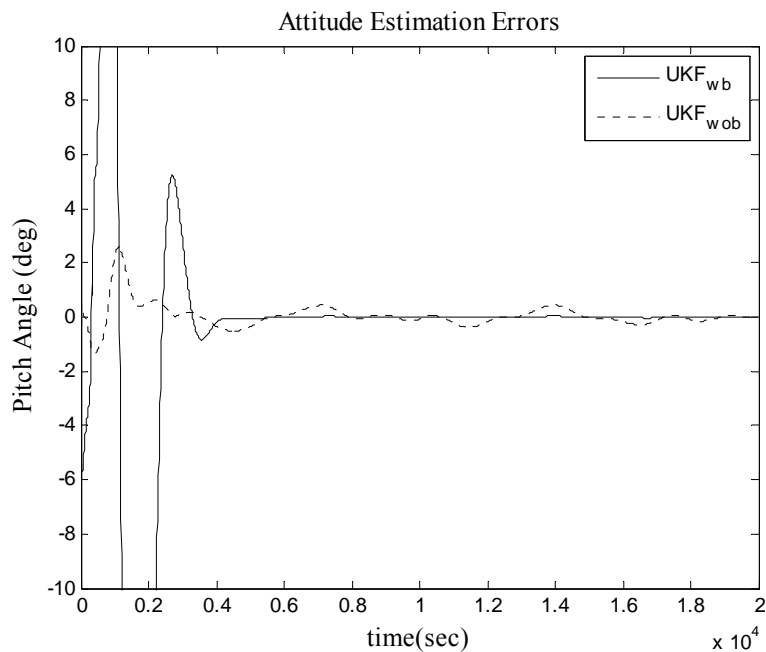


Figure 4.4: Pitch angle estimation error of the UKFs with and without magnetometer bias estimation when magnetometer bias exists in the measurements: UKF_{wb} is the filter that estimates the magnetometer biases and UKF_{wob} is the filter that disregards them.

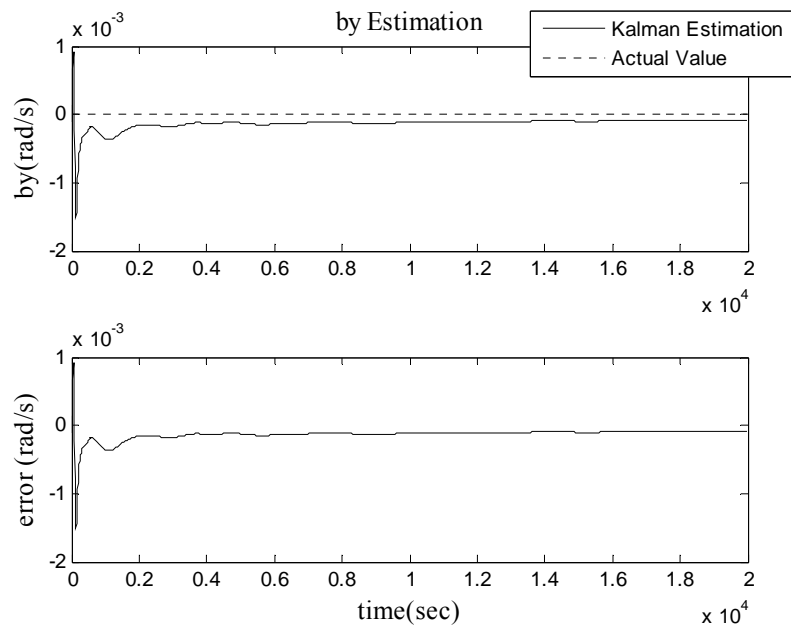


Figure 4.5: Estimation of the bias for the gyro aligned in the y axis by the UKF without magnetometer bias estimation when magnetometer bias exists in the measurements.

5. Adaptation Methods for the UKF

In this chapter we examine two different adaptation methods for the UKF: adaptation against process noise uncertainties and adaptation against the measurement faults.

The main motivation behind the adaptation against the process noise uncertainties is to find a proper tuning method for the process noise covariance of the UKF algorithm which is used for the attitude estimation and in-flight sensor calibration. As stated in the previous chapter while presenting the results for the gyro and magnetometer bias estimation, if the UKF is not tuned properly than it is not possible to increase the accuracy of the estimations. The trial and error method is always a candidate for finding the good process noise covariance matrix that makes estimation results more precise but especially for high-dimensional states this is a time-consuming and difficult process. Hence, we propose an AUKF method which tunes the process noise covariance dynamically throughout the estimations and ensures that we find the process noise covariance terms near optimality. In order to achieve that we first compare the estimation of the AUKF algorithm with the UKF that works with the analytically approximated process noise covariance for the case that such approximation is possible.

Nevertheless, for nanosatellites the interaction between the subsystems and the risk of being affected from the external disturbances are high because of the compact size of the spacecraft. That increases the possibility of giving faulty measurements for the magnetometers. Such faulty measurements affect the stability and accuracy of the estimator even when they last for few samples. The proposed RUKF algorithm is a favorable method to avoid such failures.

5.1. Adaptation against Process Noise Uncertainties

Similarly with all Kalman filtering applications, determining the process noise covariance matrix of the UKF is a challenging process especially for estimation problems with a high-dimensional state vector where states like sensor biases or system parameters are included. If the a priori statistics selected as a constant do not match with the real values, then the filter characteristics such as the accuracy or convergence speed may be affected and even a serious mismatch may cause the filter to fail in practice (Dunik *et al.* 2009). The designer has always chance to tune the process noise covariance by trial-error method but this is a

time consuming process and obtaining the optimal values is not guaranteed.

When the UKF is used for estimating only the attitude and gyro biases as a reduced-order filter then there is an analytical approximation for the process noise covariance matrix which holds true (Crassidis and Markley 2003). On the other hand, our aim is to find a proper tuning algorithm when we use the UKF also for magnetometer bias estimation. A general approach suggests that when we estimate the magnetometer biases, the bias terms can be treated and propagated as a constant in time as presented previously. Then the process noise covariance matrix must be also built regarding this fact. In this case, the analytical approximation for the process noise covariance matrix suggests that the elements of the matrix that corresponds to the magnetometer bias states should be taken as zero. Since the estimated state is constant in time this approximation is true in theory as it is shown for the estimation of the gyro scale factors in literature (Fosbury 2011). However, in practice, mainly because of the computational errors and assumptions/approximations for the models built for the filter, this method fails and the UKF cannot provide accurate estimates and usually diverges in time.

In this section we propose two AUKF algorithms for tuning the process noise covariance matrix of the UKF. The first one uses a single scale factor to perform the tuning. The second one directly estimates the process noise covariance matrix.

5.1.1. Process Noise Covariance Scaling

This section presents the novel residual based adaptation scheme for the UKF. As mentioned the UKF works well as long as the *a priori* selected constant terms for the process noise covariance matrix, $Q(k)$, match with the real values. However this is usually not a very easy process especially in practice and a challenging tuning procedure should be followed to get the best estimation characteristics for all of the parameters.

The method proposed in this section is based on a residual based adaptation scheme that is applied on the process noise covariance matrix as a correction. First, let us rewrite (4.8) as;

$$P(k+1|k) = P^*(k+1|k) + Q(k). \quad (5.1)$$

So $P^*(k+1|k)$ is the predicted covariance without the additive process noise covariance. In order to adapt the covariance an adaptive factor is put into the procedure;

$$P(k+1|k) = P^*(k+1|k) + \Lambda(k)Q(k). \quad (5.2)$$

where $\Lambda(k)$ is the adaptive factor calculated based on the residual for the state vector estimation. The residual, $\tilde{\mathbf{e}}(k+1)$, and its covariance matrix, $P_{\tilde{\mathbf{e}}}(k+1)$, may be defined as (Mohamed and Schwarz 1999);

$$\tilde{\mathbf{e}}(k+1) = \mathbf{y}(k+1) - \hat{\mathbf{y}}(k+1|k+1), \quad (5.3)$$

$$P_{\tilde{\mathbf{e}}}(k+1) = R(k+1) - H(k+1|k+1)P(k+1|k+1)H(k+1|k+1)^T \quad (5.4)$$

Here, $H(k+1|k+1)$ is the measurement matrix and $\hat{\mathbf{y}}(k+1|k+1)$ is the estimated observation vector; the derivation procedure of them will be discussed shortly.

Now let us define the real residual error of the filter as $tr[\tilde{\mathbf{e}}(k+1)\tilde{\mathbf{e}}(k+1)^T]$ and the theoretical error obtained as a result of *a priori* information as $tr[R(k+1) - H(k+1|k+1)P(k+1|k+1)H(k+1|k+1)^T]$. Here $tr(\cdot)$ is the trace of the related matrix. When the *a priori* selected $Q(k)$ matrix matches with the real value then the difference between these two error terms shall not be high and in general case the real error should not exceed the theoretical one. Hence in order to calculate the adaptive factor we can use the equality condition for these two terms:

$$tr[\tilde{\mathbf{e}}(k+1)\tilde{\mathbf{e}}(k+1)^T] = tr[R(k+1)] - tr[H(k+1|k+1)P(k+1|k+1)H(k+1|k+1)^T] \quad (5.5)$$

If we replace $P(k+1|k+1)$ with its definition from (4.17), then;

$$tr[\tilde{\mathbf{e}}(k+1)\tilde{\mathbf{e}}(k+1)^T] = tr[R(k+1)] - tr\left\{H(k+1|k+1)\left[P(k+1|k) - K(k+1)P_{vv}(k+1|k)K(k+1)^T\right]H(k+1|k+1)^T\right\} \quad (5.6)$$

After that we shall put (5.2) into (5.6) and;

$$tr[\tilde{\mathbf{e}}(k+1)\tilde{\mathbf{e}}(k+1)^T] = tr[R(k+1)] - tr\left[H(k+1|k+1)P^*(k+1|k)H(k+1|k+1)^T\right] - \Lambda(k)tr\left[H(k+1|k+1)Q(k)H(k+1|k+1)^T\right] + tr\left[H(k+1|k+1)K(k+1)P_{vv}(k+1|k)K(k+1)^T H(k+1|k+1)^T\right] \quad (5.7)$$

Finally if the knowledge of $tr[\tilde{\mathbf{e}}(k+1)\tilde{\mathbf{e}}(k+1)^T] = \tilde{\mathbf{e}}(k+1)^T \tilde{\mathbf{e}}(k+1)$ is taken into consideration then the adaptive factor can be found as (note that discretization indices are not written for the sake of readability),

$$\Lambda = \frac{tr[R] - tr[HP^*H^T] + tr[HKP_{vv}K^TH^T] - \tilde{\mathbf{e}}^T \tilde{\mathbf{e}}}{tr[HQH^T]} \quad (5.8)$$

Hence by following a simple procedure, where the process noise covariance matrix is multiplied with the adaptive factor, it is possible to adapt the UKF to get better estimation accuracy and convergence characteristics. We call this algorithm as the AUKF with covariance scaling.

Now we describe how to calculate the measurement matrix, $H(k+1|k+1)$, and the estimated observation vector, $\hat{\mathbf{y}}(k+1|k+1)$. A well known way is to follow a similar procedure with the EKF and compute the Jacobian matrix constituted of partial derivatives. However if we regard that the filter will be run adaptively for the whole process that brings about a high computational burden and also it may be considered as against the Jacobian free nature of the UKF. A Jacobian free and simpler method is proposed in this section.

From the UKF theory we know that the cross correlation matrix for the innovation sequence (4.13) can be also written by (Julier *et al.* 1996),

$$P_{xy}(k+1|k) = P(k+1|k)H(k+1|k)^T. \quad (5.9)$$

Here $H(k+1|k)$ is also the measurement matrix but formed of predicted states, not the estimated states, since the innovation sequence is the point at issue. Nonetheless, if an analogical method is followed for the residual sequence, the measurement matrix formed of estimated states, $H(k+1|k+1)$, can be computed by

$$H(k+1|k+1) = P_{xy}(k+1|k+1)^T P(k+1|k+1)^{-1} \quad (5.10)$$

where $P_{xy}(k+1|k+1)$ is the cross correlation matrix for the residual sequence. In order to calculate this matrix and also the estimated observation vector ($\hat{\mathbf{y}}(k+1|k+1)$) we must repeat the sigma point calculation procedure with the estimated states, up to the propagation (4.28-4.33). Therefore, we now have sigma points for the estimated states, as well as the

sigma points for the full quaternion vector $\hat{q}_l(k+1|k+1)$ (note that they will be also used for the next estimation step, so basically this is not an extra calculation):

$$\mathbf{x}_l(k+1|k+1) = \begin{bmatrix} \mathbf{x}_l^{\delta p}(k+1|k+1) \\ \mathbf{x}_l^\beta(k+1|k+1) \end{bmatrix} \quad l = 0 \dots 2n. \quad (5.11)$$

$$\mathbf{x}_l^f(k+1|k+1) = \begin{bmatrix} \hat{q}_l(k+1|k+1) \\ \mathbf{x}_l^\beta(k+1|k+1) \end{bmatrix} \quad l = 0 \dots 2n. \quad (5.12)$$

$\mathbf{x}_l(k+1|k+1)$ is the sigma points vector for error states and $\mathbf{x}_l^f(k+1|k+1)$ is the sigma points vector for full states. Next we calculate the estimated observation vector by using the non-propagated full sigma points:

$$\mathbf{y}_l(k+1|k+1) = h[\mathbf{x}_l^f(k+1|k+1), k], \quad l = 0 \dots 18. \quad (5.13)$$

$$\hat{\mathbf{y}}(k+1|k+1) = \frac{1}{n+\kappa} \left\{ \kappa \mathbf{y}_0(k+1|k+1) + \frac{1}{2} \sum_{l=1}^{2n} \mathbf{y}_l(k+1|k+1) \right\}. \quad (5.14)$$

Finally, the cross correlation matrix for the residual sequence can be obtained as,

$$P_{xy}(k+1|k+1) = \frac{1}{n+\kappa} \left\{ \frac{1}{2} \sum_{l=1}^{2n} [\mathbf{x}_l(k+1|k+1) - \hat{\mathbf{x}}(k+1|k+1)] [\mathbf{y}_l(k+1|k+1) - \hat{\mathbf{y}}(k+1|k+1)]^T \right\} \quad (5.15)$$

Figure 5.1 presents the overall estimation scheme for the AUKF with process noise covariance scaling.

5.1.2. Simulation Results for Process Noise Covariance Scaling

The simulations for investigating the attitude estimation and sensor calibration performance of the UKF are performed. The scenario and the simulation parameters are same as it is presented in Section 4.3. As the only difference we run the simulations for a shorter time, which is 4000sec.

Fig. 5.2 gives the norm of the attitude estimation errors (NAEE) for the Euler angles, which is formed by taking the norm of the difference between the true attitude and estimated attitude as $NAEE(k) = \sqrt{[\varphi(k) - \hat{\varphi}(k)]^2 + [\theta(k) - \hat{\theta}(k)]^2 + [\psi(k) - \hat{\psi}(k)]^2}$.

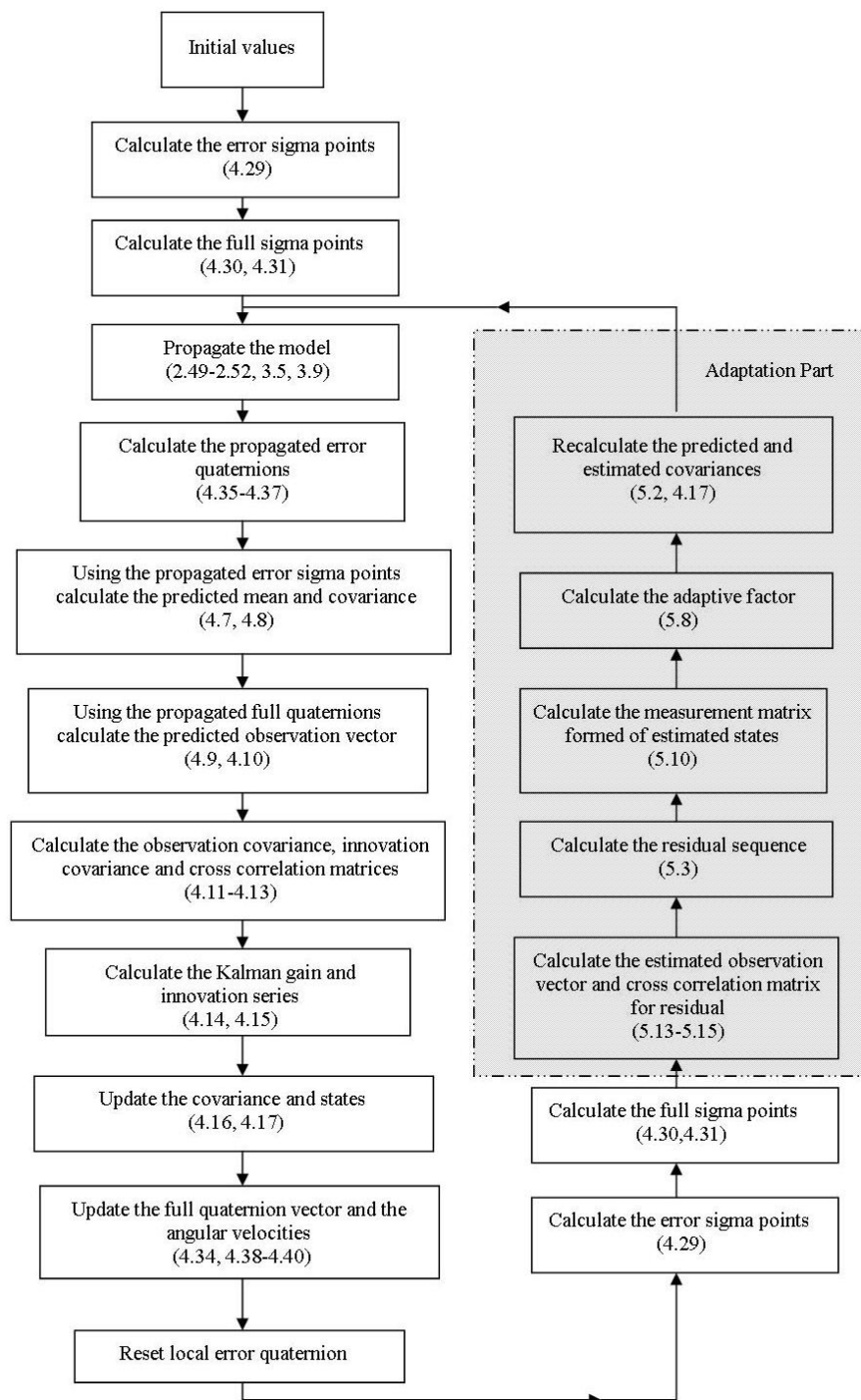


Figure 5.1: The overall estimation scheme for the AUKF with process noise covariance scaling.

The same simulation is repeated with the regular UKF in order to compare the results. As seen, the estimations by both of the filters converge to the actual value. However the AUKF overcomes the conventional UKF algorithm in the sense of accuracy and the convergence speed. The norm of the attitude error for the AUKF converges to a value below 1 deg at about 700th second. On the contrary, it takes 1700 seconds for the conventional UKF to converge to the same value. Moreover, further investigations show that through the end of the simulation, the attitude error for the AUKF settles to a value at about 0.005deg while the error for the UKF remains at about 0.02deg.

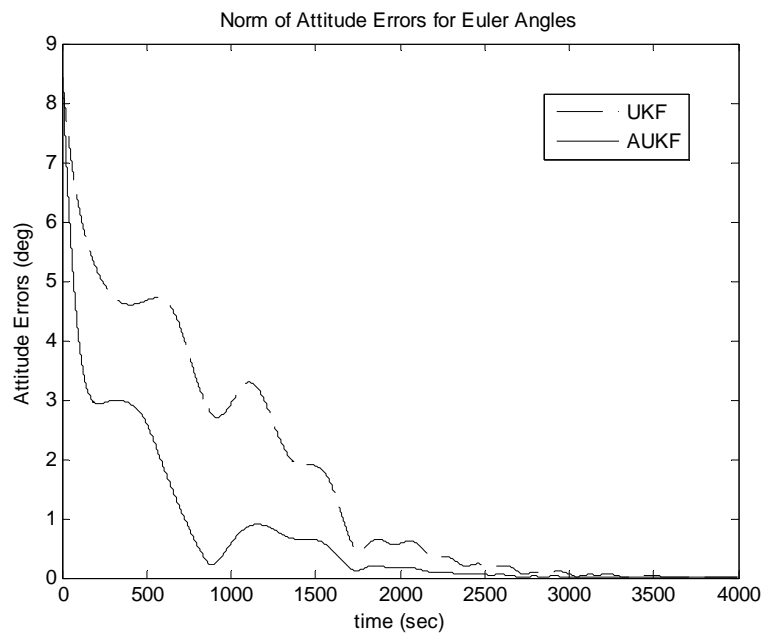


Figure 5.2: Norm of the attitude estimation errors for the conventional UKF (dashed line) and the AUKF with covariance scaling (solid line) in case of attitude, gyro bias and magnetometer bias estimation.

Therefore the proposed AUKF with process noise scaling gives reasonable results for the attitude estimation and in-orbit gyro and magnetometer calibration scenario. Nevertheless, our further investigations showed that this method has an instability issue. The initial process noise covariance matrix, which is used for initializing the algorithm, should be selected carefully; otherwise there is a risk for the filter not to converge to the actual values. Besides since the analytical approximation for the process noise covariance matrix makes the filter give almost optimal estimation results, we desire the process noise covariance of the AUKF to converge to the similar values when such approximation is possible (such as the case that we estimate only attitude and gyro biases). However when the AUKF with process noise covariance scaling is used for just the attitude and gyro bias estimation the

converged values for the process noise terms are not similar with the values found by the analytical approximation and what is more important the AUKF gives worse estimation results than the regular UKF with the analytically approximated Q . So the algorithm is working well for a scenario that we estimate attitude, gyro bias and magnetometer biases but it cannot be generalized for all the cases. The main reason of this issue is scaling the covariance matrix using only single factor.

Suppose that for getting accurate estimation results the process noise covariance should be tuned such that the ratio of Q_q / Q_{gb} is a certain constant like $Q_q / Q_{gb} = C$, where Q_q and Q_{gb} are the process noise covariance values for the attitude and gyro bias parameters, respectively and C is a constant. If these two values are initially tuned and the AUKF is started with a different ratio ($Q_q / Q_{gb} \neq C$) then it is not possible to change that and scale Q_q and Q_{gb} at different levels by using just a single scaling factor. Hence the performance of the AUKF still depends on mostly the initial tuning for the process noise covariance matrix.

As a consequence, an algorithm which directly estimates the process noise covariance terms rather than scaling by a single factor might be more feasible for increasing the estimation accuracy and easing the filter tuning procedure. Such algorithm will be presented in the next sections of this chapter.

5.1.3. Process Noise Covariance Estimation

A. Process Noise Covariance Estimation for the UKF

Adaptive estimation of the process noise covariance for the UKF is performed on the basis of a maximum likelihood estimator, which is well discussed in (Maybeck 1982; Mohamed and Schwarz 1999; Lee and Alfriend 2004) for different problems such as integrated navigation, orbit estimation etc. On the other hand, as discussed in these studies, the method must be modified (like diagonalization of the process noise covariance matrix) in accordance with the type of the problem.

The adaptive Kalman filtering problem deals with satisfying the necessary condition for the following equation (Maybeck 1982),

$$\sum_{j=j_0}^{k+1} \left[tr \left\{ C_e^{-1}(j) \frac{\partial C_e(j)}{\partial \alpha(k+1)} \right\} - \mathbf{e}^T(k+1) C_e^{-1}(j) \frac{\partial C_e(j)}{\partial \alpha(k+1)} C_e^{-1}(j) \mathbf{e}(k+1) \right] = 0, \quad (5.16)$$

where $\alpha(k+1)$ is the adaptive parameters, $tr(\cdot)$ is the trace operator, j_0 is $j_0 = k - MV + 2$ for a MV size of moving window, $\mathbf{e}(k+1)$ is the innovation sequence and C_e is the innovation covariance which may be written for the UKF as

$$C_e(k+1) = R(k+1) + P_{yy}(k+1|k) . \quad (5.17)$$

Here $R(k+1)$ and $P_{yy}(k+1|k)$ are the measurement noise and observation covariance matrices, respectively. Nonetheless the basic equation used for the process noise covariance adaptation is given as

$$\sum_{j=j_0}^{k+1} tr\left\{H^T(j)\left[C_e^{-1}(j) - C_e^{-1}(j)\mathbf{e}(k+1)\mathbf{e}^T(k+1)C_e^{-1}(j)\right]H(j)\right\} = 0 . \quad (5.18)$$

$H(k+1|k)$ is the measurement matrix and $H(k+1|k) = P_{xy}(k+1|k)^T P(k+1|k)^{-1}$ for the UKF, where $P_{xy}(k+1|k)$ is the cross correlation matrix and $P(k+1|k)$ is the predicted covariance matrix. We need to show (5.18) holds true for the UKF and it can be derived from (5.16) using the UKF equations. First let us rewrite the (5.17) in the light of formulations from (Julier et al. 1996),

$$C_e(k+1) = R(k+1) + P_{xy}^T(k+1|k)P^{-1}(k+1|k)P_{xy}(k+1|k) . \quad (5.19)$$

Then the derivative of the innovation covariance with respect to the adaptive factors becomes

$$\frac{\partial C_e(k+1)}{\partial \alpha(k+1)} = \frac{\partial R(k+1)}{\partial \alpha(k+1)} - P_{xy}^T(k+1|k)P^{-1}(k+1|k)\frac{\partial Q(k+1)}{\partial \alpha(k+1)}P^{-1}(k+1|k)P_{xy}(k+1|k) . \quad (5.20)$$

Here, while taking the derivative, we assume that $P_{xy}(k+1|k)$ and $P^*(k+1|k)$ are not a function of $\alpha(k+1)$, where $P^*(k+1|k)$ is the propagated covariance without the additive noise as $P(k+1|k) = P^*(k+1|k) + Q(k+1)$. Then regarding the equality of

$$P_{xy}(k+1|k) = P(k+1|k)H^T(k+1|k), \quad (5.21)$$

(5.20) can be rewritten as

$$\frac{\partial C_e(k+1)}{\partial \alpha(k+1)} = \frac{\partial R(k+1)}{\partial \alpha(k+1)} - H(k+1|k) \frac{\partial Q(k+1)}{\partial \alpha(k+1)} H^T(k+1|k) . \quad (5.22)$$

If we replace (5.22) in (5.16) we get,

$$\sum_{j=j_0}^{k+1} tr \left\{ \left[C_e^{-1}(j) - C_e^{-1}(j) \mathbf{e}(k+1) \mathbf{e}^T(k+1) C_e^{-1}(j) \right] \left[\frac{\partial R(j)}{\partial \alpha(k+1)} - H(j) \frac{\partial Q(j-1)}{\partial \alpha(k+1)} H(j)^T \right] \right\} = 0 . \quad (5.23)$$

Finally if we consider that the measurement noise covariance R is completely known and independent of α and take $\alpha_i = Q_{ii}$, then the (5.23) reduces to the same equation as (5.18).

After that, next step is to use this basic equation (5.18) in order to find out a definition for the covariance matrix of the system noise. This procedure is same as it is presented in (Maybeck 1982; Mohamed and Schwarz 1999) and not repeated here for the brevity. Consequently, the estimation of the $Q(k)$ can be written as,

$$Q^* = \Delta \mathbf{x}(k+1) \Delta \mathbf{x}^T(k+1) + P(k+1|k) - P(k+1|k+1) - Q(k), \quad (5.24)$$

where $Q(k)$ is the current process noise covariance and $\Delta \mathbf{x}(k+1)$ is the state residual defined as the difference between the estimated and predicted state as

$$\Delta \mathbf{x}(k+1) = \hat{\mathbf{x}}(k+1|k+1) - \hat{\mathbf{x}}(k+1|k) . \quad (5.25)$$

Furthermore, as known, the attitude estimator is sensitive against any kind of variations in the process noise covariance matrix. Therefore directly forcing the estimated process noise covariance matrix into the estimator at the next step may cause stability issues especially if the initial process noise covariance matrix is not appropriately selected. One possible method is to consider the Q^* within a low pass filter such as

$$Q(k+1) = \gamma Q^* + (1-\gamma)Q(k). \quad (5.26)$$

Here γ is the scale factor which may be determined by the trial-error method. This idea has other examples in the literature (Lee and Alfriend 2004) and yields to more stable estimation characteristic for the attitude estimator.

B. Process Noise Covariance for the Attitude Estimator

In (Crassidis and Markley 2003) the analytical approximation for the process noise covariance matrix, which is used for the UKF based attitude estimator, is given as

$$Q = \begin{bmatrix} (\sigma_v^2 \Delta t + \frac{1}{3} \sigma_u^2 \Delta t^3) I_{3 \times 3} & -(\frac{1}{2} \sigma_u^2 \Delta t^2) I_{3 \times 3} \\ -(\frac{1}{2} \sigma_u^2 \Delta t^2) I_{3 \times 3} & (\sigma_u^2 \Delta t) I_{3 \times 3} \end{bmatrix}. \quad (5.27)$$

Here Δt is the sampling time.

In this sense, if we include also the magnetometer biases into the state vector then according to the theory, the 9×9 process noise covariance matrix must be (Fosbury 2011):

$$Q = \begin{bmatrix} (\sigma_v^2 \Delta t + \frac{1}{3} \sigma_u^2 \Delta t^3) I_{3 \times 3} & -(\frac{1}{2} \sigma_u^2 \Delta t^2) I_{3 \times 3} & 0_{3 \times 3} \\ -(\frac{1}{2} \sigma_u^2 \Delta t^2) I_{3 \times 3} & (\sigma_u^2 \Delta t) I_{3 \times 3} & 0_{3 \times 3} \\ 0_{3 \times 3} & 0_{3 \times 3} & 0_{3 \times 3} \end{bmatrix}. \quad (5.28)$$

However as aforementioned, this approximation fails in practice for an UKF that is used for the attitude, gyro bias and magnetometer bias estimation. Hence we use the adaptive estimation algorithm for the noise covariance given by (5.24-5.26).

The process noise covariance matrix estimated by (5.26) is a non-diagonal matrix because of the state residual term. So specifically for the attitude estimation problem we modify it such that it fits in the form given as

$$Q = \begin{bmatrix} Q_q I_{3 \times 3} & Q_{q_gb} I_{3 \times 3} \\ Q_{q_gb} I_{3 \times 3} & Q_{gb} I_{3 \times 3} \end{bmatrix}, \quad (5.29)$$

when the attitude and gyro biases are estimated and a form given as

$$Q = \begin{bmatrix} Q_q I_{3 \times 3} & Q_{q_gb} I_{3 \times 3} & 0_{3 \times 3} \\ Q_{q_gb} I_{3 \times 3} & Q_{gb} I_{3 \times 3} & 0_{3 \times 3} \\ 0_{3 \times 3} & 0_{3 \times 3} & Q_{mb} I_{3 \times 3} \end{bmatrix}, \quad (5.30)$$

when the attitude, gyro bias and magnetometer bias are estimated. Here Q_q , Q_{gb} and Q_{mb} are the terms of the process noise covariance matrix which correspond to the attitude quaternion, gyro bias and magnetometer bias respectively and Q_{q_gb} are the terms for the noise covariance in between the quaternion and gyro bias states.

5.1.4. Simulation Results for Process Noise Covariance Estimation

In this section, the proposed AUKF algorithm with process noise covariance estimation is tested via simulations for the nanosatellite model. Two scenarios have been taken into consideration: In the first one, only the attitude and gyro bias terms are estimated and in the second one, the magnetometer biases are also included into the estimated state vector. The main aim of realizing the first scenario is to test the converged values of the process noise covariance in a case that we have its analytical approximation. In this sense same scenarios are also performed with the regular UKF algorithm which uses the analytically approximated process noise covariance matrix. For the specific gyro characteristics the analytically approximated process noise covariance matrix becomes

$$Q = \begin{bmatrix} (8.46E-14)I_{3 \times 3} & -(1.305E-21)I_{3 \times 3} \\ -(1.305E-21)I_{3 \times 3} & (2.61E-20)I_{3 \times 3} \end{bmatrix}, \quad (5.31)$$

$$Q = \begin{bmatrix} (8.46E-14)I_{3 \times 3} & -(1.305E-21)I_{3 \times 3} & 0_{3 \times 3} \\ -(1.305E-21)I_{3 \times 3} & (2.61E-20)I_{3 \times 3} & 0_{3 \times 3} \\ 0_{3 \times 3} & 0_{3 \times 3} & 0_{3 \times 3} \end{bmatrix}, \quad (5.32)$$

for two different scenarios, respectively.

The simulation parameters such as the initial attitude errors and orbital parameters for the spacecraft are same as they are given in Section 4.3. For the low-pass filtering given with (5.26) γ is taken as $\gamma = 0.01$ in both scenarios.

A. When the AUKF is used for Attitude and Gyro Bias Estimation

In this scenario two different UKFs are examined for the attitude and gyro bias estimation. The first one uses the analytically approximated covariance matrix (5.31) and labeled as UKF_a in the graphs. The second one is the AUKF that tunes the covariance matrix by the use of the proposed process noise covariance estimation algorithm.

Fig. 5.3 gives the Euclidean norm for the attitude estimation errors in terms of the Euler angles. The mean of 10 different runs for each filter is plotted in the figure. It is clear that the AUKF and the UKF with the analytically approximated covariance show similar performance. Nonetheless, if we examine the converged values for the elements of the adaptively estimated process noise covariance matrix (5.33) we see that the difference between these values and the analytically calculated values is not high (comparing matrices given with 5.31 and 5.33). We think that such difference (especially for non-diagonal

terms) might be caused by the computational errors and yet the matrix given with (5.31) is an approximation found under some assumptions, not an exact equivalent. Moreover, regarding the simulation results we can state that a difference in such order does not have a significant effect on the accuracy of the estimation and the performance of two filters are at the same level.

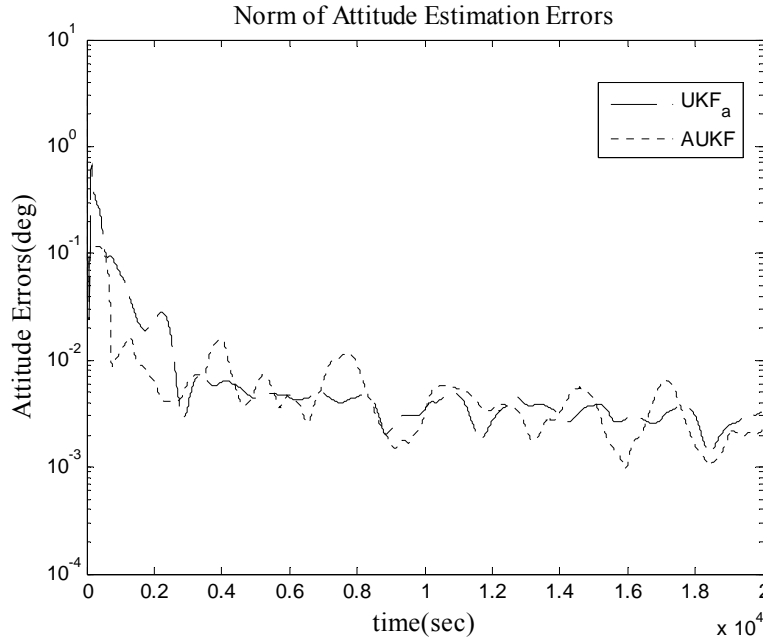


Figure 5.3: Norm of the attitude estimation errors for the UKF_a and AUKF in case where attitude and gyro biases are estimated.

$$\hat{Q}_{adap} = \begin{bmatrix} 5.440E-11 & 0 & 0 & -4.824E-14 & 0 & 0 \\ 0 & 4.630E-10 & 0 & 0 & -6.031E-14 & 0 \\ 0 & 0 & 1.785E-10 & 0 & 0 & -1.127E-14 \\ -4.824E-14 & 0 & 0 & 7.160E-17 & 0 & 0 \\ 0 & -6.031E-14 & 0 & 0 & 7.989E-18 & 0 \\ 0 & 0 & -1.127E-14 & 0 & 0 & 1.322E-17 \end{bmatrix}. \quad (5.33)$$

Fig. 5.4 gives the Euclidean norm of the gyro bias estimation errors. The results for the estimation of the gyro biases are similar and it shows that the AUKF with process noise covariance estimation performs well in a similar manner with the UKF_a. As a result we may state that the AUKF approach for tuning the process noise covariance provides similar results with an UKF that is analytically tuned. That shows us the method works well and it tunes the terms of the process noise covariance matrix such that the filter gives estimates close to the optimal accuracy.

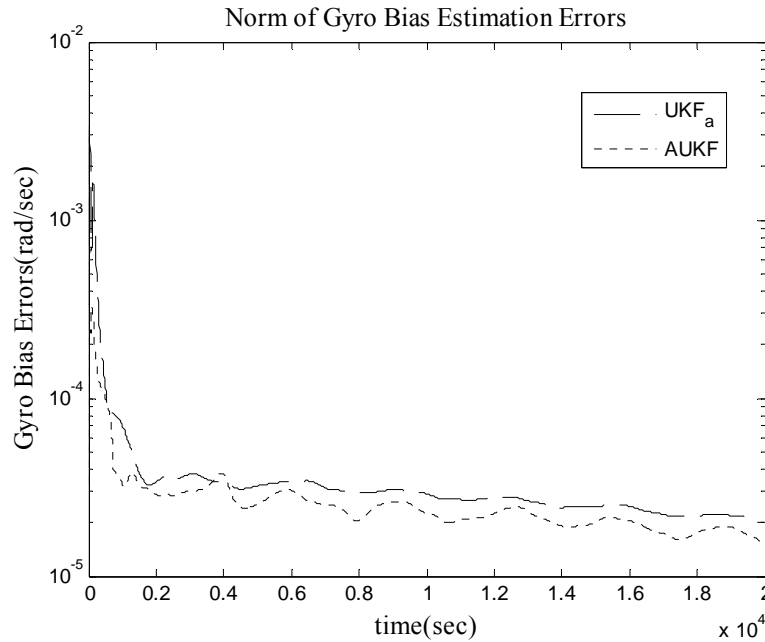


Figure 5.4: Norm of the gyro bias estimation errors for the UKF_a and AUKF in case where attitude and gyro biases are estimated.

B. When the AUKF is used for Attitude, Gyro Bias and Magnetometer Bias Estimation

In this scenario initially two different UKFs are examined for the attitude, gyro bias and magnetometer bias estimation. The first one uses the analytically approximated covariance matrix such as (5.32) and labelled as UKF_a in the graphs. The second one is the AUKF that tunes the covariance matrix by the use of the proposed covariance estimation algorithm.

Fig. 5.5 and 5.6 give the norm of the attitude and gyro bias estimation errors respectively. The mean of 10 different runs for each filter are presented. As seen, this time the AUKF gives better estimation results than the UKF with the analytically approximated process noise covariance matrix and actually the results obtained by UKF_a are far from being accurate. As discussed the main reason for such estimation characteristics is assuming that the process noise covariance for the magnetometer biases is zero. That means we have perfect initial guess for the magnetometer biases and the filter shall trust the propagation model more than the incoming measurements. The magnetometer bias estimation results also support this statement and clearly show that the UKF_a is incapable of estimating these parameters (Fig. 5.7).

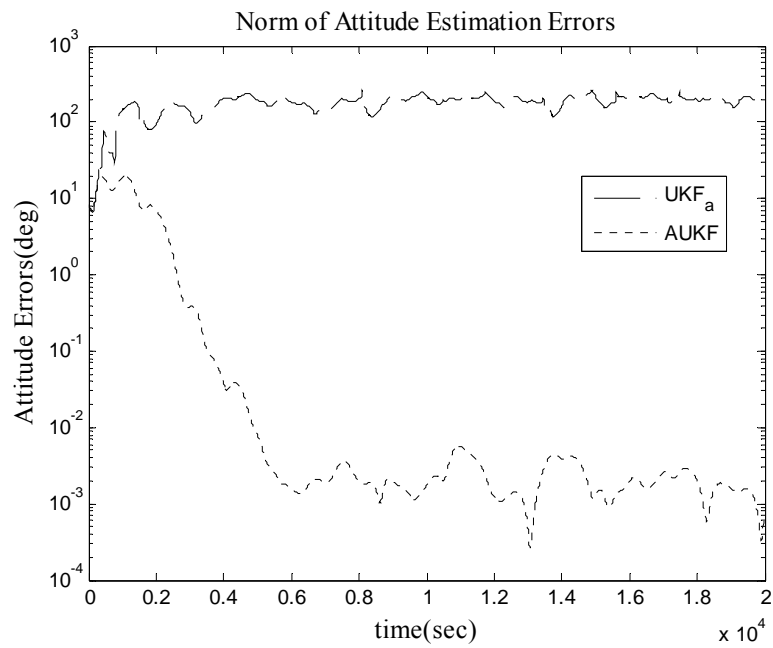


Figure 5.5: Norm of the attitude estimation errors for the UKF_a and AUKF in case where attitude, gyro biases and magnetometer biases are estimated.

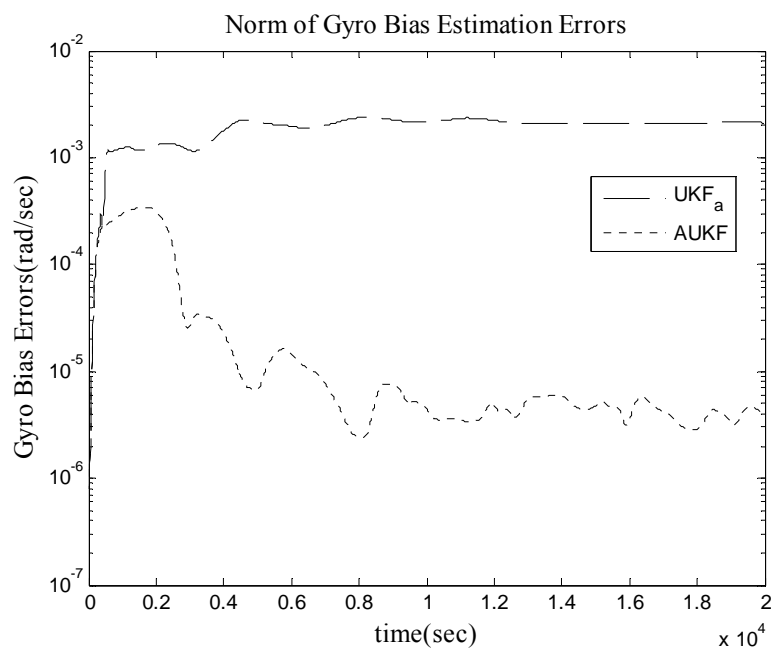


Figure 5.6: Norm of the gyro bias estimation errors for the UKF_a and AUKF in case where attitude, gyro biases and magnetometer biases are estimated.

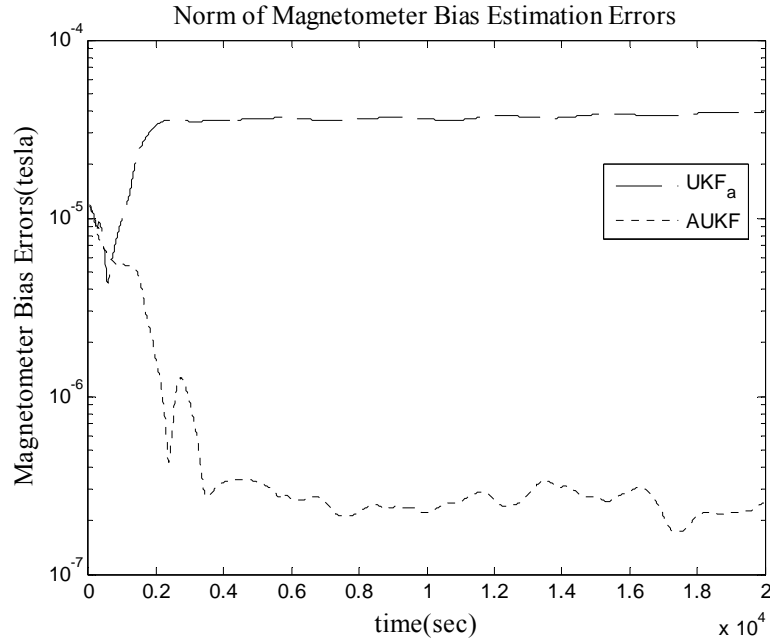


Figure 5.7: Norm of the magnetometer bias estimation errors for the UKF_a and AUKF in case where attitude, gyro biases and magnetometer biases are estimated.

The converged values for the terms of the Q matrix (5.34) shows us the values that correspond to the attitude and gyro bias states differ from the first scenario's results and the analytically approximated values. Besides, obviously the elements that correspond to the magnetometer biases are not zero in contrast with the analytical approximation.

$$\hat{Q}_{adapt} = \begin{bmatrix} 2.015E-7 & 0 & 0 & -1.047E-10 & 0 & 0 & 0 & 0 & 0 \\ 0 & 4.956E-7 & 0 & 0 & -1.757E-10 & 0 & 0 & 0 & 0 \\ 0 & 0 & 2.385E-7 & 0 & 0 & -9.987E-11 & 0 & 0 & 0 \\ -1.047E-10 & 0 & 0 & 1.178E-13 & 0 & 0 & 0 & 0 & 0 \\ 0 & -1.757E-10 & 0 & 0 & 8.214E-14 & 0 & 0 & 0 & 0 \\ 0 & 0 & -9.987E-11 & 0 & 0 & 6.573E-14 & 0 & 0 & 0 \\ 0 & 0 & 0 & 0 & 0 & 0 & 7.515E-18 & 0 & 0 \\ 0 & 0 & 0 & 0 & 0 & 0 & 0 & 1.000E-17 & 0 \\ 0 & 0 & 0 & 0 & 0 & 0 & 0 & 0 & 6.568E-18 \end{bmatrix} \quad (5.34)$$

For the second scenario we run additional simulations assuming that we have the perfect initial guess for the magnetometer biases. In other words, the initial error for the magnetometer bias estimations was taken as zero in the filter algorithm while the initial attitude error kept as similar with the first case. As Fig.5.8 shows even in this case the UKF_a estimations do not converge to the real values. The results for the attitude and gyro bias estimation are similar. Further investigations show that the UKF_a may perform well only if we have the perfect initial guess for all the estimated parameters (such as zero initial

attitude, gyro and magnetometer bias error). However this is simply contradictory with the nature of the filtering concept since we use the UKF to estimate the parameters for which we usually have poor *a priori* knowledge, specifically the parameters like sensor bias.

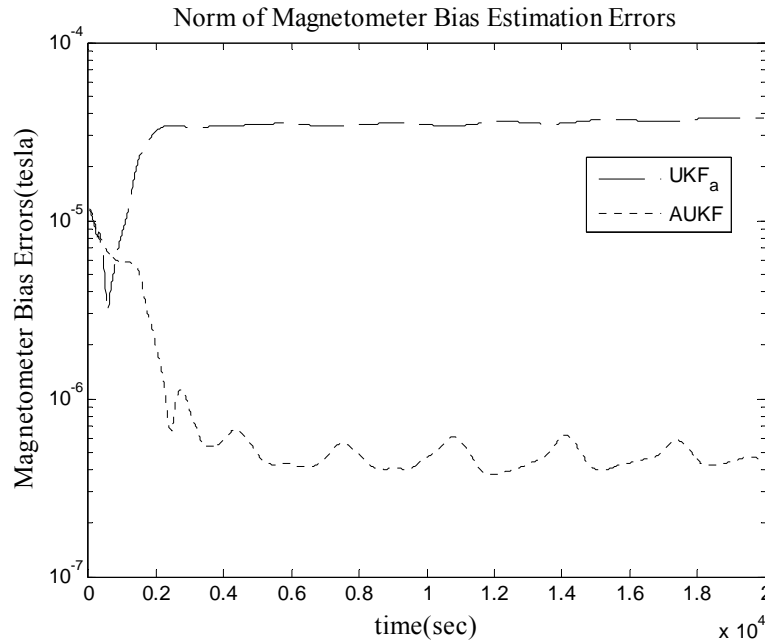


Figure 5.8: Norm of the magnetometer bias estimation errors for the UKF_a and AUKF in case where attitude, gyro biases and magnetometer biases are estimated (zero initial error for magnetometer biases).

Now we already proved that the analytical approximation for calculating the process noise covariance is not usable when we perform in-orbit magnetometer calibration. On the other hand our intention was to find a proper algorithm where the Q is tuned automatically in order to provide more accurate results than a filter tuned by the trial-error method. As a result the overall system performance for the UKF used for attitude estimation and in-orbit gyro and magnetometer estimation would increase. Hence we need to compare the results of the AUKF with the results of the UKF, which were presented in Section 4.3.

In Fig. 5.9 the pitch angle estimation errors for these two filters are given. As seen the accuracy for the attitude estimation is significantly increased when the AUKF algorithm is used. That is an outcome of running the filter with the proper process noise covariance matrix. This is also clear in the results for magnetometer bias estimation (Fig. 5.10). As a matter of fact the main reason for the better attitude estimation accuracy is the increase in the magnetometer bias estimation performance when the AUKF is used. Moreover there is a visible improvement in the convergence speed of the filter.

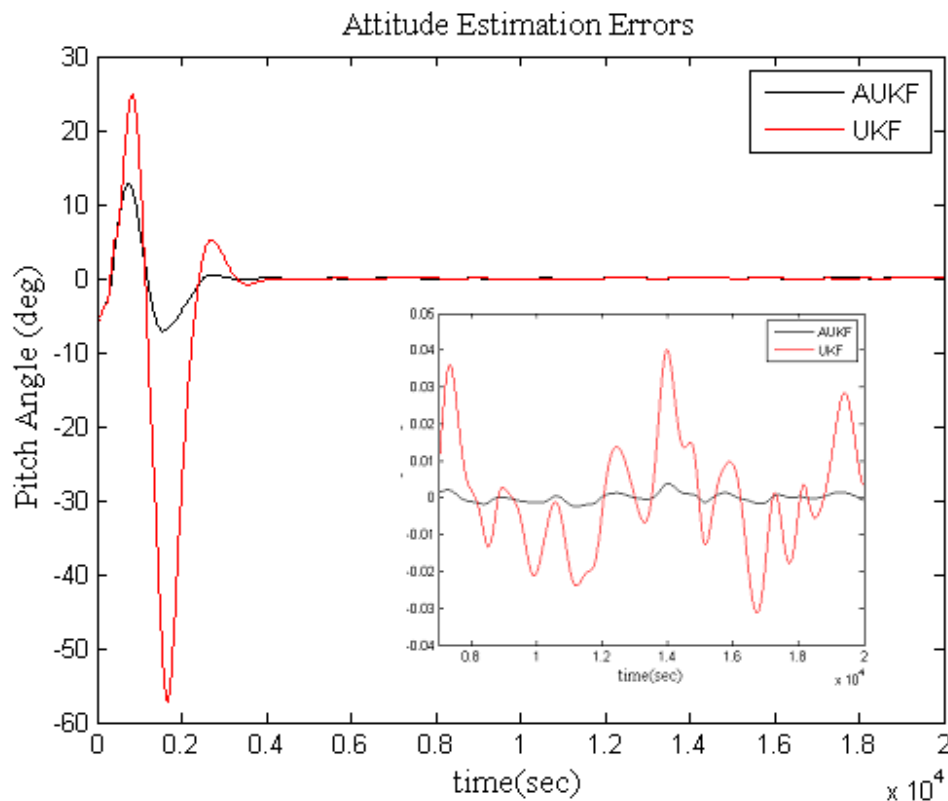


Figure 5.9: Pitch angle estimation error for attitude, gyro and magnetometer bias estimation scenario. Results for the UKF tuned by trial and error method are given with red line and the results for the AUKF are given with black line.

In conclusion, although analytical approximation for the process noise covariance matrix gives sufficiently accurate estimation results for the case we use the UKF for estimation of attitude and gyro biases, such method fails when we include terms constant in time into the state vector, such as magnetometer biases. On the other hand, it is always possible to tune the filter by trial-error method but it is a time consuming and difficult process. The proposed adaptive tuning method and so the AUKF algorithm is considerably simpler. If we compare the AUKF with the filter that uses analytically approximated covariance, when such approximation is possible (as in the first scenario), we see that both filters give similar results. Therefore we may state that the given adaptation method is an easy way of tuning the filter especially in the absence of any analytical approximation for the calculation of Q matrix and by using the AUKF it is possible to get accurate estimation results close to the optimality.

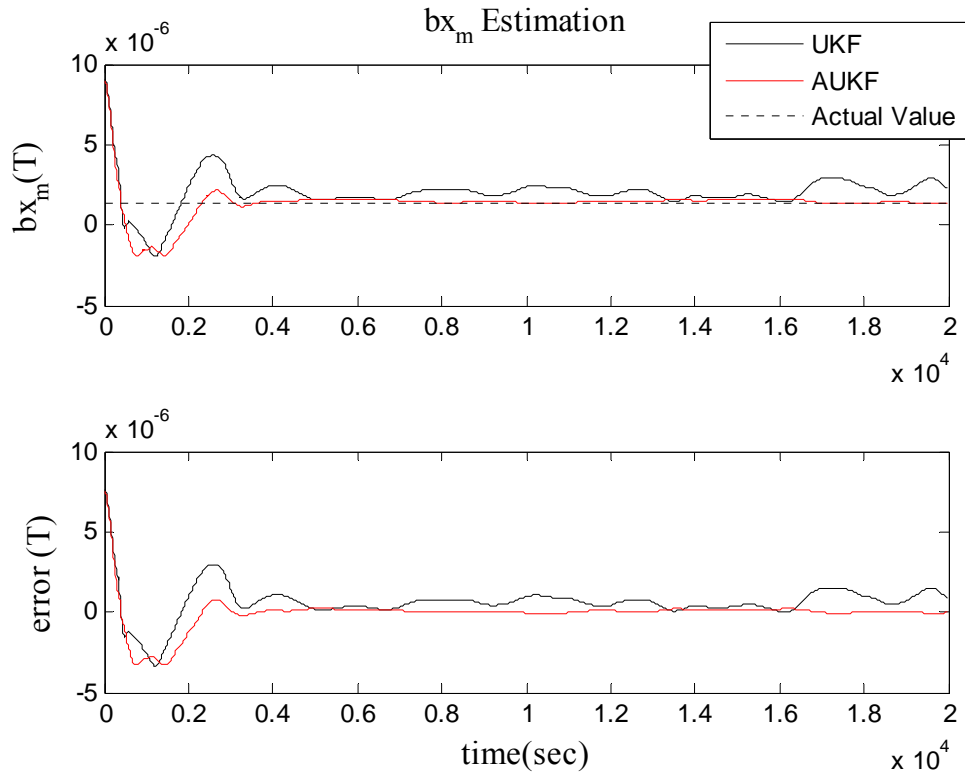


Figure 5.10: Estimation of the bias for the magnetometer aligned in the x axis for attitude, gyro and magnetometer bias estimation scenario. Results for the UKF tuned by trial and error method are given with black line and the results for the AUKF are given with red line.

5.2. Robust UKF against Measurement Malfunctions

For nanosatellite missions the interaction between the subsystems is higher than usual because of the compactness of the satellite. Besides, the external disturbances such as the ionospheric currents have noteworthy effects on the spacecraft. These facts may cause the magnetometers to give faulty measurements. Such faulty measurements affect the stability and accuracy of the UKF even when they last for few samples.

The UKF work accurately when there is no fault in the measurement system. On the contrary, in case of a fault such as abnormal measurements, step-like changes or sudden shifts in the measurement channel etc. the filter deteriorates and the estimation outputs become faulty.

Therefore, a robust algorithm must be introduced such that the filter is insensitive to the measurements in case of malfunctions and the estimation process is corrected without affecting the remaining good estimation behavior.

The robustness of the filter is secured by scaling the measurement noise covariance matrix in case of fault. In this sense two different approaches may be used: Scaling by a single scale factor or scaling by a scale matrix built of multiple scale factors. In general, despite its relative simplicity, using single scale factor is not a healthy procedure since the filter should be insensitive just to the measurements of the faulty sensor, not to the all sensors including the ones working properly (Soken and Hajiyev 2010). In contrast a matrix built of multiple scale factors might be preferred since in this method the relevant terms of the measurement noise covariance are fixed, individually.

The robust algorithm affects characteristic of the filter only when the condition of the measurement system does not correspond to the model used in the synthesis of the filter. Otherwise the UKF work with the regular algorithm.

The essence of the adaptation procedure against the measurement malfunctions is to compare the real and theoretical values of the innovation covariance matrix. When there is a sensor fault in the system, the real error will exceed the theoretical one. In this case we may ensure the robustness of the filter against the sensor fault by adapting the R matrix, which is a diagonal matrix, formed of the measurement process noise covariances. The adaptation procedure basically aims at finding an appropriate multiplier for the R, such that the real and theoretical values of the innovation covariance match. As discussed, this multiplier might be either as a single factor or a matrix formed of multiple factors. In case we use a single factor, matching the real and theoretical values of the innovation covariance means that we basically increase all the terms of the R matrix and impose to the UKF that the measurements are faulty. However we do not isolate which sensor is malfunctioning. On the contrary when we use multiple scale factors we correct the necessary term of the R matrix (the term which corresponds to the sensor with the faulty measurement). In other word we make the UKF disregard just the measurements of the faulty sensor.

5.2.1. Adaptation Using Single Scale Factor

As stated the essence of the adaptation is the covariance matching. For single scale factor approach we match the trace of the covariances such that

$$\text{tr} \left[e(k+1) e^T(k+1) \right] = \text{tr} \left[P_{yy}(k+1|k) + S_s(k) R(k+1) \right], \quad (5.35)$$

where $P_{yy}(k+1|k)$ is the observation covariance, $R(k+1)$ is the measurement noise covariance and $S_s(k)$ is the introduced single scale factor. We may rewrite the equation as

$$\text{tr}[e(k+1)e^T(k+1)] = \text{tr}[P_{yy}(k+1|k)] + S_s(k)\text{tr}[R(k+1)]. \quad (5.36)$$

Then, regarding $\text{tr}[e(k+1)e^T(k+1)] = e^T(k+1)e(k+1)$ the single scale factor can be obtained

$$S_s(k) = \frac{e^T(k+1)e(k+1) - \text{tr}[P_{yy}(k+1|k)]}{\text{tr}[R(k+1)]}. \quad (5.37)$$

The scale factor affects the Kalman gain as;

$$K(k+1) = P_{xy}(k+1|k)[P_{yy}(k+1|k) + S_s(k)R(k+1)]^{-1}. \quad (5.38)$$

Here $K(k+1)$ is the Kalman gain and $P_{xy}(k+1|k)$ is the cross correlation matrix.

In case of sensor fault the scalar scale factor will take a larger value and that will increase all terms of the innovation covariance. Eventually the Kalman gain will decrease and the measurements will be disregarded in the state update process (or taken into consideration with lesser weight than the regular case). In such approach the information about the faulty sensor isolation does not have any significance; all of the current information from the measurements is left out and the UKF relies mostly on the propagation information during the estimation.

5.2.2. Adaptation Using Multiple Scale Factors

Firstly, we add a matrix built of multiple scale factors, $S_m(k)$, into the algorithm in order to tune the measurement noise covariance matrix and match the real and theoretical innovation covariances,

$$\frac{1}{\xi} \sum_{j=k-\xi+1}^k e(j+1)e^T(j+1) = P_{yy}(k+1|k) + S_m(k)R(k+1). \quad (5.39)$$

Here, ξ is the width of the moving window. Left hand side of the equation represents the real innovation covariance while the right hand side stands for the theoretical innovation covariance. Then, if we re-arrange the equation, it is clear that we can get the scale matrix by,

$$S_m(k) = \left\{ \frac{1}{\xi} \sum_{j=k-\xi+1}^k \mathbf{e}(j+1)\mathbf{e}^T(j+1) - P_{yy}(k+1|k) \right\} R^{-1}(k+1). \quad (5.40)$$

In case of a measurement fault for one of the sensors then the corresponding term of the scale matrix will be a relatively larger term and that will increase the measurement noise covariance of this sensor in the R matrix. Eventually this faulty measurement will be disregarded (or regarded with a lower gain) by the filter. On the other hand, the scale matrix affects the estimation procedure only when the measurements are faulty. Otherwise, in case of normal operation, the scale matrix will be a unit matrix as $S_m(k) = I_{z \times z}$, where z is the size of the innovation vector.

Nonetheless, as ξ is a limited number because of the number of the measurements and the computations performed with the computer implies errors such as the approximation and round off errors; $S_m(k)$ matrix that is calculated by the use of (5.40) may not be diagonal and may have diagonal elements which are “negative” or lesser than “one”. $S_m(k)$ matrix should be diagonal because only its diagonal terms have significance on the adaptation since each diagonal term corresponds to the noise covariance of each measurement (for the adaptation procedure $S_m(k)$ matrix is multiplied with the diagonal R matrix). Besides the measurement noise covariance matrix must be positive definite (that is why the multiplier $S_m(k)$ matrix cannot have negative terms) and also any term of this matrix cannot decrease in time for this specific problem since there is no possibility for increasing the performance of the onboard sensor (that is why the multiplier $S_m(k)$ matrix cannot have terms less than one).

Therefore, in order to avoid such situations, composing the scale matrix by the following rule is suggested:

$$S^* = \text{diag}(s_1^*, s_2^*, \dots, s_z^*) \quad (5.41)$$

$$s_i^* = \max\{1, S_{ii}\} \quad i = 1, z. \quad (5.42)$$

Here, S_{ii} represents the i^{th} diagonal element of the matrix $S_m(k)$. Apart from that point, if the measurements are faulty, $S^*(k)$ will change and so affect the Kalman gain as;

$$K(k+1) = P_{xy}(k+1|k) \left[P_{yy}(k+1|k) + S^*(k)R(k+1) \right]^{-1}. \quad (5.43)$$

In case of any kind of malfunction, the element(s) of the scale matrix, which corresponds to the faulty component(s) of the innovation vector, increases and so the terms in the related column(s) of the Kalman gain decreases. As a consequence, the effect of the faulty innovation term on the state update process reduces and accurate estimation results can be obtained even in case of measurement malfunctions.

5.2.3. Fault Detection Procedure

As aforementioned, we use the RUKF only in case of the fault and in all other cases, the filter run following its regular algorithms. The fault detection is realized via a kind of statistical information. In order to achieve that, following two hypotheses may be proposed:

- γ_0 ; the system is normally operating
- γ_1 ; there is a malfunction in the estimation system.

Then we may introduce the following statistical functions for the RUKF

$$\beta(k) = \mathbf{e}^T(k+1) \left[P_{yy}(k+1|k) + R(k+1) \right]^{-1} \mathbf{e}(k+1), \quad (5.44)$$

This function has χ^2 distribution with z degree of freedom, where z is the dimension of the innovation vector.

If the level of significance, α , is selected as,

$$P\{\chi^2 > \chi_{\alpha,z}^2\} = \alpha; \quad 0 < \alpha < 1, \quad (5.45)$$

the threshold value, $\chi_{\alpha,z}^2$ can be determined. Hence, when the hypothesis γ_1 is correct, the statistical value of $\beta(k)$ will be greater than the threshold value $\chi_{\alpha,s}^2$, i.e.:

$$\begin{aligned} \gamma_0 : \beta(k) &\leq \chi_{\alpha,s}^2 && \forall k \\ \gamma_1 : \beta(k) &> \chi_{\alpha,s}^2 && \exists k \end{aligned} \quad (5.46)$$

5.2.4. Simulation Results

A series of simulations were performed in order to test and compare the proposed RUKF algorithms. For just this simulation case in order to understand the affects of using single or multiple scale factors it is assumed that the sensors are fully calibrated. After deciding

the proper adaptation method the results will be applied to the UKF for attitude estimation and sensor calibration, which has been discussed so far.

The simulations are performed for 7000seconds for the nanosatellite for which the orbital parameters and the sensor characteristics were given before in Section 4.3.

The initial attitude errors in the simulations are set to 50 degrees for all three axes. Besides, the initial value of the covariance matrix is taken as $P_0 = \text{diag}[0.5 \ 0.5 \ 0.5 \ 10^{-4} \ 10^{-4} \ 10^{-4}]$ while the process noise covariance matrix is selected as $Q = \text{diag}[10^{-7} \ 10^{-7} \ 10^{-7} \ 10^{-12} \ 10^{-12} \ 10^{-12}]$. For the RUKF with multiple scale factors the size of the moving window is taken as $\xi = 30$.

Nonetheless, for the fault detection procedure, $\chi_{\alpha,z}^2$ is taken as 7.81 and this value comes from chi-square distribution when the degree of freedom is 3 and the reliability level is 95%.

Three different scenarios are taken into consideration for simulating the fault in the measurements; the continuous bias, fault of zero output and measurement-noise increment. For each scenario a series of simulations are run by the RUKF and as well the conventional UKF algorithm.

A. Continuous Bias Failure

In this scenario, a constant value is added to the measurements of the magnetometer aligned in the x axis between the 3000th and 3200th seconds for a period of 200 seconds such that;

$$B_x(\mathbf{q}, t) = B_x(\mathbf{q}, t) + 20000nT \quad t = 3000 \dots 3200 \text{sec}.$$

The constant term, selected as $20000nT$, almost doubles the magnetometer output.

In Fig.5.11 the attitude estimation error of the UKF and RUKF are given for the pitch angle. The RUKF that uses single scale factor is plotted with dotted line and labeled as RUKF_s while the RUKF with multiple scale factors is plotted with dashed line and labeled as RUKF_m. Apparently, in case of fault the estimation accuracy for the conventional UKF algorithm deteriorates. The RUKF with single scale factor lessens the effect of the fault but still the filter is not fully recovered and after the measurement fault ends at 3200th sec. the RUKF_s estimations show a fluctuating behavior. Because the RUKF_s disregards the measurements of all three magnetometers as it increases all terms of the R matrix via multiplication with a single large scale factor (see Fig.5.12 for the variation of the single

scale factor). Instead of isolating the faulty sensor and leaving out just its measurements, the RUKF_s considers all of the measurements as faulty and throughout this period it mostly relies on the propagation values. In this case especially for a filter with relatively higher process noise covariance, Q , the estimation errors accumulate and the filter starts to diverge from the actual values. The Table 5.1, which gives the absolute values of error at 3050th and 3150th seconds, supports this interpretation. Clearly the estimation error for the RUKF_s at the 3150th sec is higher than the one at the 3050th sec. Hence the single scale factor approach may be useful only for faults which lasts a short period. On the contrary the RUKF with the multiple scale factors does not have such limitation and keeps its estimation accuracy without being affected from the fault. An examination on the scale matrix at an instant between the 3000th and 3200th seconds of the simulation shows that the algorithm works properly; $S^* = \text{diag}(4427 \ 1 \ 1.59)$. Since the fault is in the measurements of the magnetometer aligned in the x axis, the correction must be applied to the first term of the R matrix as in this case. The large first diagonal term of the scale matrix decreases the terms in the first column of the Kalman gain and so the faulty innovation term (the first term of the innovation vector) is disregarded in the state update process.

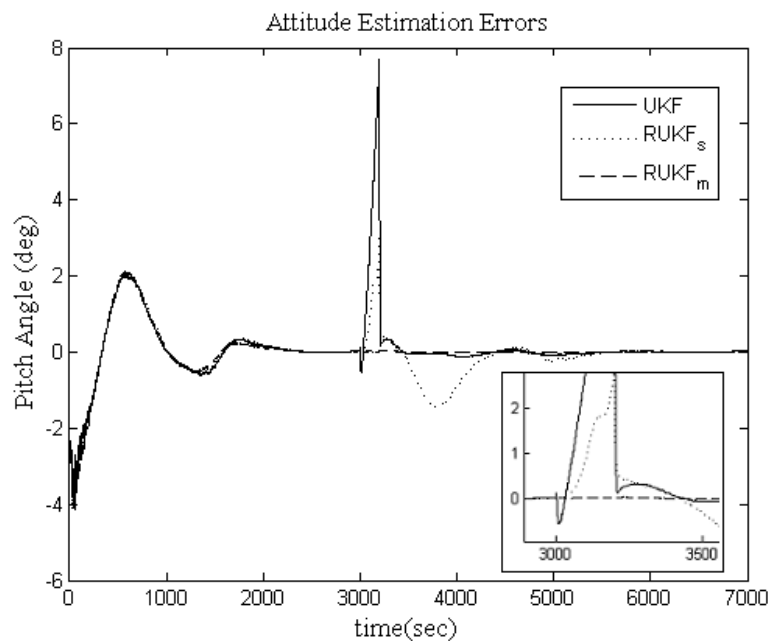


Figure 5.11: Pitch angle estimation error for the UKF and RUKF in case of continuous bias.

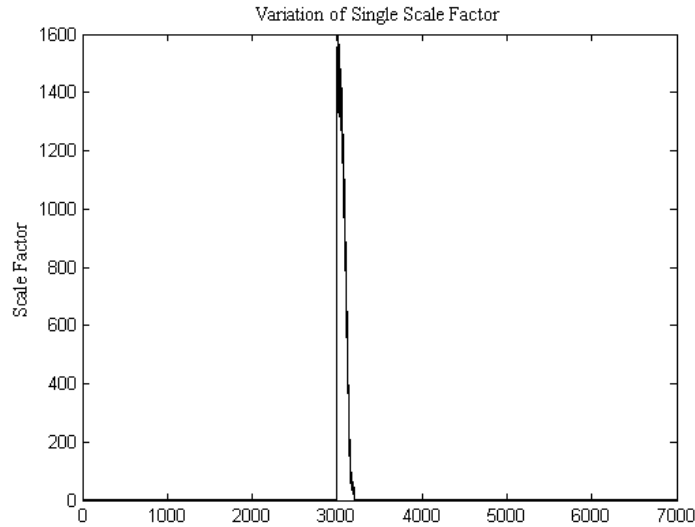


Figure 5.12: Variation of the single scale factor for the RUKF in case of continuous bias.

Table 5.1: Absolute estimation errors in case of continuous bias: Regular UKF, RUKF with single scale factor (SSF) and RUKF with multiple scale factor (MSF).

Parameter	Abs. Err. Values for Regular UKF		Abs. Err. Values for RUKF with SSF		Abs. Err. Values for RUKF with MSF	
	3050 s.	3150 s.	3050 s.	3150 s.	3050 s.	3150 s.
φ (deg)	10,580	10,835	0,1901	0,4936	0,0207	0,0430
θ (deg)	0,6945	5,1327	0,1116	1,8268	0,0033	0,0178
ψ (deg)	0,6131	0,8453	0,0862	2,6225	0,0041	0,0030

B. Measurement Noise Increment Failure

In this scenario, the measurement noise of the magnetometer aligned in x axis is multiplied with a constant between the 3000th and 3200th seconds for a period of 200 seconds. In fault case the standard deviation of this magnetometer becomes $\sigma_{m_x}^f = 300 \times 100nT$.

In Fig.5.13, the estimation results for the UKF and RUKF are given. As can be observed, again the UKF fails about giving accurate estimation results in case of fault and the noisy measurements make the estimations deteriorate for a longer period than the fault itself. For this simulation case it takes 3000 seconds for the filter to satisfy accuracy less than 0.1 deg. after the fault removes. On the other hand in case of measurement noise increment both

approaches for robust Kalman filtering that are scaling with single and multiple factors give accurate estimation results. Unlike the first fault case this time single scale factor works properly because of the fault's characteristic. Since the noise in the measurements is random, the filter does not work continuously with the robust algorithm for the whole 200 seconds. Moreover the scale factor may take values that are closer to one when the robust algorithm is running. In other words the filter tunes itself depending on the magnitude of the noise and does not disregard the measurements for the whole fault period; it only does when the $\chi^2_{\alpha,z}$ threshold is exceeded and the magnitude of the noise is high such that the scale factor takes large values. Variation of the single scale factor confirms that (Fig. 5.14). Hence specifically for this fault scenario the RUKF_s and RUKF_m do not have any significant difference in the sense of estimation accuracy (Table 5.2).

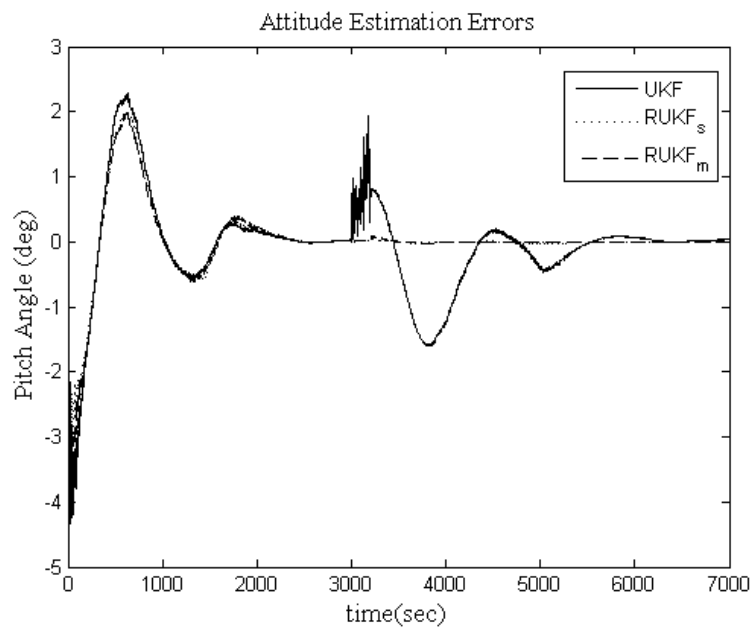


Figure 5.13: Pitch angle estimation error for the UKF and RUKF in case of measurement noise increment.

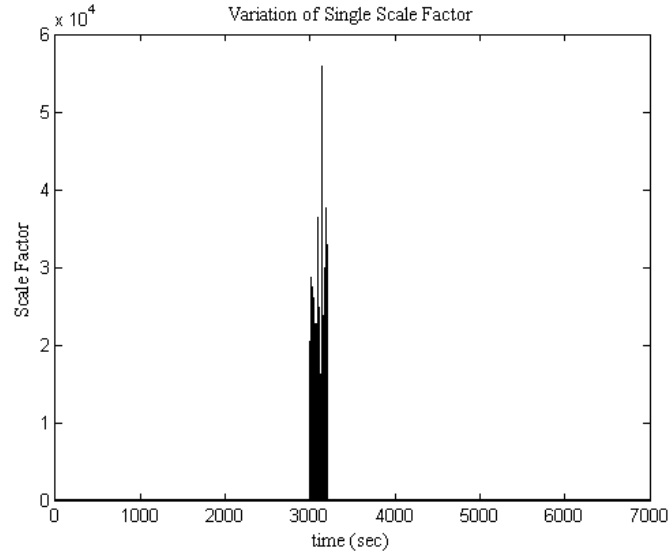


Figure 5.14: Variation of the single scale factor for the RUKF in case of measurement noise increment.

Table 5.2: Absolute estimation errors in case of measurement noise increment: Regular UKF, RUKF with single scale factor (SSF) and RUKF with multiple scale factor (MSF).

Parameter	Abs. Err. Values for Regular UKF		Abs. Err. Values for RUKF with SSF		Abs. Err. Values for RUKF with MSF	
	3050 s.	3150 s.	3050 s.	3150 s.	3050 s.	3150 s.
φ (deg)	3,4186	4,3199	0,0010	0,0242	0,0269	0,0412
θ (deg)	0,2853	1,3830	0,0134	0,0048	0,0062	0,0174
ψ (deg)	0,9533	0,9003	0,0026	0,0049	0,0017	0,0015

C. Zero Output Failure

The third failure case, which is fault of zero output, is simulated by simply making the measurement output of one of the magnetometers zero so it measures $0nT$ for 200 seconds between the 3000th and 3200th seconds. In order to test the algorithm this time the fault is implemented to the magnetometer aligned in the z axis:

$$B_z(\mathbf{q}, t) = 0 + \eta_{1z} \quad t = 3000 \dots 3200 \text{ sec.}$$

In Fig.5.15 the estimation results for the UKF and RUKF are given. Obviously, same as the first simulation scenario, the UKF cannot achieve accurate estimation whereas the RUKF with the single scale factor can overcome the fault only for a short period. Because of taking none of the measurements into consideration the RUKF_s estimations get worse when the robust algorithm runs longer than 50 seconds. The single scale factor behaves in a similar manner with its trend for the continuous bias fault scenario (Fig. 5.16). Moreover, the results show us when the filter is not robust, the zero output failure has a high detractive impact on the estimation accuracy that lasts for a very long period. Even though the filter's response may vary when it is designed with different parameters (such as the Q matrix) simulations show that a fault may affect the filter for a longer period than its length. Therefore if the magnetometer measures 0 even for just few seconds, it is not possible to compensate that with a filter other than the robust ones. In this sense the estimation results for the RUKF_m clearly signify the importance of using the proposed algorithm. The RUKF_m is not affected from the fault and can perform accurate estimation even when the fault lasts long, by simply disregarding the measurements of the faulty magnetometer and working on the basis of the measurements from two properly operating magnetometers (Table 5.3 may be seen for further examination). The sample for the multiple scale factors in case of fault validates that the RUKF_m disregards the measurements of the magnetometer aligned in the z axis as it supposed to be $S^* = \text{diag}(1.44 \quad 1 \quad 4024)$.

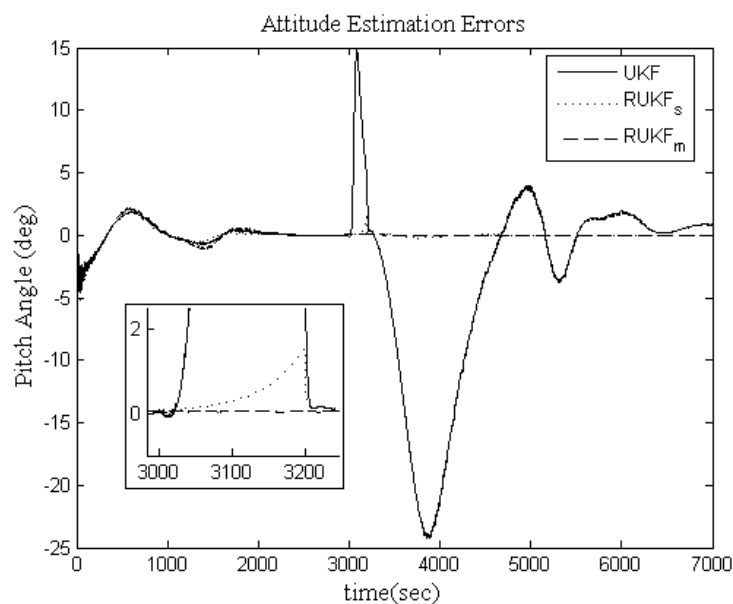


Figure 5.15: Pitch angle estimation error for the UKF and RUKF in case of zero output failure.

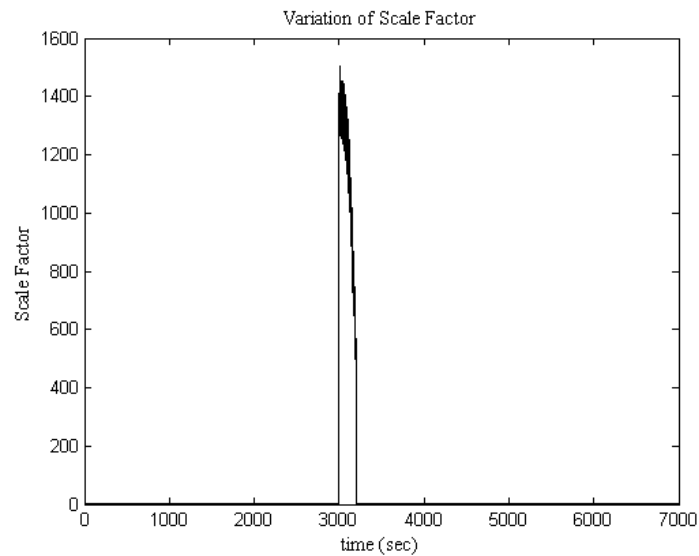


Figure 5.16: Variation of the single scale factor for the RUKF in case of zero output failure.

Table 5.3: Absolute estimation errors in case of zero output failure: Regular UKF, RUKF with single scale factor (SSF) and RUKF with multiple scale factor (MSF).

Parameter	Abs. Err. Values for Regular UKF		Abs. Err. Values for RUKF with SSF		Abs. Err. Values for RUKF with MSF	
	3050 s.	3150 s.	3050 s.	3150 s.	3050 s.	3150 s.
φ (deg)	9,7561	42,492	0,0321	0,2176	0,0892	0,0567
θ (deg)	7,0059	8,1779	0,0293	0,3733	0,0521	0,0576
ψ (deg)	9,6897	41,673	0,0114	0,1908	0,0163	0,0191

In conclusion the simulation results show that the RUKF performs well when a specific measurement fault is the point at issue. On the other hand, the conventional UKF fails at giving accurate estimation results for the period of the fault and as well for some additional time that passes before the filter converges again. When two proposed methods for the adaptation, the RUKF with single scale factor and RUKF with multiple scale factors, are compared, obviously the latter one gives better estimation results under all conditions. Hence we will use the RUKF_m algorithm when the overall attitude estimation scheme is built for the nanosatellite in Chapter 7.

6. The Residual Magnetic Moment Estimation

The RMM is the main disturbance source for nanosatellites and has a high deteriorating effect on the ADCS accuracy as discussed in (Sakai *et al.* 2008; Inamori *et al.* 2009; Steyn and Hashida 2001; Suehiro 2010; Hosonuma *et al.* 2012). In order to increase the accuracy of the magnetorquers based attitude control method first we need to cancel out the disturbance caused by the RMM. An efficient way of doing so is to use a feedforward cancellation technique, and when this technique is used, the performance depends on the accuracy of the RMM estimation. Hence for all the mission phases, as a prerequisite for accurate attitude control, the RMM must be estimated precisely.

In literature there are various recent dated researches discussing about the RMM estimation (Sakai *et al.* 2008; Inamori *et al.* 2009). As a drawback the RMM components are considered to be constant in time. However, in practice, these parameters may change with sudden shifts because of the instantaneous variations in the onboard electrical current. Such instantaneous variations in the current may be caused by switching on/off of the onboard electronic devices or going into/out of eclipse. In such cases, the UKF (or observer in general) cannot catch the new value of the parameter quickly if it is designed with a small process noise covariance in order to increase steady state estimation accuracy. The main issue is, especially if we use the feedforward cancellation technique for the RMM compensation, then, as discussed, the estimation accuracy is essential and so the UKF must be designed with small process noise covariance. In other words, the inherent tracking capacity of the UKF that can be provided by choosing a high process noise covariance must be sacrificed in order to increase the overall system performance. Therefore, if we want to design an UKF with good tracking capability, as well as the high steady state accuracy, then the filter should be adaptively designed such that it gives both good estimation results when there is no change in the parameter and good tracking performance when the parameter is changed.

In this chapter we present an in-orbit RMM estimation method for the nanosatellite. Unlike the existing studies in the literature, unexpected abrupt changes in the RMM are also considered. Regarding the fact that the change in the RMM is unexpected and the amount of the shift cannot be predicted, we propose a novel adaptation method which is applied on the estimation covariance. Sudden shifts in the mean of the RMM terms are detected by a

low pass filter applied to the normalized innovation of the UKF. Then a weighting function is calculated regarding the amount of the shift and the estimation covariance is scaled for the next step using this function. Compared to the standard methods that reinitialize the filter or increase the process noise covariance intuitively after each change detection, the proposed method does not need any a priori information about the magnitude of the shift and assures both accurate estimation and good tracking performance for shifts with different magnitudes. Besides it is simple without any excessive extra computational load.

6.1. In-Orbit Estimation of Time-Varying RMM

For the specific problem, the estimated state vector is composed of the body angular rates with respect to the inertial frame and RMM terms as given with

$$\mathbf{x} = \begin{bmatrix} \boldsymbol{\omega}_{BI} \\ \mathbf{M} \end{bmatrix}. \quad (6.1)$$

For RMM estimation we use a second UKF other than the reduced-order UKF that is run for attitude, gyro bias and magnetometer bias estimation. The integration scheme for these two filters will be given in Chapter 7.

The nonlinear process model is obtained by discrete-time integration of

$$\frac{d\boldsymbol{\omega}_{BI}}{dt} = J^{-1} \left[\mathbf{N}_c + (\mathbf{M}_r \times \mathbf{B}) - \boldsymbol{\omega}_{BI} \times (J \boldsymbol{\omega}_{BI}) \right], \quad (6.2)$$

and (2.45). The (6.2) is the rewritten form of (2.40) for the case where the disturbance torques other than the RMM are negligible. Note that the magnetometers that are carried onboard directly supply the \mathbf{B} information, and now we assume that the magnetometers are calibrated using the technique proposed previously. Besides the body angular rates with respect to the inertial frame, $\boldsymbol{\omega}_{BI}$, are measured using the onboard gyros, which are also in-flight calibrated with the UKF algorithm discussed in the previous chapters.

Nevertheless, since the onboard gyros directly supply $\boldsymbol{\omega}_{BI}$ information, the measurement model may be represented with linear equation as

$$\tilde{\mathbf{y}}_k = \begin{bmatrix} I_{3 \times 3} & \mathbf{0}_{3 \times 3} \end{bmatrix} \mathbf{x}_k + \mathbf{v}_k \quad (6.3)$$

where $I_{3 \times 3}$ and $\mathbf{0}_{3 \times 3}$ are 3×3 identity and null matrices, respectively.

For the magnetometer measurements, which provide \mathbf{B} information for dynamic modeling, the sensor noise is characterized by zero mean Gaussian white noise with a standard deviation of $\sigma_m = 300nT$; whereas, the gyro random error assumed as $\sigma_v = 1 \times 10^{-3} [\text{deg}/\sqrt{h}]$ (these values are same as the sensor values presented in Section 4.3). In the first scenario, where the RMM terms are constant and there is no abrupt change in time, the real RMM terms are $\mathbf{M} = (0.1, 0.02, -0.05) Am^2$ and the process noise covariance matrix of the second UKF is selected as

$$\mathbf{Q} = \begin{bmatrix} (1E-20)I_{3 \times 3} & 0_{3 \times 3} \\ 0_{3 \times 3} & (1E-10)I_{3 \times 3} \end{bmatrix}. \quad (6.4)$$

In Fig.6.1 the estimation result for the RMM in the x axis is presented. In the top plot, the UKF estimation is given together with the actual value of the estimated parameter and in the lower plot the estimation error is shown. As seen the UKF accurately estimates the RMM terms. In order to make a better understanding of the performance the Root Mean Squared Error (RMSE) for the RMM terms of the state vector ($x_j(k)$ such that $j = 4..6$) is calculated in between the 300th and 500th seconds (for 2000 samples since $\Delta t = 0.1\text{sec}$.):

$$RMSE_j = \sqrt{\frac{1}{2000} \sum_{k=300}^{500} [x_j(k) - \hat{x}_j(k)]^2} \quad j = 4..6, \quad (6.5)$$

where $x_j(k)$ and $\hat{x}_j(k)$ are the real and estimated values of the j^{th} state. As a result the RMSE is $2.626 \times 10^{-4} Am^2$, $2.584 \times 10^{-4} Am^2$ and $2.673 \times 10^{-4} Am^2$, respectively for M_x , M_y and M_z estimations. That means the RMM estimation is accurate enough regarding the overall attitude control requirements and the magnetic disturbance can be compensated efficiently with a feed forward cancellation technique.

In the second scenario, this time the instantaneous change is realized as the change in the RMM terms at the 2000th second such that

$$\mathbf{M} = \begin{cases} [0.1 & 0.02 & -0.05]^T Am^2 & t < 2000\text{sec} \\ [0.25 & 0.1 & -0.15]^T Am^2 & t \geq 2000\text{sec} \end{cases} \quad (6.6)$$

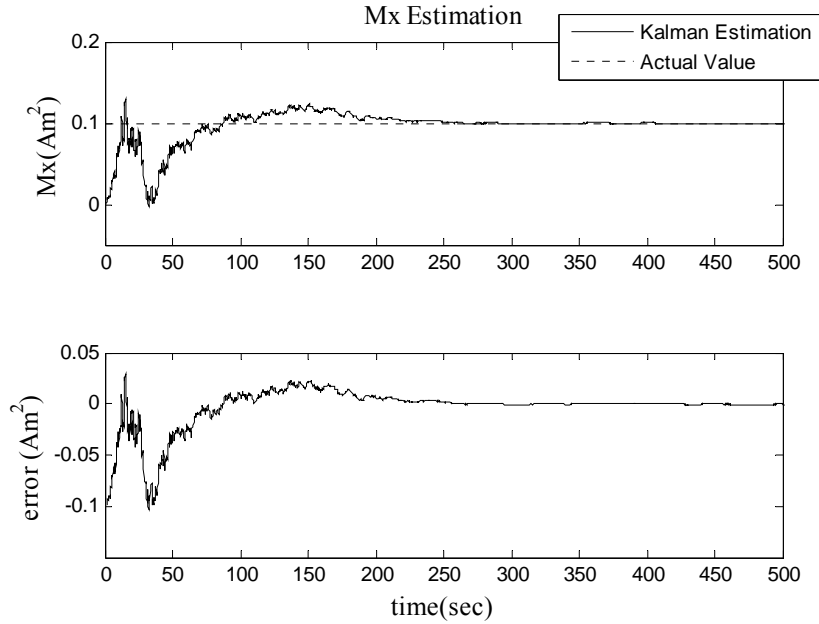


Figure 6.1: Estimation of the RMM in x axis.

and the same scenario is repeated for two different process noise levels, high and low, in order to clearly demonstrate the effect of the process noise covariance on the trade-off between the steady state accuracy and tracking capability of the filter. For low noise level, the Q matrix is selected the same as in (6.4). For high noise, the Q matrix is chosen as

$$Q = \begin{bmatrix} (1E-20)I_{3 \times 3} & 0_{3 \times 3} \\ 0_{3 \times 3} & (1E-6)I_{3 \times 3} \end{bmatrix}. \quad (6.7)$$

The Fig. 6.2 presents the estimation results of the RMM in x axis for these two different noise levels. Obviously, the UKF tuned with low process noise has a poor tracking capability when the estimated parameter is changed and it takes almost one third of the orbital period (the orbital period of the satellite for the performed simulation is 6400sec.) for the filter to converge again to the required estimation accuracy (accepted as $\pm 0.001 Am^2$ for the RMM estimation). Further examinations show that such change in the estimated RMM terms also causes deterioration of the angular rate estimations (Fig.6.3). Conversely, the UKF with high noise is more agile to catch the new values of the RMM terms but performs noisy estimations with low accuracy during the steady-state regime. Table 6.1 shows the absolute estimation error of the filters for three different sampling times.

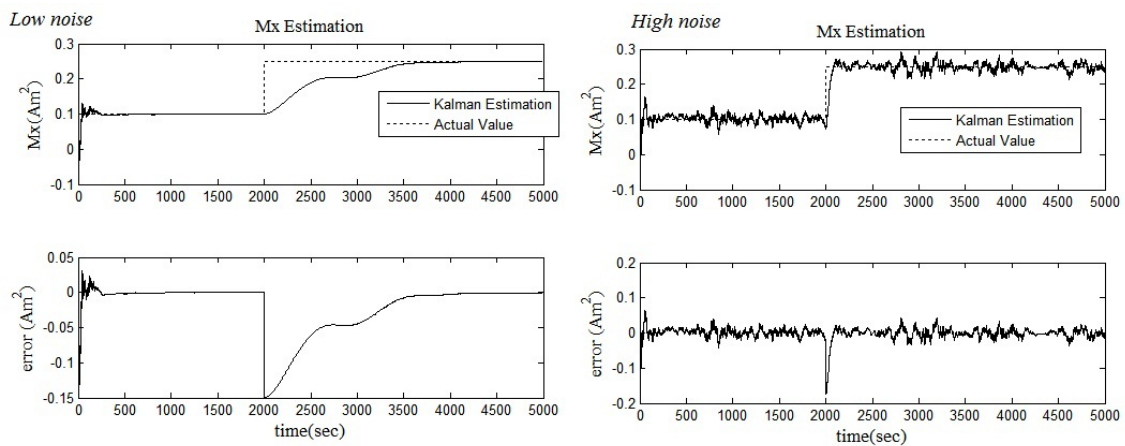


Figure 6.2: Estimation of the RMM in x axis in case of sudden change for two different process noise levels.

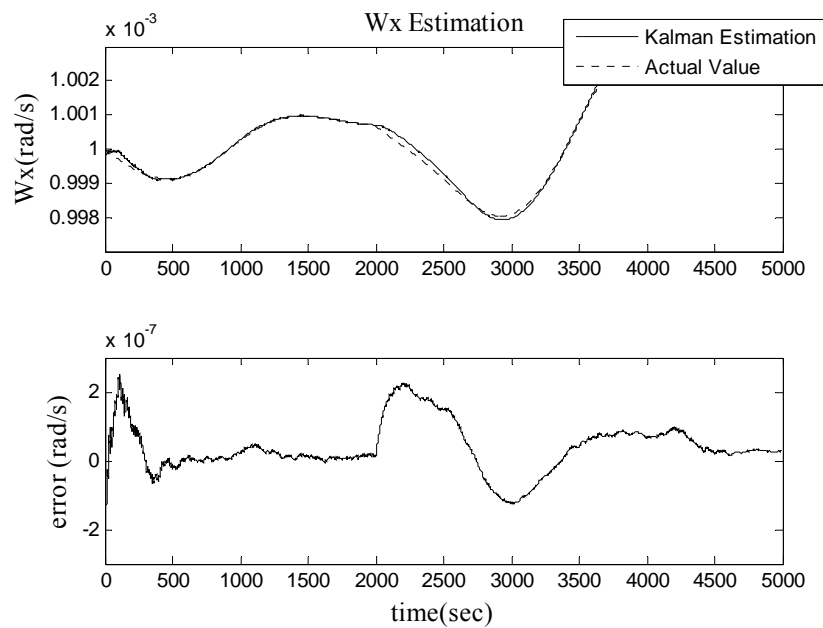


Figure 6.3: Estimation of the angular rate about x axis by the UKF with low process noise in case of sudden change.

Table 6.1: Absolute values of error for the RMM estimation in case of sudden change.

Absolute Values of Estimation Error for the RMM Estimation						
	<i>UKF with Low Noise</i>			<i>UKF with High Noise</i>		
	1000 th sec.	2500 th sec.	4000 th sec.	1000 th sec.	2500 th sec.	4000 th sec.
$M_x (Am^2)$	0.000020	0.061680	0.002544	0.007702	0.002422	0.002908
$M_y (Am^2)$	0.000482	0.025425	0.000085	0.006528	0.003433	0.011384
$M_z (Am^2)$	0.000567	0.016087	0.004357	0.000547	0.036143	0.013680

The table more clearly represents the fact that although the UKF with high process noise can agilely catch the new value of the RMM terms after the sudden change, the steady state accuracy of the estimation is not high enough for satisfying good attitude control performance.

The investigations in this section signify that if there is a necessity for both highly accurate RMM estimations during the steady state and good tracking speed when the states change suddenly, the KF must be built adaptively such that the filter parameters are tuned with respect to the requirements at that moment. The simplest method for achieving this is to use a change detector first for detecting the abrupt changes in the states and then increase the process noise covariance or estimation covariance of the filter in order to speed up the tracking process. The next section introduces the novel method for change detection and KF adaptation, which we propose as an advanced approach for solving this problem.

6.2. Change Detection and UKF Adaptation

The existing methods used for augmenting the tracking capability of a filter, which is fundamentally designed with low Q values for steady state accuracy, are only concerned with the change time (or alarm time) for starting the adaptation of the filter. These methods disregard the magnitude of the change or assume that it is known *a priori* (Basseville and Nikiforov 1993). Hence, the performed adaptation is specific for just a single magnitude and cannot be generalized. The value of the Q or P matrices selected after the change detection (Q_{alarm} and P_{alarm}) works well for this specific condition but fails to provide the required performance when a change with a different magnitude occurs. This failure might be either as being late for tracking the new value of the state or showing unnecessary fluctuations because of the overestimated Q_{alarm} and P_{alarm} values (Q and P matrices increased to a unnecessarily high level) (Hartikainen and Ekelin 2006).

In this section, first we present the change detection method used for sensing the abrupt changes in the estimated RMM terms. Then the novel procedure for the adaptation of the UKF is proposed and the performance of the method is examined by comparing with the existing techniques.

6.2.1. Change Detection

The essence of change detection for the KF in general is to apply a low-pass filter to the normalized innovation sequence of the filter. For vector valued measurements (or innovation sequence) the sum of the normalized innovation sequence is used (Gustafsson 2000). The sum of the normalized innovation sequence for the UKF is

$$Z_n(k+1) = \frac{1}{\sqrt{n_i}} \mathbf{1}_{n_i} \{P_{yy}(k+1|k) + R(k+1)\}^{-1/2} \{\mathbf{y}(k+1) - \hat{\mathbf{y}}(k+1|k)\}. \quad (6.8)$$

Here n_i is the size of the innovation vector and $\mathbf{1}_{n_i}$ is unit vector with n_i unit elements, by which the sum of the elements of the normalized innovation sequence is taken.

One of the well known change detectors (or stopping rules) is the CUSUM test (Page 1954), which should be used as a two-sided algorithm in order to detect both the increase and decrease in the mean of the estimated parameter. In other words, two statistical parameters should be checked simultaneously for detecting the changes in both directions. Another approach is to use the Geometric Moving Average (GMA) (Roberts 1959) which is simpler as a result of being one-sided. In this study, we preferred to implement the GMA test for change detection because of this simplicity and also its quicker response to the adaptation which will be shown with the numerical example. The GMA test is defined as;

$$g(k+1) = \lambda g(k) + (1-\lambda)Z_n(k+1) \quad \text{alarm if } \begin{cases} g(k+1) > \xi \\ g(k+1) < -\xi \end{cases}. \quad (6.9)$$

Here, λ is the forgetting factor used for tuning the low-pass effect, $g(k+1)$ is the GMA parameter to be tested for the change detection, where $g(0) = 0$, and ξ is the threshold value. The value of ξ must be determined carefully since a high value will make the detector insensitive against changes with small magnitude, whereas a small value will increase the chance of false alarms. In Fig. 6.4 the variation of the GMA in case of a change in the estimated RMM terms is given. The figure shows how the GMA behaves for the UKF with low process noise (6.4) as in the second scenario presented in the previous section. The forgetting factor is taken as $\lambda = 0.997$, which means the current observations

are weighted less and the low-pass effect is high. For this scenario, ξ might be selected as $\xi = 0.2$ which is small enough to detect changes with small magnitude and sufficiently away from the highest value that GMA takes during the steady-state regime such that the false alarm chance is reduced.

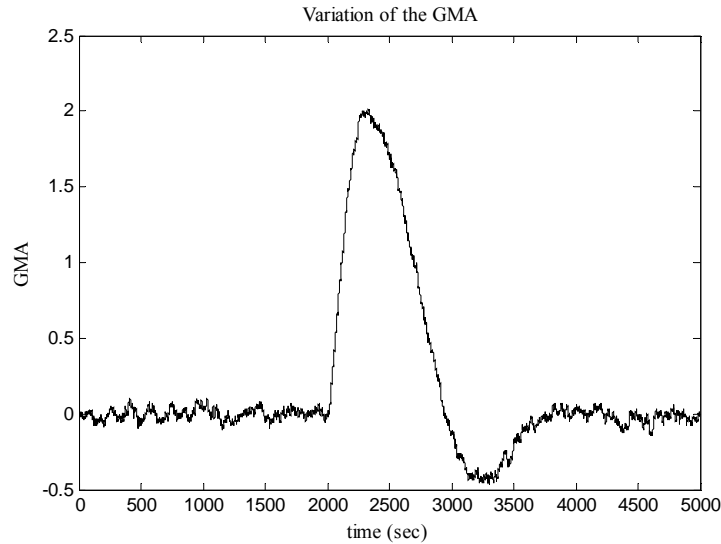


Figure 6.4: Variation of the GMA in case of change in the estimated RMM terms (change at 2000th second).

The next step after the change detection is to adapt the UKF appropriately such that the filter agilely catches the new values of the estimated states with similar performance for every different change conditions. This will be also the main contribution of the chapter in the sense of change detection and adaptation.

6.2.2. The Adaptation of the UKF

The proposed adaptation method for the KF is based on the idea of increasing the estimation covariance of the filter after detecting the change. Instead of a correction on the process noise covariance, we preferred this method because of the known upper limit for the increase in the estimation covariance. In case of a change, the estimation covariance can be increased upmost to its initial value, which is basically similar to reinitializing the filter. Unlike the existing methods, the level of increase is not same for all change conditions and it is determined regarding the magnitude of the shift in the estimated RMM terms.

The adaptation is carried out such that the new value of the estimated covariance after the change detection is

$$P(k+1|k+1) = \{1 - \Omega(k+1)\} \left\{ \left[I - K(k+1)H(k) \right] P(k+1|k) \right\} + \Omega(k+1)P_0, \quad (6.10)$$

where $K(k+1)$ is the optimal Kalman gain, P_0 is the initial value of the covariance matrix and $\Omega(k+1)$ is the weighting function which takes a value from 0 to 1. For this problem the weighting function is selected as

$$\Omega(k+1) = \exp \left[- \left(t_{\xi_1} - t_{\xi_2} \right) / \mathcal{G} \right]. \quad (6.11)$$

Here \mathcal{G} is the tuning parameter selected intuitively regarding the general trend of the GMA function and t_{ξ_1} and t_{ξ_2} are the time steps that the GMA exceeds the thresholds of ξ_1 and ξ_2 , respectively. Note that $t_{\xi_1} > t_{\xi_2}$ and χ_1 might be selected as $\xi_1 = \xi$ where ξ is the threshold that the adaptation is started as introduced via (6.9).

When the magnitude of the shift is large the GMA follows a steeper trend while exceeding the threshold and so the $t_{\xi_1} - t_{\xi_2}$ difference takes a small value. Consequently, the $\Omega(k+1)$ becomes closer to its upmost limit, 1, and the P_0 is weighted more for the adaptation. On the contrary, if the magnitude of the shift is smaller, then the GMA acts slower and the time difference between the instants that the GMA exceeds successive thresholds of ξ_2 and ξ_1 becomes large ($t_{\xi_1} - t_{\xi_2}$ takes a large value). Therefore the weighting function $\Omega(k+1)$ approaches to 0 and the P matrix increases slightly with a smaller impact from the P_0 .

Fig. 6.5 gives the overall estimation scheme for the RMM by the UKF including the change detection and adaptation procedures. Note that in case we use the UKF (6.10) differs as

$$P(k+1|k+1) = \{1 - \Omega(k+1)\} \left[P(k+1|k) - K(k+1)P_{vv}(k+1|k)K^T(k+1) \right] + \Omega(k+1)P_0. \quad (6.12)$$

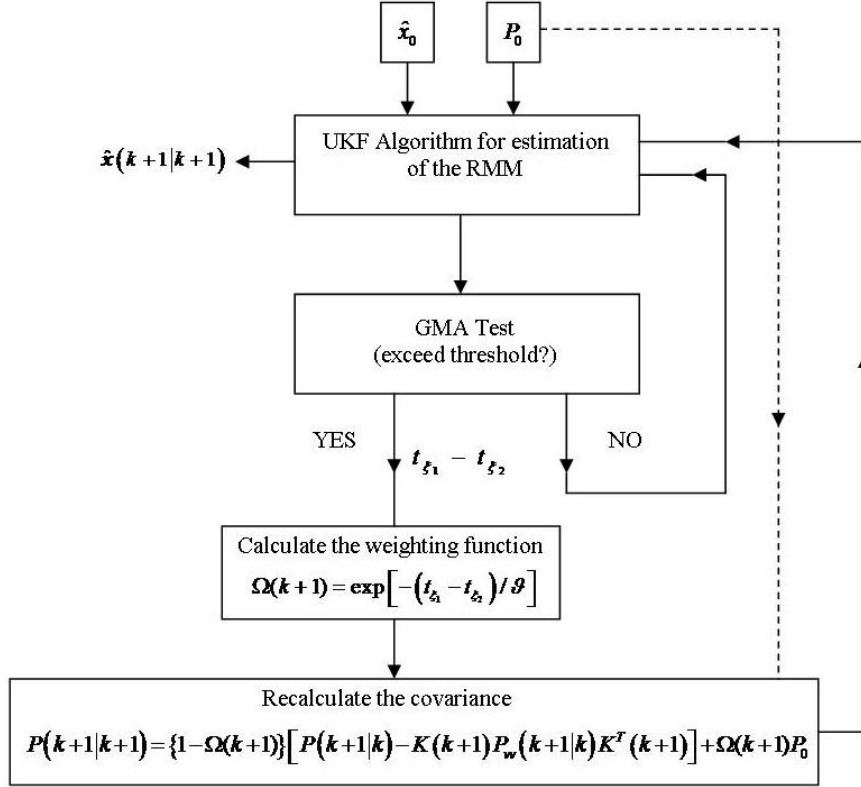


Figure 6.5: The RMM estimation scheme in case of sudden change.

Remark on Stability. In the essence, the applied adaptation procedure is not different from restarting the KF when a change detected (Gustafsson 1996; Stenlund and Gustafsson 2001). Here, the key point is not to start the filter again with the initial covariance but to use a covariance value that is calculated regarding the magnitude of the change.

In this sense, a similar approach with the one of Kalman filter may be followed to check whether the stability of the KF is affected as a result of the applied adaptation method. From (Hajiyev and Caliskan 2003) it is known that the following characteristic polynomial of the system can be used for stability analyses of a Kalman filter:

$$\text{Characteristic polynomial} = \{zI - [F(k) - K(k+1)H(k)F(k)]\}. \quad (6.13)$$

where z denotes the usual z -transform variable and $F(k)$ is the systems dynamics matrix which is a Jacobian matrix for nonlinear case.

The roots of this polynomial provide information about the filter stability. If all the roots lie inside the unit circle in the z -plane, the filter is stable; conversely, if any root lies on or outside the unit circle, the filter is unstable. As a matter of terminology, the roots of the characteristic polynomial are the same as the eigenvalues of

$$\left[F(k) - K(k+1)H(k)F(k) \right]. \quad (6.14)$$

Regarding this fact and evaluating the stability of the KF within one step, it is clear that the stability of the filter will be affected only if there is a modification on the Kalman gain such that the process or measurement noise covariances ($Q(k)$ and $R(k)$ respectively) are adapted. For all other cases the stability will be assured if the regular KF without any modification is stable.

Furthermore the stability of the UKF may be examined as a special case. As discussed in (Dymirkovsky *et al.* 2012; Xiong *et al.* 2009) the stability of the UKF strictly depends on the positive-definiteness of the process and measurement noise covariance matrices; as long as this certain condition is satisfied, the estimation error of the UKF remains bounded even for large initial estimation errors. Therefore the proposed adaptation method does not have a detractive effect on the stability of the UKF used for the RMM estimation. If the abrupt changes of the RMM do not happen so often, there is no problem with the convergence as the original estimator is stable.

Remark on Determination of the Tuning Parameters and Thresholds. There are four parameters to be determined for the proposed change detection and KF adaptation algorithm: λ , the forgetting factor for the GMA test; \mathcal{G} , the tuning parameter for the weighting function; and the thresholds of ξ_1 and ξ_2 , which determine the t_{ξ_1} and t_{ξ_2} time steps used as an input to the weighting function. Besides since $\xi_1 = \xi$, ξ_1 is also the threshold that the adaptation is started.

The forgetting factor, λ , is the first parameter to be tuned. It determines the low-pass filtering effect and $0 \leq \lambda < 1$. A value closer to 1 means higher low-pass effect and selecting $\lambda = 0$ means thresholding the normalized innovation sequence, $Z_n(k+1)$, directly, which is also one option (Gustafsson 2000). The forgetting factor should be chosen regarding the characteristics of the KF. Especially the level of the measurement noise covariance, $R(k)$, has a remarkable effect on the normalized innovation output of the filter. If the measurement noise is smaller (such that we have more accurate sensors) than the

low-pass filtering effect must be increased with a λ closer to 1 to get a smoother GMA parameter.

Then as the next step, the thresholds of ξ_1 and ξ_2 should be selected regarding the design criteria of $\xi_1 > \xi_2$. Since ξ_1 is also the threshold where the adaptation is started it must be determined carefully. It must be small enough to detect changes with small magnitude and sufficiently away from the highest value that GMA takes during the steady-state regime such that the false alarm chance is reduced. Suppose that for a fixed λ value, we have smaller measurement noise. In this case the GMA output will be more noisy so the threshold of $\xi = \xi$ should be selected as a higher value. On the other hand, selection of ξ_2 does not need to be so precise; it only affects the level of the tuning parameter \mathcal{G} . In this sense $\xi_2 = 0.75\xi_1$ is a good candidate.

Lastly, the tuning parameter for the weighting function, \mathcal{G} , must be selected regarding the trend of the GMA for a KF without adaptation and the values of t_{ξ_1} and t_{ξ_2} . For a change with the possible highest magnitude the \mathcal{G} should be selected such that the $\Omega(k+1)$ approaches to 1.

6.3. Simulation Results

The proposed change detection and adaptation algorithm is tested for the UKF based RMM estimation. Two different change conditions are investigated. The first change, which is imposed to the RMM terms at the 2000th second, is relatively larger in magnitude while the second change at the 7000th second is smaller. The real values for the RMM terms change as

$$\mathbf{M} = \begin{cases} \begin{bmatrix} 0.1 & 0.02 & -0.05 \end{bmatrix}^T Am^2 & t < 2000 \text{ sec} \\ \begin{bmatrix} 0.25 & 0.1 & -0.15 \end{bmatrix}^T Am^2 & 2000 \text{ sec} \geq t \geq 7000 \text{ sec} \\ \begin{bmatrix} 0.2 & 0.07 & -0.10 \end{bmatrix}^T Am^2 & t \geq 7000 \text{ sec} \end{cases} . \quad (6.15)$$

The process noise covariance matrix of the UKF is as given with (6.4). For the change detection and UKF adaptation algorithm the thresholds are selected as $\xi = \xi_1 = 0.2$ and $\xi_2 = 0.15$, while the tuning parameter \mathcal{G} is taken as $\mathcal{G} = 40$. As mentioned the selection for the β depends on the selected values for ξ_1 , ξ_2 and the characteristics of the UKF.

The same simulation scenario is repeated with an UKF without change detection and adaptation, as well with an UKF which is reinitialized with P_0 after each change detection.

In Fig. 6.6, the estimation results for the RMM in the x axis is given. As seen the regular UKF algorithm without adaptation is slow about catching the new values especially when the change is large in magnitude (as at 2000th sec.). On the other hand, when we integrate a change detector into the algorithm and perform an adaptation on the UKF after each change detection, the UKF speeds up remarkably. However, if we perform the adaptation regardless the magnitude of the shift, as performed with the UKF reinitialized after each change detection, then specifically for small shifts we may meet with undesirable fluctuations until the estimations are attenuated to the accurate steady state values (see zoomed subfigure *a* of Fig.6.6). The proposed adaptation algorithm takes the magnitude of the shift into consideration when deciding the value of the filter covariance for the next step after detecting the change. Therefore, as well as increasing the filter's agility for catching the new value, it prevents from the undesirable fluctuations as a result of increasing the covariance accordingly for that magnitude of shift. Similar results are obtained for the estimation of other RMM terms (Fig. 6.7 and Fig. 6.8).

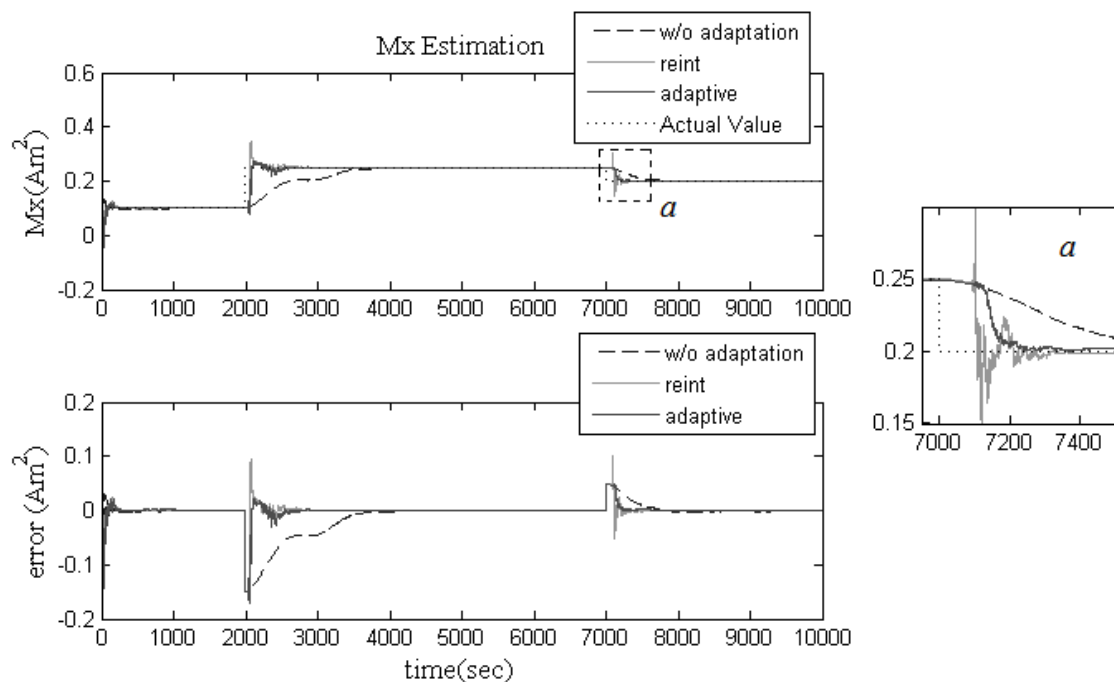


Figure 6.6: Estimation of the RMM in x axis in case of sudden change: The UKF without change detection and adaptation is referred as “w/o adaptation”; the UKF, which is reinitialized after each change detection, is named as “reint”; and the proposed estimation algorithm is shown as “adaptive”.

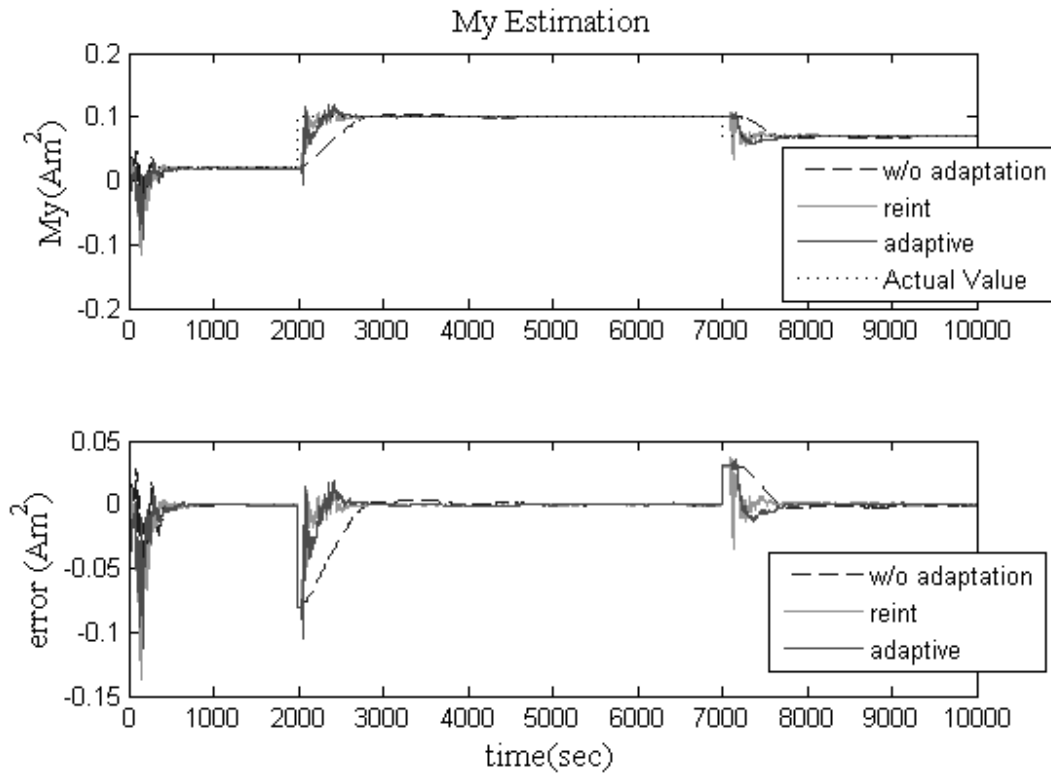


Figure 6.7: Estimation of the RMM in y axis in case of sudden change: The UKF without change detection and adaptation is referred as “w/o adaptation”; the UKF, which is reinitialized after each change detection, is named as “reint”; and the proposed estimation algorithm is shown as “adaptive”.

As a further examination on the proposed algorithm, we checked the alarm time, $t_{\xi_1} - t_{\xi_2}$ difference, which is important for reflecting the magnitude of the detected change into the adaptation algorithm, and the value of the weighting function for the changes at 2000th and 7000th seconds (Table 6.2). As seen, for the change with relatively larger magnitude $t_{\xi_1} - t_{\xi_2}$ takes a smaller value that increases the value of the weighting function and vice versa for the change with smaller magnitude. Nonetheless, as expected the alarm time is later for lesser changes.

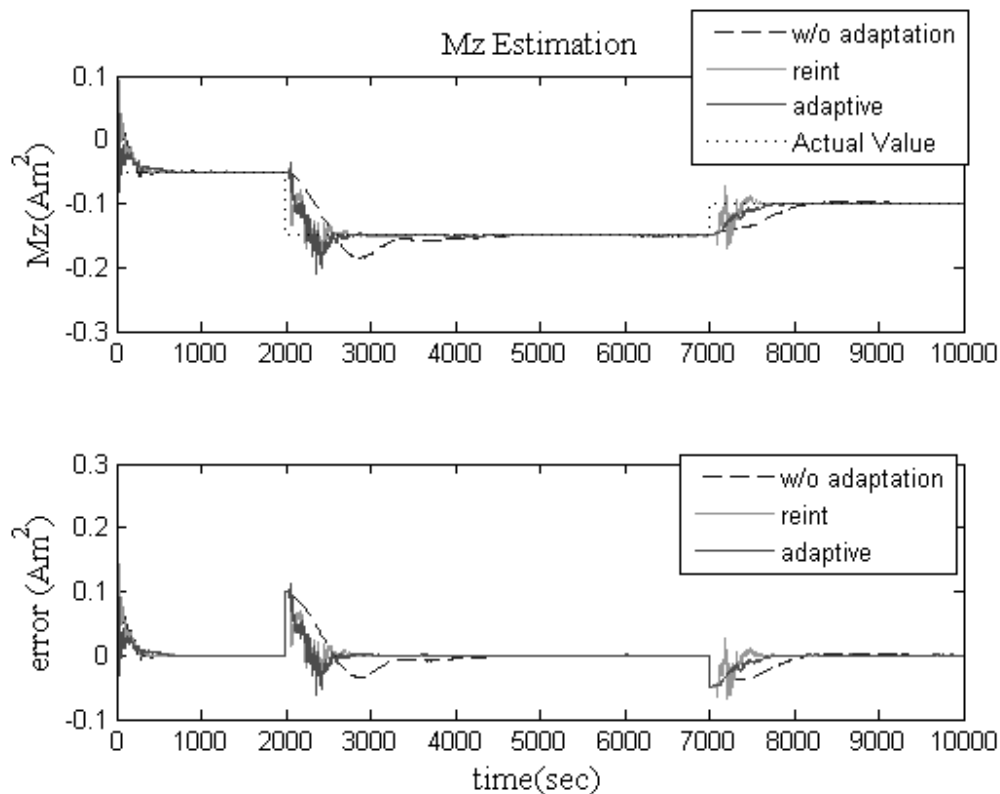


Figure 6.8: Estimation of the RMM in z axis in case of sudden change: The UKF without change detection and adaptation is referred as “w/o adaptation”; the UKF, which is reinitialized after each change detection, is named as “reint”; and the proposed estimation algorithm is shown as “adaptive”.

Table 6.2: Alarm time and the adaptation values for the proposed UKF adaptation algorithm.

	Change at 2000th sec.	Change at 7000th sec.
Alarm time	2032.4 sec.	7085.6 sec.
$(t_{\xi_1} - t_{\xi_2})$	36	142
Ω	0.4066	0.0287

In Fig. 6.9, the variation of the GMA for the proposed algorithm is shown together with the GMA for the regular UKF without adaptation. As aforementioned the GMA has a quick response to the adaptation and immediately after the adaptation begins it goes down below

the threshold. That indicates the adaptation on the filter covariance (6.12) is performed only for few steps and then the filter works with the regular covariance update procedure.

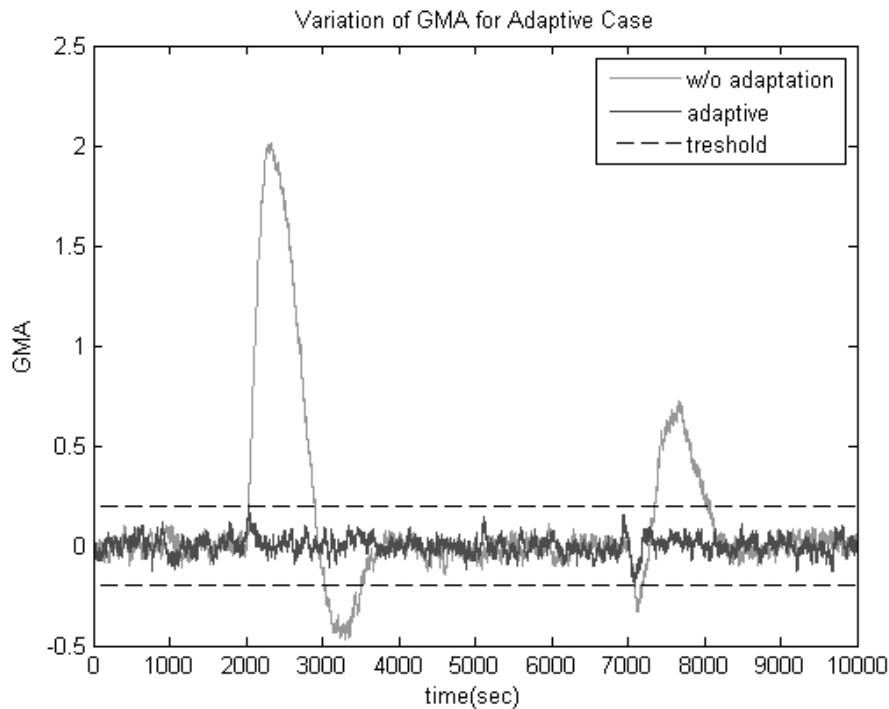


Figure 6.9: Variation of the GMA in case of change in the estimated RMM terms: The GMA for the regular UKF and UKF with the proposed change detection and adaptation procedure.

As a result the proposed change detection and KF adaptation procedure works well. By applying this algorithm on the UKF for the RMM estimation problem the agility of the UKF for catching the new values of the changed parameters can be increased remarkably, whereas the filter is originally designed for steady state accuracy with low process noise covariance. We preferred to apply the adaptation on the filter covariance matrix but similar procedure may be followed for an adaptation of the Q . But in this case the determination of the upper bound for the Q , which we select as P_0 for the covariance adaptation, is seen as an empirical problem.

7. Demonstration of the Proposed Attitude Determination Scheme

In this chapter the proposed estimation algorithms are integrated in order to get a full attitude estimation scheme for the nanosatellite. First by using a unique integration technique, the AUKF and RUKF algorithms are integrated for building a Robust Adaptive Unscented Kalman Filter (RAUKF), which is both adaptively tuned and robust against measurement malfunctions. Then this filter is integrated with the UKF based RMM estimator and a two-stage filtering algorithm that estimates the attitude, attitude rate, magnetometer & gyro biases and RMM is obtained.

The proposed overall estimation scheme is demonstrated for nanosatellite attitude estimation. The effects of each discussed method, such as the Q adaptation, are clearly shown. The performance of the overall scheme is analyzed regarding the goals set initially and comparing with the existing methods.

7.1. Integration of the Filters

7.1.1. The RAUKF Algorithm

The AUKF and RUKF algorithms presented in Chapter 5 are solutions for different problems but the main intention for building the algorithms was same: increasing the attitude determination accuracy of the nanosatellite. The AUKF is used as a tuning algorithm for the process noise covariance of the filter in order to ease the difficult tuning procedure and make the filter more efficient in the sense of estimation accuracy. On the other hand the RUKF is a filter which is adapted as a measure against the possible measurement faults in the harsh space environment. In this section we integrate these two filters. The new filter is named as the RAUKF.

The given AUKF algorithm applies the adaptation on the Q matrix while the RUKF scales the R matrix against the measurement malfunctions. The integration of these two adaptation techniques is an open topic and there are numerous researches in the literature (Hajiyev and Soken 2013; Almagbile *et al.* 2010). Indeed there is no any stable integration method when

both the R and Q matrices are estimated based on the innovation covariance (Almagbile *et al.* 2010). On the other hand the Q estimation method presented in this thesis is based on the residual covariance and the adaptation method for the R matrix is an innovation covariance based scaling method, not the direct estimation of the matrix itself. Hence these two methods can be run at the same time. Fig. 7.1 shows the integration method with the key steps of the RAUKF.

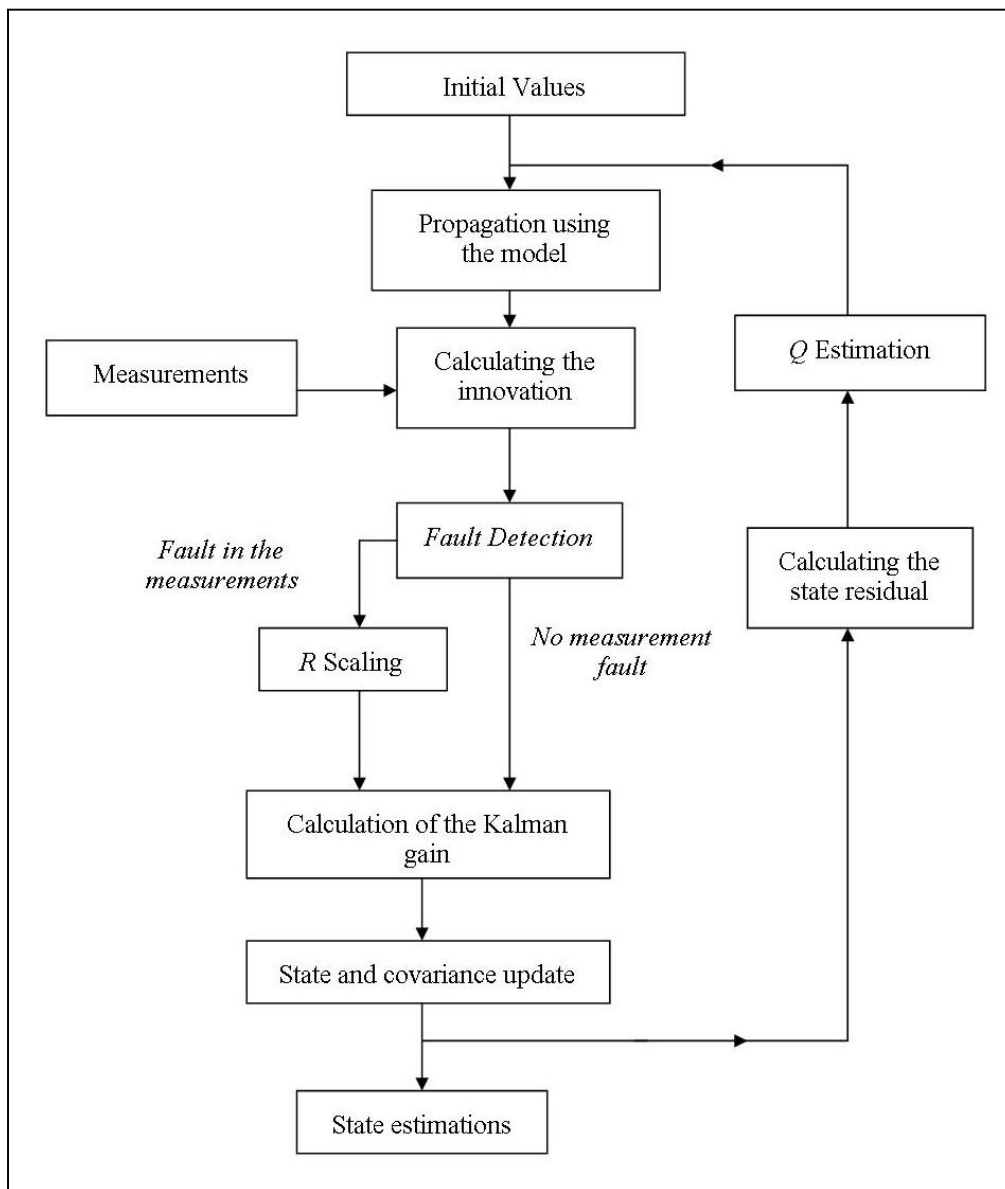


Figure 7.1: The proposed RAUKF.

Nonetheless, there are two important points which should be regarded while designing the RAUKF:

- The R scaling is performed only when a fault is detected in the measurements as given in 5.2.3. In all other cases the filter runs with the regular algorithm only with the Q estimation (when there is no fault the algorithm is same as the AUKF with process noise covariance estimation).
- The scale factor for the AUKF in (5.26) should be selected carefully. If more aggressive adaptation is performed (such that $\gamma \approx 1$) the stability of the RAUKF might be affected in case of a measurement fault when both R and Q adaptations are necessary.

7.1.2. Integration of the RAUKF with the RMM Estimator

The RAUKF algorithm presented in the previous section estimates the attitude, gyro bias and magnetometer bias for the nanosatellite. As stated in the Chapter 6, while discussing the RMM estimation scheme, the UKF used for the RMM estimation takes the already calibrated magnetometer and gyro measurements as inputs. The calibrated magnetometer measurements supply the \mathbf{B} information for the propagation model (6.2) and the calibrated gyro measurements are used as the measurements (6.3). In other words, the calibrated gyro and magnetometer measurements are prerequisite for running the second UKF and estimating the RMM accurately. Hence these two filters, the RAUKF and UKF for the RMM estimation should be serially run as proposed in Fig. 7.2.

Here, the RAUKF, which is the first filter, uses the magnetometer and gyro measurements, \mathbf{B}_{mes} and $\boldsymbol{\omega}_{mes}$ respectively. As discussed, this filter estimates the attitude $\hat{\mathbf{q}}$, gyro biases $\hat{\mathbf{b}}_{gyro}$ and magnetometer biases $\hat{\mathbf{b}}_{mag}$. Then these estimated bias terms are used for calibrating the sensors and so correcting the measurements as $\mathbf{B}_{mes} - \hat{\mathbf{b}}_{mag}$ and $\boldsymbol{\omega}_{mes} - \hat{\mathbf{b}}_{gyro}$. These corrected measurements are the inputs for the second filter that mainly estimates the RMM ($\hat{\mathbf{M}}$). In addition to the RMM terms the attitude rates, $\hat{\boldsymbol{\omega}}$, are also estimated by the second UKF (estimating the attitude rate is necessary as an essence of the filtering algorithm since we use the spacecraft dynamics as the propagation model and the measurement inputs are the gyro measurements). The estimated RMM terms are then used for cancelling out the magnetic disturbance torque either by a feedforward or feed-back cancellation technique. The disturbance torque is counteracted with the torque produced by the magnetorquers. The integration of the RAUKF and the UKF based RMM estimator forms the overall attitude estimation scheme for the nanosatellite.

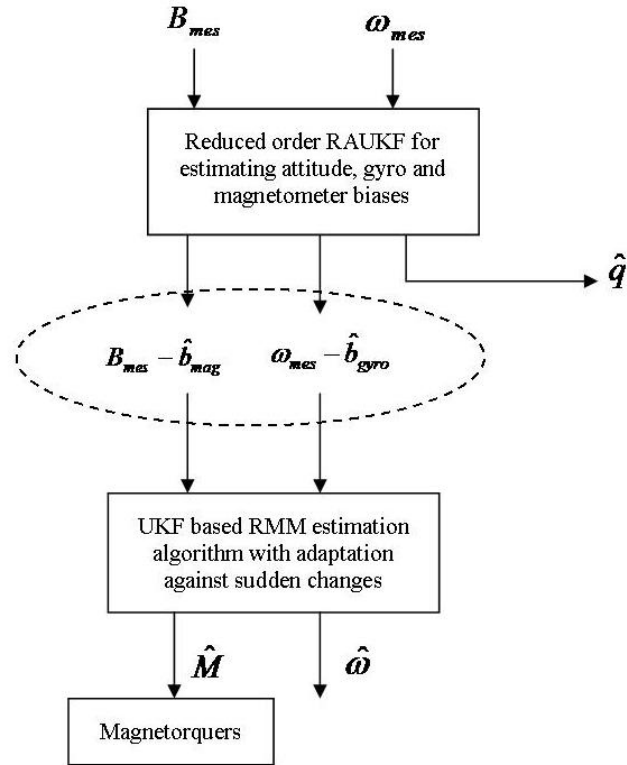


Figure 7.2: Integration of the RAUKF with the RMM estimator: The overall attitude estimation scheme.

7.2. Overall Attitude Estimation Scheme

7.2.1. Demonstration of the Overall Attitude Estimation Scheme

In order to test the overall attitude estimation scheme, a series of simulations were performed. First we showed the effects of the Q adaptation by comparing a regular UKF with the RAUKF. In other words, the overall attitude estimation scheme is run using both the RAUKF and regular UKF as the first filter. Then the results for the UKF and RAUKF are compared in case of measurement malfunction to clarify the necessity of the R adaptation. The advantages of using the RAUKF for the first stage of the filtering algorithm is clearly shown by the discussing the estimation results of the both first and second filters. In the end, an abrupt instantaneous change is simulated for the real RMM terms to be estimated and the RMM estimation results by the second filter are given comparing the cases with and without the P adaptation (6.12).

For robust filtering (R adaptation) the adaptation via multiple scale factors (5.40) is preferred since the previous investigations showed that it gives better estimation results under all conditions. For the Q adaptation process, noise covariance estimation method is used (5.24-5.26).

The reduced order RAUKF is run for estimating the attitude, gyro bias and sensor biases and the UKF with the P adaptation is run for the RMM and attitude rate estimation. The simulations are performed for a hypothetical nanosatellite. The satellite is assumed to be a 3U cubesat with dimensions of $10\text{cm} \times 10\text{cm} \times 30\text{cm}$, an approximate mass of 3kg and an approximate inertia matrix of $J = \text{diag}(0.055 \ 0.055 \ 0.017)\text{kg.m}^2$. A real mission example for a similar 3U nanosatellite might be seen in (Reijneveld and Choukroun 2012).

Nonetheless the orbit of the satellite is assumed as circular. The inclination for the satellite's orbit is $i = 31^\circ$ and the distance between the centre of the masses of the Earth and satellite is $r_0 = 7450\text{km}$.

For the magnetometer measurements, the sensor noise is characterized by zero mean Gaussian white noise with a standard deviation of $\sigma_m = 300\text{nT}$ (Sakai et al. 2011) and the constant magnetometer bias terms are accepted as $\bar{b}_m = [0.14 \ 0.019 \ 0.37]^T \times 10^4\text{nT}$, which is reasonable when compared to the values in (Sakai et al. 2011; Han et al. 2012). Moreover, the gyro random error is taken as $\sigma_v = 2.47[\text{arcsec} / \sqrt{s}]$, whereas the standard deviation of the gyro biases is $\sigma_u = 6.36 \times 10^{-4}[\text{arcsec} / \sqrt{s^3}]$ (Sakai et al. 2006a).

As the filter parameters for the RAUKF, κ is selected as $\kappa = -2$ where $f = 2(a+1)$ and $a = 1$. For the second UKF that is used for the RMM estimation κ is $\kappa = -3$. Initial attitude errors are set to 30, 25 and 25 deg for pitch, yaw and roll axes respectively. The initial estimation values for the gyro and magnetometer biases, attitude rate and RMM are all taken as 0. Besides, the initial value of the covariance matrix is $P_0 = \text{diag}[0.1 \ 0.1 \ 0.1 \ 10^{-7} \ 10^{-7} \ 10^{-7} \ 10^{-3} \ 10^{-3} \ 10^{-3}]$ for the first filter and $P_0 = \text{diag}[10^{-6} \ 10^{-6} \ 10^{-6} \ 0.01 \ 0.01 \ 0.01]$ for the second filter. For the RAUKF the initial the value of the process noise covariance matrix is,

$$Q = \begin{bmatrix} (1 \times 10^{-3})I_{3 \times 3} & -(1.5 \times 10^{-7})I_{3 \times 3} & 0_{3 \times 3} \\ -(1.5 \times 10^{-7})I_{3 \times 3} & (1 \times 10^{-10})I_{3 \times 3} & 0_{3 \times 3} \\ 0_{3 \times 3} & 0_{3 \times 3} & (1 \times 10^{-12})I_{3 \times 3} \end{bmatrix}. \quad (7.1)$$

For the RMM estimator UKF the Q is fixed as,

$$Q = \begin{bmatrix} (1 \times 10^{-5}) I_{3 \times 3} & 0_{3 \times 3} \\ 0_{3 \times 3} & (1 \times 10^{-7}) I_{3 \times 3} \end{bmatrix}. \quad (7.2)$$

Moreover, for the RAUKF's fault detection procedure, $\chi_{\alpha,z}^2$ is taken as 7.81 and this value comes from chi-square distribution when the degree of freedom is 3 and the reliability level is 95%.

We tested the RAUKF for the continuous bias failure. Hence a constant value is added to the measurements of the magnetometer aligned in the x axis between the 30000th and 30200th seconds for a period of 200 seconds such that;

$$B_x(\mathbf{q}, t) = B_x(\mathbf{q}, t) + 20000nT \quad t = 30000 \dots 30200 \text{ sec}$$

A deviation in the bias with this amount is reasonable when the values given in (Sakai *et al.* 2011) are taken into consideration.

For testing the second UKF with the adaptation against the sudden changes, the change is realized in the RMM terms at the 30000th second such that

$$\mathbf{M} = \begin{cases} \begin{bmatrix} 2 \times 10^{-5} & 1 \times 10^{-5} & -1 \times 10^{-5} \end{bmatrix}^T Am^2 & t < 3000 \text{ sec} \\ \begin{bmatrix} 3 \times 10^{-5} & 2 \times 10^{-5} & -2 \times 10^{-5} \end{bmatrix}^T Am^2 & t \geq 3000 \text{ sec} \end{cases}. \quad (7.3)$$

A. Effects of the Q Adaptation

In Fig. 7.3 the pitch angle estimation results that we get in case we use the regular UKF or the proposed RAUKF at the first stage (as the first filter) of the overall scheme are given in the same plot. As clearly seen, especially from the zoomed subplot, the results obtained by the RAUKF are far more accurate. As discussed in the previous chapters, this is mainly because of the nearly optimal values of the Q matrix for the RAUKF that we cannot easily obtain by the trial-error method.

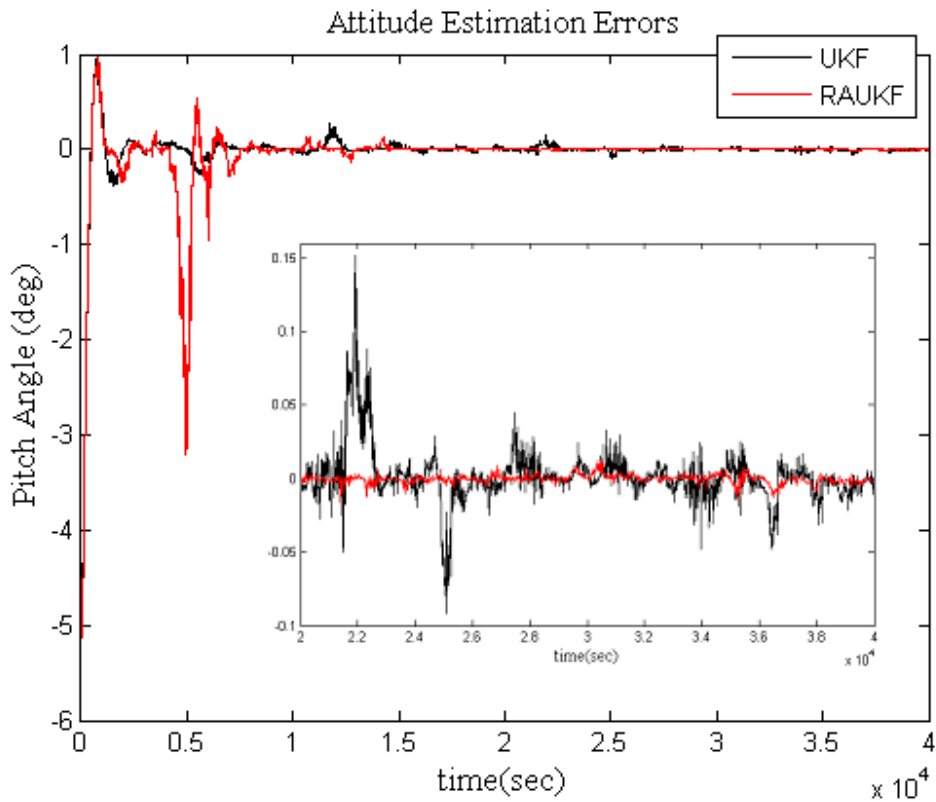


Figure 7.3: Estimation of the pitch angle via the RAUKF (red line) and UKF (black line) as a part of the overall estimation scheme.

In Fig. 7.4 the estimation result for the RMM in the z axis is given. The RMM output of the second filter is plotted again in case we use a regular UKF or RAUKF at the first stage of the overall scheme. Apparently, and as expected, the performance of the first filter affects the second filter's estimation accuracy. When we use the RAUKF, which means a better estimation performance as shown with Fig. 7.3, the RMM terms can be estimated more accurately by the second filter. Besides, in this case the second filter has better convergence characteristic. The second filter for the RMM estimation is dependent to the magnetometer and gyro bias information from the first filter (RAUKF) and its performance is highly affected from the accuracy of the RAUKF. Unless the estimations for magnetometer and gyro biases converge to the real values, the second filter cannot give good estimation results. The precision of the gyro bias estimations is specifically important for the second filter since it uses the gyro outputs as the measurements.

The estimation results obtained for the other parameters such as the magnetometer biases are similar and the estimation scheme built with the RAUKF gives better estimation results.

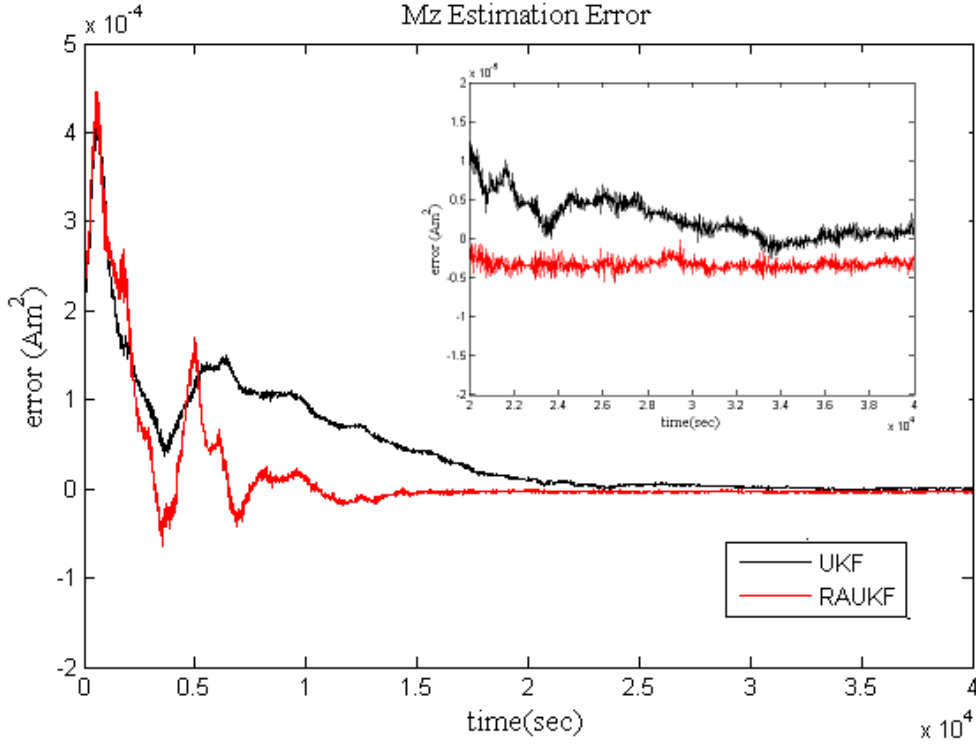


Figure 7.4: Estimation of the RMM term in z axis via the RAUKF (red line) and AUKF (black line) as a part of the overall estimation scheme.

B. Effects of the R Adaptation

The same scenario is repeated by considering a sensor malfunction in between 30000th and 30200th seconds this time. Fig. 7.5 gives the pitch angle estimation result comparing the cases that the first filter is the RAUKF or just the regular UKF. As expected the UKF estimations deteriorates in case of measurement fault and it takes an additional 1000 seconds for the filter to converge again and satisfy estimation results with error less than 0.1deg.

If we examine the results for the RMM estimation (Fig. 7.6) we see that any malfunction in the magnetometer measurements and so deterioration in the estimation of the first stage highly affects the performance of the second filter and the RMM estimation. This is also because the second filter considers additional bias in the magnetometer measurements as a variation in the RMM. Since $\mathbf{B}_{mes} - \hat{\mathbf{b}}_{mag}$ is an input to the second filter, which is used within the propagation model, an abrupt change in the measurements, \mathbf{B}_{mes} , is sensed by the second UKF as a variation in the RMM terms. As given with (2.44) the magnetic

disturbance torque is formulated as $N_{md} = M_r \times B$. For this specific simulation example the additional bias in the B_x is considered by the second filter as a change in the M_y and M_z terms because of the cross product and its detractive effect is clear in Fig. 7.6. On the other hand, when the first filter is robust against measurement malfunctions it senses any abrupt variation in the measurements and by counteracting the fault for the estimation procedure it also prevents the second filter from any kind of error.

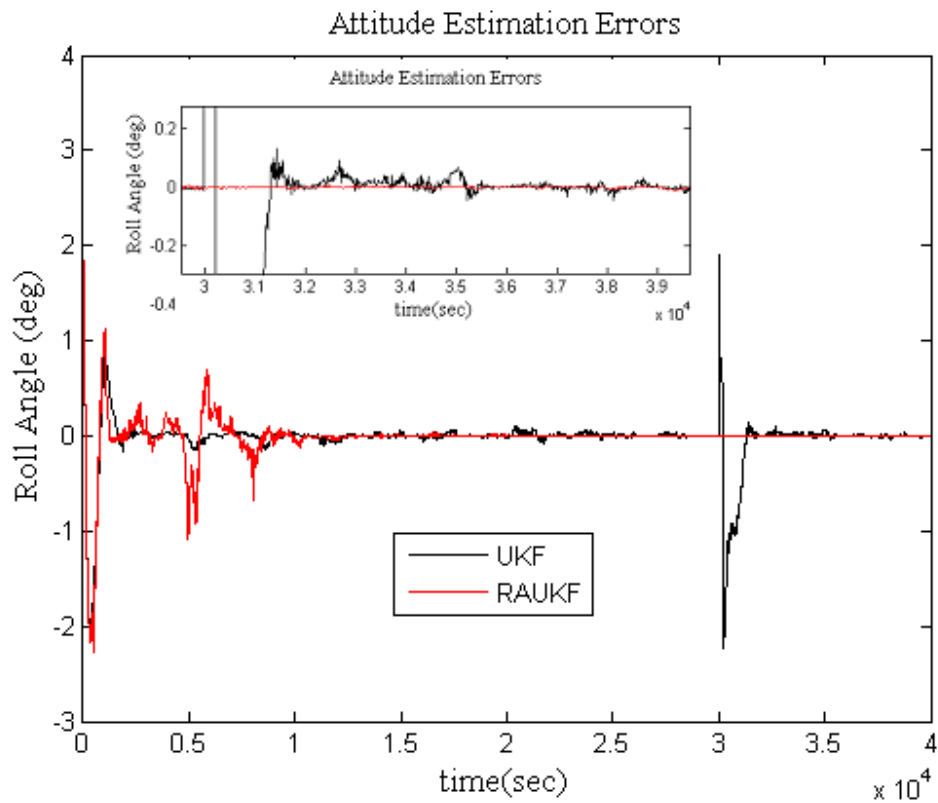


Figure 7.5: Estimation of the roll angle via the RAUKF (red line) and UKF (black line) as a part of the overall estimation scheme in case of measurement malfunction.

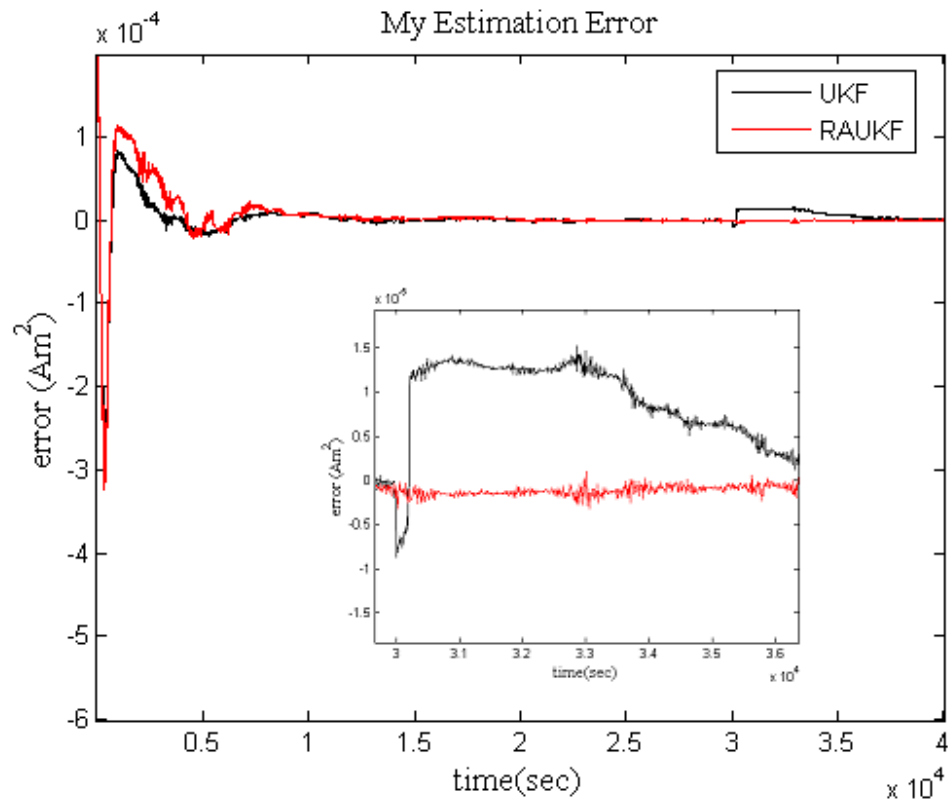


Figure 7.6: Estimation of the RMM term in y axis via the RAUKF (red line) and AUKF (black line) as a part of the overall estimation scheme in case of measurement malfunction.

C. Effects of the P Adaptation

In this last part basically the outputs of the second filter are tested against instantaneous changes in the estimated RMM parameters. At 30000th second the abrupt change is simulated as given with (7.3) and the second filter is run both with and without P adaptation. As expected the UKF with the proposed P adaptation procedure quickly catches the new value of the RMM term while it takes more than 5000 seconds for the regular filter without adaptation to converge and satisfy the desired estimation accuracy (Fig.7.7).

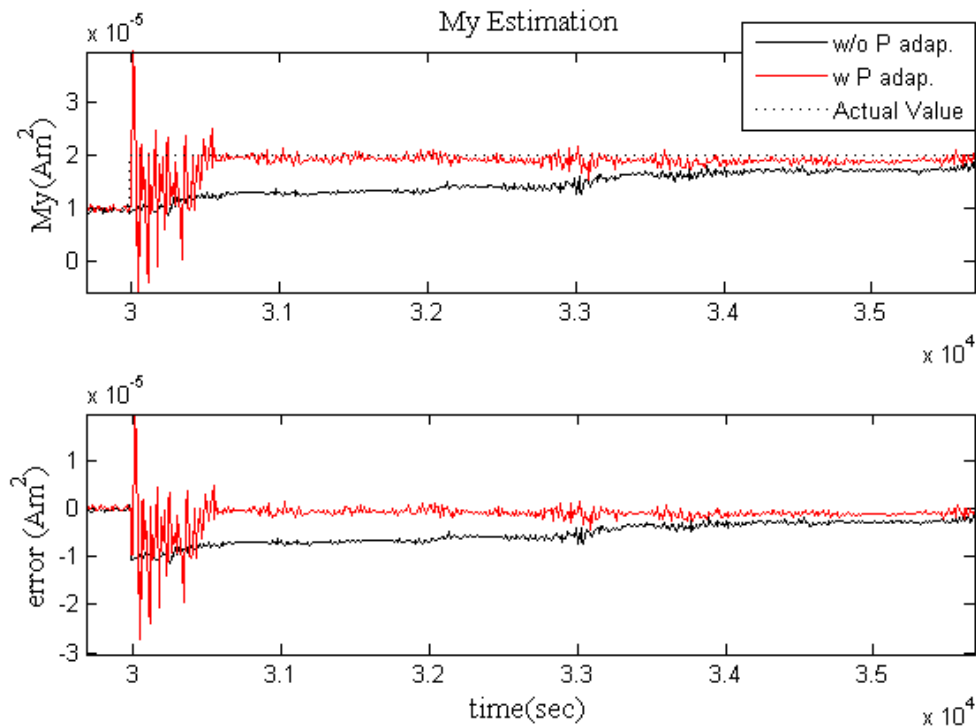


Figure 7.7: Estimation of the RMM term in y axis via the UKF with P adaptation (red line) and UKF without P adaptation (black line) as a part of the overall estimation scheme in case of instantaneous change in the estimated RMM parameters (figure is zoomed to the estimations in between 30000th and 35000th seconds).

7.2.2. Performance Comparison

Another essential evaluation for the overall scheme is examining the accuracy of the attitude estimations. By using the proposed method it is possible to determine the attitude of the nanosatellite with an accuracy higher than 0.01deg , which is much better than the goal set as 0.1deg initially. That shows us it is possible to increase the attitude determination accuracy of a nanosatellite, which has magnetometers, gyros and magnetorquers onboard, to a level at around 0.01deg when the magnetometers and gyros are in-orbit calibrated, the estimator is adaptively tuned and robust against measurement faults.

Furthermore, the proposed overall attitude estimation scheme provides RMM estimation with an absolute error less than $\%10$ of the magnitude of the actual values and that is

sufficient for feedforward cancellation technique which will be used as a part of the attitude control algorithm.

The only drawback of the proposed algorithm is the increased computational load when compared with the classical methods such as estimating only the attitude and gyro biases by the EKF. In Table 7.1 a stage by stage evolution for the computational load of the proposed algorithms is given. The main increment is caused by using the UKF instead of the EKF and that increases the load 2.82 times. In this specific case we think the main reason for such increase is the transformations between the full and error attitude representations and necessity for applying these transformations to all sigma points. On the other hand, if we had preferred using the EKF we would not be able to achieve high accuracy and there will be possibility for filter to not converge to the real values even for a simple problem as discussed in (Crassidis and Markley 2003). When the overall scheme is compared with the UKF based algorithm for estimating just the attitude and the gyro biases, the computational load is almost doubled. However, this is normal if we regard that there are two filters running serially for the overall scheme.

Table 7.1: Comparison of the computational load of proposed algorithms with the EKF. (*) Here EKF is built as the Multiplicative Extended Kalman Filter which uses quaternions for the attitude representation.

The Algorithm	Computational load (EKF^(*)=100)
<i>The regular UKF algorithm for attitude and gyro bias estimation</i>	282
<i>The regular UKF algorithm for attitude, gyro bias and magnetometer bias estimation</i>	398
<i>The AUKF algorithm for attitude, gyro bias and magnetometer bias estimation</i>	459
<i>The RAUKF algorithm for attitude, gyro bias and magnetometer bias estimation</i>	470
<i>The overall attitude estimation scheme</i>	566

In summary the overall attitude estimation scheme increases the accuracy of the attitude determination procedure significantly but sacrifices the computational performance. A tradeoff between them might be done by the designer regarding the mission requirements.

8. Conclusion and Recommendations

The main results of the thesis are summarized in the chapter and recommendations for the future work are given.

The primary aim of this thesis was to propose an accurate attitude determination and control method for nanosatellites with magnetic sensors and actuators. In this context several practical problems that appear when the magnetometers and magnetorquers are used as the attitude hardware are addressed and possible solution techniques were proposed. These are:

- In-orbit calibration of the magnetometers and gyros by using a single UKF algorithm was realized. This is a practical calibration method, and the magnetometers are efficiently calibrated without concerning about the on-ground calibration procedure.
- Two techniques were proposed for process noise covariance adaptation of the UKF and by using the appropriate one the UKF which is used for attitude estimation and in-orbit sensor calibration was adapted. It was shown that the estimation and calibration performance was remarkably improved. Such method might be useful both for actual implementation onboard or to determine the optimal Q values for the UKF by tests before using in the real time application.
- Single and multiple scale factor based adaptation techniques were examined for building an UKF robust against the measurement malfunction. The proposed algorithms were tested for the attitude estimation of the nanosatellite and the results were compared for various measurement failure cases.
- An estimation algorithm for the RMM was given regarding the sudden changes in the estimated parameters. A novel method for change detection and KF adaptation was proposed. Simulation results showed that the presented algorithm works properly for the RMM estimation in case of sudden changes. Using this algorithm we guaranteed that the filter has both good steady-state accuracy and tracking capability.

- An overall attitude estimation method for the nanosatellite carrying magnetometers, gyros and magnetorquers was presented and tested. The performance of the overall attitude estimation scheme is evaluated by demonstrations for a hypothetical nanosatellite.

Possible further discussions on these topics may be:

- Possible methods for reducing the computational load of the overall attitude estimation algorithm might be searched.
- The change detection method for the RMM estimation should be tested for false alarms.
- The KF adaptation method given for the RMM estimation is based on multiplication of the filter covariance with a scalar determined by the weighting function. Using a matrix instead of the scalar might be better especially if the change in all of the estimated parameters is not in the same magnitude.
- The proposed overall attitude determination method for nanosatellites might be tested with applications.

Bibliography

- Almagbile, A., Wang, J. and Ding, W. (2000). "Evaluating the Performance of Adaptive Kalman Filter Methods in GPS/INS Integration," *Journal of Global Positioning Systems*, **9**(1), 33-40.
- Bak, T. (1999). *Spacecraft Attitude Determination – a Magnetometer Approach*. Ph.D. thesis, Aalborg University, Denmark.
- Basseville, M. and Nikiforov, I.V. (1993). *Detection of Abrupt Changes: Theory and Application*, Prentice Hall, New Jersey, USA.
- Bhat, S.P. (2005). "Controllability of Nonlinear Time-Varying Systems: Applications to Spacecraft Attitude Control Using Magnetic Actuation," *IEEE Transactions on Automatic Control*, **50**(11), 1725-1735.
- Bouwmeester, J., and Guo, J. (2010). "Survey of Worldwide Pico- and Nanosatellite Missions, Distributions and Subsystem Technology," *Acta Astronautica*, **67**, 854-862. DOI:10.1016/j.actaastro.2010.06.004
- Brockett, R. W. (1983). "Asymptotic stability and feedback stabilization." in *Differential Geometric Control Theory*, (Eds. R. W. Brockett, R. S. Millman, and H. H. Sussmann), 1983.
- Candini, G.P., Piergentili, F. and Santoni, F. (2012). "Miniaturized Attitude Control System for Nanosatellites," *Acta Astronautica*, **81**, 325-334. DOI: 10.1016/j.actaastro.2012.07.027
- Cao, Y. And Tian, X. (2009). "An Adaptive UKF Algorithm for Process Fault Prognostics." *Proc. of the 2009 Second International Conference on Intelligent Computation Technology and Automation*, Zhangjiajie, PRC, **2**, 487-490. DOI: 10.1109/ICICTA.2009.352
- Crassidis, J.L. and Markley, F.L. (2003). "Unscented Filtering for Spacecraft Attitude Estimation." *Journal of Guidance, Control and Dynamics*, **26**(4), 536-542. DOI: 10.2514/2.5102
- Crouch, P.E. (1984). "Spacecraft Attitude Control and Stabilization: Applications of Geometric Control Theory to Rigid Body Models," *IEEE Transactions on Automatic Control*, **AC-29**(4), 321-331.
- Dunik, J., Simandl, M. and Straka, O. (2009). "Methods for estimating state and measurement noise covariance matrices: aspects and comparison," *Proc. 15th IFAC Symposium on System Identification*, Saint-Malo, France, 972-977.

- Dymirkovsky, G., Jing, Y. and Xu, J. (2012). "Discrete-time Unscented Kalman Filter: Comprehensive Study of Stochastic Stability," *Proc. Itzhack Y. Bar-Itzhack Memorial Symposium on Estimation, Navigation, and Spacecraft Control*, Haifa, Israel.
- Farrenkopf, R. L. (1978). "Analytic Steady-state Accuracy Solutions for Two-common Spacecraft Attitude Estimators." *Journal of Guidance, Control and Dynamics*, **1**(4), 282-284.
- Fosbury, A.M. (2011). "Steady-state Accuracy Solutions of More Spacecraft Attitude Estimators." *Proc. AIAA Guidance, Navigation, and Control Conference*, Portland, USA.
- Geng, Y. and Wang, J. (2008). Adaptive estimation of multiple fading factors in Kalman filter for navigation applications, *GPS Solutions*, **12**(4), 273-279. DOI: 10.1007/s10291-007-0084-6
- Gustafsson, F. (1996). "Estimation and Change Detection of Tire-Road Friction Using the Wheel Slip", *Proc. IEEE International Symposium on Computer-Aided Control System Design*, Michigan, USA.
- Gustafsson, F. (2000). *Adaptive Filtering and Change Detection*, John Wiley&Sons, Chichester, England.
- Hajiyev, C. and Caliskan, F. (2003) *Fault Diagnosis and Reconfiguration in Flight Control Systems*, Kluwer Academic Publishers, Boston, USA.
- Hajiyev, C. and Soken, H.E. (2013). "Robust Adaptive Unscented Kalman Filter for Attitude Estimation of Pico Satellites," *Published Online: International Journal of Adaptive Control and Signal Processing*, DOI: 10.1002/acs.2393
- Han, J., Song, Q., and He, Y. (2009). "Adaptive Unscented Kalman Filter and Its Applications in Nonlinear Control." in: *Kalman Filter: Recent Advances and Applications*, InTech Open Access Publisher, Rijeka, Croatia.
- Han, K., Wang, H., Xiang, T. and Jin, Z. (2012). "Magnetometer Compensation Scheme and Experimental Results on ZDPS-1A Pico-satellite." *Chinese Journal of Aeronautics*, **25**, 430-436.
- Hartikainen, E. and Ekelin, S. (2006). "Enhanced Network-State Estimation using Change Detection", *Proc. 31st IEEE Conference on Local Computer Networks*, Florida, USA.
- Hosonuma, T., Inamori, T. and Nakasuka, S. (2012). "A Precise Attitude Determination and Control Strategy for Small Astrometry Satellite Nano-Jasmine", *Proc. 26th AIAA/USU Conference on Small Satellites*, Logan, USA.
- Inamori, T., Nakasuka, S. and Sako, N. (2009). "In-orbit Magnetic Disturbance Estimation and Compensation Using UKF in Nano-satellite Mission," *Proc. AIAA Guidance, Navigation, and Control Conference*, Chicago, USA.

- Julier, S.J., Uhlmann, J.K. and Durrant-Whyte, H.F., (1995). "A New Approach for Filtering Nonlinear Systems." *Proc. of American Control Conference*, **3**, 1628-1632. DOI: 10.1109/ACC.1995.529783
- Julier, S., Uhlmann, J. and Durrant-Whyte, H.F., (1996). "A General Method for Approximating Nonlinear Transformations of Probability Distributions," URL: <http://citeseer.ist.psu.edu/viewdoc/summary?doi=10.1.1.46.6718> [cited 17 May 2009].
- Julier, S., Uhlmann, J. and Durrant-Whyte, H.F. (2000). "A New Method for the Nonlinear Transformation of Means and Covariances in Filters and Estimators." *IEEE Transactions on Automatic Control*, **45**(3), 477-482. DOI: 10.1109/9.847726
- Jwo, D., and Tseng, C. (2009). "Fuzzy Adaptive Interacting Multiple model Unscented Kalman Filter for Integrated Navigation." *Proc. 18th IEEE International Conference on Control Applications Part of 2009 IEEE Multi-conference on Systems and Control*, Saint Petersburg, Russia, 1684-1689. DOI: 10.1109/CCA.2009.5281068
- Jwo, D., and Chung, F. (2010). "Fuzzy Adaptive Unscented Kalman Filter for Ultra-Tight GPS/INS Integration." *Proc. of the 2010 International Symposium on Computational Intelligence and Design*, 229-235. DOI: 10.1109/ISCID.2010.148
- Kim, K.H., Lee, J.G. and Park, C.G. (2006). "Adaptive two-stage Kalman filter in the presence of unknown random bias." *International Journal of Adaptive Control and Signal Processing*, **20**(7), 305-319. DOI: 10.1002/acs.900.
- LaValle, S.M. (2006). *Planning Algorithms*. Cambridge University Press, Cambridge, UK.
- Lee, D. J., and Alfriend, K.T. (2004). "Adaptive Sigma Point Filtering for State and Parameter Estimation." *Proc. AIAA/AAS Astrodynamics Specialists Conference and Exhibit*, Rhode Island, USA.
- Liu, J., and Lu, M. (2009). "An Adaptive UKF Filtering Algorithm for GPS Position Estimation." *Proc. 5th International Conference on Wireless Communications, Networking and Mobile Computing*, Beijing, PRC, 1-4. DOI: 10.1109/WICOM.2009.5305046
- Markley, F.L., Crassidis, J.L. and Cheng, Y. (2005). "Nonlinear attitude filtering methods," *Proc. AIAA Guidance, Navigation, and Control Conference and Exhibit*, San Francisco, USA.
- Maybeck, P.S. (1982). *Stochastic Models, Estimation and Control*. Vol. II. Academic Press, New York, USA.
- Mehra, R.K. (1970). "On the identification of variances and adaptive filtering," *IEEE Transactions on Automatic Control*, **15**(2), 175-184.
- Mehra, R.K. (1972). "Approaches to adaptive filtering," *IEEE Transactions on Automatic Control*, **17**(10), 693-698.
- Mohamed, A.H., and Schwarz, K.P. (1999). "Adaptive Kalman Filtering for INS/GPS." *Journal of Geodesy*. **73**(4), 193-203.

- Morin, P. and Samson, C. (1997). "Time-varying Exponential Stabilization of a Rigid Spacecraft with Two Control Torques," *IEEE Transactions on Automatic Control*, **42**(4), 528-534.
- Murray, R.M. and Sastry, S.S. (1993). "Nonholonomic Motion Planning: Steering Using Sinusoids," *IEEE Transactions on Automatic Control*, **38**(5), 700-716.
- Odelson, B.J., Rajamani, M.R. and Rawlings, J.B. (2006). "A new autocovariance least-squares method for estimating noise covariances," *Automatica*, **42**(2), 303-308.
- Page, E. S. (1954). "Continuous Inspection Schemes," *Biometrika*, **41**(1-2), 100-115.
- Pong, C. M., et al. (2012). "High-Precision Pointing and Attitude Determination and Control of ExoplanetSat," *Proc. AIAA Guidance, Navigation and Control Conference*, Minneapolis, USA.
- Reijneveld, J. and Choukroun, D. (2012). "Attitude Control of the Delfi-n3Xt Satellite," *Proc. AIAA Guidance, Navigation and Control Conference*, Minneapolis, USA.
- Rendleman, J. D. (2009). "Why SmallSats?" *Proc. AIAA SPACE 2009 Conference & Exposition*, Pasadena, USA.
- Reyhanoglu, M. and Drakunov, M. (2008). "Attitude Stabilization of Small Satellites Using Only Magnetic Actuation," *Proc. 34th Annual Conference of IEEE on Industrial Electronics*, Florida, USA.
- Roberts, S.W. (1959). "Control Chart Tests Based on Geometric Moving Averages," *Technometrics*, **1**(3), 239-250.
- Sakai, S., Fukushima, Y., Ohno, A. and Saito, H. (2006a). "In-orbit Performance Evaluation of Temperature Controlled Small Fiber Optical Gyro on Microsatellite <REIMEI>," *Proc. International Conference on Optical Fiber Sensors*, Cancún, Mexico.
- Sakai, S., Fukushima, Y., Saito, H. and Kaneda, R. (2006b). "Studies on Magnetic Attitude Control System for the REIMEI Microsatellite," *Proc. AIAA Guidance, Navigation, and Control Conference*, Keystone, USA.
- Sakai, S., Fukushima, Y. and Saito H. (2008) "Design and on-orbit Evaluation of Magnetic Attitude Control System for the "REIMEI" Microsatellite," *Proc. 10th IEEE International Workshop on Advanced Motion Control*, Trento, Italy.
- Sakai S. and et al. (2011) "Real-time estimation of the bias error of the magnetometer only with the gyro sensors," *Proc. of the 27th International Symposium on Space Technology and Science*, Okinawa, Japan.
- Sekhvat P., Gong, Q. and Ross, I.M (2007). "NPSAT1 Parameter Estimation Using Unscented Kalman Filter." *Proc.2007 American Control Conference*, IEEE, New York, USA, 4445-4451.
- Silani, E. and Lovera, M. (2005). "Magnetic Spacecraft Attitude Control: A Survey and Some New Results," *Control Engineering Practice*, **13**, 357-371.

- Shi, Y., Han, C. and Liang, Y. (2009). "Adaptive UKF for Target Tracking with Unknown Process Noise Statistics." *Proc. 12th International Conference on Information Fusion*, Seattle, USA, 1815-1820.
- Sofyali, A. and Jafarov, E. M. (2012). "Purely Magnetic Spacecraft Attitude Control by Using Classical and Modified Sliding Mode Algorithms," *Proc. 12th IEEE Workshop on Variable Structure Systems*, Mumbai, India.
- Soken, H.E., Aslan, A.R. and Hajiyev, C. (2010). "Attitude Determination and Control of Future Small Satellites," *Proc. NATO AVT-171 Workshop: Multifunctional Structures and System Technologies for Small Spacecraft (RTO-MP-AVT-171)*, Antalya, Turkey.
- Soken, H.E. and Hajiyev, C. (2010). "Pico satellite attitude estimation via Robust Unscented Kalman Filter in the presence of measurement faults." *ISA Transactions*, **49**(3), 249-256. DOI:10.1016/j.isatra.2010.04.001.
- Soken H. E. and Sakai, S. (2011). "UKF Based On-Orbit Gyro and Magnetometer Bias Estimation as a Part of the Attitude Determination Procedure for a Small Satellite," *Proc. 11th International Conference on Control Automation and Systems*, 1891-1896, Seoul, Korea.
- Soken, H.E., and Hajiyev, C. (2012). "UKF-Based Reconfigurable Attitude Parameter Estimation and Magnetometer Calibration." *IEEE Transactions on Aerospace and Electronic Systems*, **48**(3), 2614 – 2627.
- Soken, H.E., Hajiyev C. and Sakai, S. (2012a). "Robust Kalman Filtering with Multiple Scale Factors for Small Satellite Attitude Estimation", *Proc. Itzhack Y. Bar-Itzhack Memorial Symposium on Estimation, Navigation, and Spacecraft Control*, Haifa, Israel.
- Soken, H.E., Hajiyev C. and Sakai, S. (2012b). "Robust Kalman Filtering for Small Satellite Attitude Estimation in the Presence of Measurement Faults," *Submitted for: European Journal of Control*.
- Soken H.E. and Sakai, S. (2012a). "Residual Based Adaptive Unscented Kalman Filter for Satellite Attitude Estimation," *Proc. AIAA Guidance, Navigation, and Control Conference*, Minneapolis, USA. DOI: 10.2514/6.2012-4476
- Soken, H.E. and Sakai, S. (2012b) "Adaptive Unscented Kalman Filter for Small Satellite Attitude Estimation", *Proc. 2012 Asia-Pacific International Symposium on Aerospace Technology*, Jeju, Korea.
- Soken H.E. and Sakai, S. (2012c) "Adaptive Tuning of the UKF for Satellite Attitude Estimation," *Submitted for: ASCE Journal of Aerospace Engineering*.
- Soken, H.E., Hajiyev C. and Sakai, S. (2013a). "Robust Kalman Filtering with Single and Multiple Scale Factors for Small Satellite Attitude Estimation" in: *Advances in Estimation, Navigation, and Spacecraft Control* (Eds. Choukroun, D., Oshman, Y., Thienel J. and Idan M.), Springer (under review).

- Soken, H.E., Sakai S. and Wisniewski, R. (2013b). "In-Orbit Estimation of Time-Varying Residual Magnetic Moment," *Submitted for: IEEE Transactions on Aerospace and Electronic Systems*.
- Soken H.E. and Sakai, S. (2013). "In-Orbit Estimation of Time-Varying Residual Magnetic Moment for Small Satellite Applications," *Accepted for: AIAA Guidance, Navigation, and Control Conference*, Boston, USA.
- Song, Q. and He, Y. (2009). "Adaptive Unscented Kalman Filter for Estimation of Modelling Errors for Helicopter." *Proc. 2009 IEEE International Conference on Robotics and Biomimetics*, Guilin, PRC, 2463-2467. DOI: 10.1109/ROBIO.2009.5420406
- Stenlund, B. and Gustafsson, F. (2002). "Avoiding Windup in Recursive Parameter Estimation", *Preprints of reglermöte*, Linköping, Sweden.
- Steyn, W.H. and Hashida, Y. (2001). "In-Orbit Attitude Performance of the 3-Axis Stabilised SNAP-1 Nanosatellite", *Proc. 15th AIAA/USU Conference on Small Satellites*, Logan, USA, 2001.
- Suehiro, T. (2010). "Satellite Design Methodology to Suppress Time-varying Residual Magnet Effects on Attitude for Nano-Satellites," *Proc. 18th IFAC Symposium on Automatic Control in Aerospace*, Nara, Japan, 2010.
- Vinther, K., Jensen, K.F., Larsen, J.A., and Wisniewski, R. (2011). "Inexpensive Cubesat Attitude Estimation Using Quaternions and Unscented Kalman Filtering." *Automatic Control in Aerospace [online journal]*, **4**(1).
- Wang, D., Jia, Y., Jin, L. and Xu, S. (2013). "Control Analyses of an Underactuated Spacecraft under Disturbance," *Acta Astronautica*, **83**, 44-53.
- Wang P. Shtessel, Y.B. and Wang Y. (1998). "Satellite Attitude Control Using Only Magnetorquers," *Proc. Thirtieth Southeastern Symposium on System Theory*, Morgantown, USA.
- Wisniewski, R. (1996). *Satellite Attitude Control Using Only Electro-magnetic Actuation*. Ph.D. thesis, Aalborg University, Denmark.
- Wisniewski, R. (2012). Private Communication.
- Wertz, J.R. (1988). *Spacecraft Attitude Determination and Control*, Kluwer Academic Publishers, Dordrecht, Holland.
- Xiong, K., Liu L.D. and Zhang, H. Y. (2009). "Modified Unscented Kalman Filtering and Its Application in Autonomous Satellite Navigation," *Aerospace Science and Technology*, **13**, 238-246.
- Yoshimura, Y., Matsuno, T. and Hokamoto S. (2011). "Three Dimensional Attitude Control of Underactuated Satellite with Thrusters," *International Journal of Automation Technology*, **5**(6), 892-899.

Appendix A: Attitude Control of the Magnetically Actuated Nanosatellite

In this thesis we discussed several issues regarding the design of an attitude determination scheme for a nanosatellite with magnetic sensors and actuators. Undoubtedly, attitude control for such satellites is also an important problem which should be solved for proposing a complete attitude determination and control method. On the other hand, attitude control by means of solely magnetic actuators (i.e. magnetorquers) forms a standalone issue because of its complexity, so we believe it should be considered as a part of another study. In this appendix, we review the pure magnetic attitude control problem by referring to well known studies and summarize our recent work which might be a candidate for solving the problem by an approach different than the ones in the literature.

A.1. A Review for the Attitude Control by Magnetic Actuation

One of the main issues for increasing the ADCS performance of a nanosatellite with magnetic sensor and actuator is the accuracy and applicability of the method used for pure magnetic attitude control. Pure magnetic attitude control refers pointing the satellite using only magnetorquers as the actuators. Using magnetic coils for the attitude control purpose is not a new topic and the first investigations go back to 1960s. Nonetheless, since the feasibility of the periodic control techniques for the magnetic attitude control was proved (Wisniewski 1996), it has been more and more popular because of its advantages for small satellite applications. A comprehensive survey for magnetic attitude control can be found in (Silani and Lovera 2005). There are also more recent studies which propose different approaches to the problem (Reyhanoglu and Drakunov 2008; Sofyali and Jafarov 2012). The main drawback of all researches on the pure magnetic attitude control is the dependency to the orbital periodic variation of the Earth's magnetic field. This is because of the inherent constraint of the problem: the applied control torque must lie in the plane orthogonal to the magnetic field vector as given in Fig. A1. In figure, \mathbf{B} is the magnetic field vector of the Earth, \mathbf{N}_{req} is the required torque for attitude control purpose and \mathbf{N}_{mag} is the applicable magnetic control torque which is orthogonal to the vector \mathbf{B} . For defining the problem explicitly, we may rewrite Eq.2.42 as

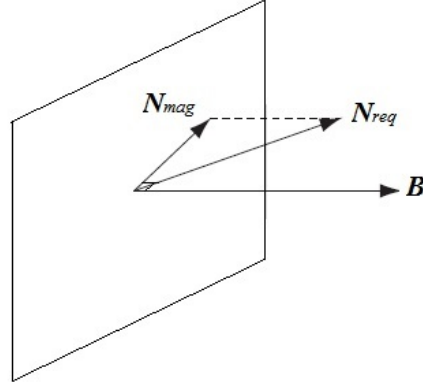


Figure A.1: Limitations of the magnetic attitude control.

$$N_c = M_c \times B = B(b)M_c, \quad (\text{A.1})$$

where,

$$B(b) = \begin{bmatrix} 0 & B_z & -B_y \\ -B_z & 0 & B_x \\ B_y & -B_x & 0 \end{bmatrix}. \quad (\text{A.2})$$

Here, for $B(b)$ matrix $\text{rank}[B(b)] = 2$. So, the satellite is instantaneously underactuated and we cannot apply a control torque about all three axes in an independent manner. Full controllability is only guaranteed if the spacecraft experiences a variation in the direction of the magnetic field along each orbit such that (Silani and Lovera 2005),

$$\bigcup_{t=0,T} \text{span}_{col}(B(t)) = R^3. \quad (\text{A.3})$$

Here, T is the orbital period of the satellite. Hence, three axis stabilization is possible only if the orbit of the satellite experiences a variation of the magnetic field which is sufficient for stabilizability. This condition strictly depends on the inclination of the orbit; the controllability tends to increase with the orbit inclination and the satellite with solely magnetic actuators is almost uncontrollable in equatorial orbits.

A.2. Discussion on the Recent Studies

Our recent study on this problem is to search for a method to control the attitude of the satellite by means of solely magnetorquers without any dependence to the orbital periodicity of the Earth's magnetic field. In this sense an analogy with a satellite with two

control inputs about two axes (e.g. a satellite with two thrusters) might be useful. In this case the satellite dynamic equations are written as

$$\frac{d\omega_x}{dt} = \left(\frac{J_y - J_z}{J_x} \right) \omega_y \omega_z + \frac{T_x}{J_x}, \quad (\text{A.4})$$

$$\frac{d\omega_y}{dt} = \left(\frac{J_z - J_x}{J_y} \right) \omega_z \omega_x + \frac{T_y}{J_y}, \quad (\text{A.5})$$

$$\frac{d\omega_z}{dt} = \left(\frac{J_x - J_y}{J_z} \right) \omega_x \omega_y \quad (\text{A.6})$$

Obviously this system is an underactuated system and there is no torque input for controlling the angular velocity around the z axis, ω_z . However, some researchers show that using only two control torques, three-dimensional angular velocities and/or attitude of a satellite can be controlled and in order to achieve that, non-integrable constraints should be utilized (Yoshimura *et al.* 2011; Crouch 1984). A system with non-integrable constraints is called nonholonomic and states of such system can be controlled even if the number of the actuators is less than the number of generalized coordinates. A car with its limited configuration for parallel parking (i.e. parallel parking problem) is a good example for nonholonomic systems and has been widely discussed for path planning issues (LaValle 2006).

Before designing the controller for the underactuated satellite system (A.4-A.6) it must be proven that the system is controllable. Such examination is covered by the studies on nonlinear controllability and as the first step the system should be expressed in the control-affine form:

$$\dot{x} = g_0(x) + \sum_{i=1}^m u_i g_i(x). \quad (\text{A.7})$$

Here, g_0 is the drift vector (dynamics), g_i are the control vector fields and u_i are the control inputs such that $i=1\dots m$.

Then, as discussed in (Crouch 1984) the geometric control theory can be applied to the spacecraft's dynamic model and the controllability can be analyzed using the Lie algebra and concept of Lie brackets. Assuming g_1 and g_2 are two control vector fields, the standard definition of the Lie bracket is

$$g_3 = [g_1, g_2] = \frac{\partial g_2}{\partial x} g_1(x) - \frac{\partial g_1}{\partial x} g_2(x). \quad (\text{A.8})$$

Basically if the new vector fields (e.g. $g_3 \dots g_n$) calculated by Lie bracketing the others produces motion in all directions of the state space that is not accessible with the existing control inputs (Lie algebra rank condition is satisfied) that means the system is controllable. For the example of satellite with two thrusters such analyses might be seen in details in (Crouch 1984; Wang *et al.* 2013).

After showing that the system is controllable the controller can be designed. Nonetheless, the closed loop control of nonholonomic systems is very difficult, especially because of fundamental restrictions that prohibit the existence of smooth feedback controllers which asymptotically stabilize a point (Brockett 1983; Murray and Sastry 1993). A nonholonomic system can be stabilized only by means of smooth time-varying or discontinuous (e.g. sliding-mode) feedback control laws. Same methodology should be followed for a satellite with two control inputs as extensively discussed in the literature (Morin and Samson 1997; Wang *et al.* 2013; Yoshimura *et al.* 2011).

The controller design procedure for a satellite with solely magnetic actuators might be similar when we want to control the satellite without any dependence to the orbital variation of the Earth's magnetic field. In (Bhat 2005) a controllability analysis using the Lie brackets is performed but assuming that the spacecraft experiences a variation of the magnetic field along the orbit. For our case such analysis must be performed assuming that the magnetic field in the orbit coordinate system is constant and in the body coordinates the terms of \mathbf{B} depends only on the attitude of the spacecraft such that $\mathbf{B} = \mathbf{B}(\mathbf{q})$. In this case the control vector fields will be,

$$\mathbf{N}_c = \mathbf{M}_c \times \mathbf{B} = \underbrace{\begin{bmatrix} 0 \\ -B_z(\mathbf{q}) \\ B_y(\mathbf{q}) \end{bmatrix}}_{g_1} M_{C_x} + \underbrace{\begin{bmatrix} B_z(\mathbf{q}) \\ 0 \\ -B_x(\mathbf{q}) \end{bmatrix}}_{g_2} M_{C_y} + \underbrace{\begin{bmatrix} -B_y(\mathbf{q}) \\ B_x(\mathbf{q}) \\ 0 \end{bmatrix}}_{g_3} M_{C_z} \quad (\text{A.9})$$

Here M_{C_x} , M_{C_y} and M_{C_z} are magnetic control inputs (magnetic dipole for each torquer) and g_1 , g_2 and g_3 are control vector fields.

Specifically for pure magnetic control, the problem arises from the linear dependence of three vector fields g_1 , g_2 and g_3 , which is not in question for a satellite with two thrusters. Because $\text{rank}[\mathbf{B}(b)] = 2$ and it means that we cannot use all three of the control vector

fields to derive another level of Lie bracket and gain dimension in terms of control. Two main ideas to proceed are:

- Start derivation for an underactuated system such that we have two magnetic torquers. Neglect the torquer in one direction.
- Perform coordinate transformation to some axis team where one of the control terms is always parallel to the magnetic field vector so does not produce any torque. A similar problem is investigated in (Wang *et al.* 1998) for an isoinertial satellite ($J_x = J_y = J_z$). In this case the spacecraft dynamics and kinematics must be represented in this new coordinate system.

In summary, the problem of attitude control by means of solely magnetorquers without any dependence to the orbital periodicity of the Earth's magnetic field is analogous to the attitude control by two thrusters since both systems are instantaneously underactuated. Therefore a similar methodology might be followed for first proving the controllability of the system and then designing the controller. On the other hand, for pure magnetic control, a modification such as the coordinate transformation might be necessary.